Summer 8-19-2016

Long-Acting Antiretroviral Nanoformulation Development and Subcellular Trafficking

Dongwei Guo
University of Nebraska Medical Center

LONG-ACTING ANTIRETROVIRAL NANOFORMULATION DEVELOPMENT AND SUBCELLULAR TRAFFICKING

by

Dongwei Guo

A Dissertation

Presented to the Faculty of the Graduate School in the University of Nebraska Medical Center in Partial Fulfillment of the Requirements for the Degree of Doctor of Philosophy

Department of Pharmaceutical Science
Under the Supervision of Dr. Howard E. Gendelman

University of Nebraska Medical Center, Omaha, Nebraska

June 2016

Supervisory Committee:

Howard E. Gendelman, M.D.	Michael D. Boska, Ph.D.
JoEllyn M. McMillan, Ph.D.	Jered C. Garrison, Ph.D.

Long-Acting Antiretroviral Nanoformulation Development and Subcellular Trafficking

Dongwei Guo, Ph.D.

University of Nebraska Medical Center, 2016

Supervisor: Howard E Gendelman, M.D.

The introduction of nanoformulated antiretroviral therapeutic regimens is a promising alternative to standard once a day oral treatment of HIV infection. Our lab has pioneered this effort and was successful in harnessing mononuclear phagocytes (monocytes, dendritic cells and macrophages) as nanoformulated drug carriers. The approach was developed as Trojan horses for drug transport, delivery and distribution to sites of viral replication in order to facilitate microbial elimination in HIV sanctuaries. However, the remaining challenges for current antiretroviral nanoformulations include to formulate a broad range of hydrophilic short-acting drugs, and to elucidate the mechanism of sequestered nanoparticles in macrophages at the subcellular level. To this end, we developed a two-step synthesis to create a long-acting lamivudine (2',3'-dideoxy-3'-thiacytidine, 3TC). A stable hydrophobic pro-drug crystal formulation was produced by poloxamer drug encasement. Conversion of the hydrophilic 3TC significantly extended its bioavailability facilitated by chemical drug conjugation to a fatty acid and creating a myristoylated drug. A folate targeted poloxamer 407 coated a newly formed nanocrystalline pro-drug markedly improving cell uptake, bioavailability and pharmacokinetic profiles. Reduced cytotoxicity and robust antiretroviral activities were also achieved. The nanoparticle interactions at the subcellular level were investigated vial nanoformulated protease inhibitor. Quantitative SWATH-MS proteomics for complete

recording of fragment ion peptide precursors in biological sample. and cell profiling were applied for endolysosomal trafficking for HIV-1 assembly and nanoformulation depot formation. We believe these findings unveil new opportunities for nanoformulated antiretroviral therapy and have brought the idea of long-acting antiretroviral therapy closer to the clinical translation.

Acknowledgement

I would like to give my sincerely acknowledgement to my mentor and adviser Dr. Howard E Gendelman, who provided constant support and help to accomplish this work. I have been extremely lucky to have a mentor who cared so much about my work, who responded to my questions so promptly. He taught me not only to become a troubleshooter, a creative thinker, and a great scientist but also to be a diligent, upright and an enthusiastic person. From him, I learned what a real scientist is.

I also would like to thank members of my graduate supervisory committees, Drs. Michael D Boska, JoEllyn M McMillan, and Jered C Garrison, for their valuable guidance, suggestions and encouragement during my PhD training period. I would like to thank Dr. JoEllyn McMillan for her professional guidance during my studies. I would like to thank Dr. Boska and Dr. Garrison for scientific training and my research skill fostering.

I would like to thank the China Scholarship Council for financial support in the past years. I would like to thank the UNMC Graduate Studies and Department of Pharmaceutical Sciences. I would like to thank all the UNMC core facility staff and members in the UNMC animal facility for their extreme cooperation.

I would also like to thank all the members from Dr. Gendelman's lab, past and present. I wish to especially thank Dr. Xinming Liu for his professional advice through out this project. I would like to thank Dr. Benson Edagwa for his guidance on chemical synthesis, Dr. Arainga Ramirez for her training on biological analysis, and Dr. Tianyuzi Li for her help on MRI data analysis. I would like to thank Dr. Gang Zhang for teaching me biological assay methods. I would like to thank Dr. Pavan Puligujja, Tian Zhou and Zhiyi Lin for help on animal sacrifice, and Diana Palandri for UPLC analysis. I would also like to thank Dr. Shantanu Balkundi, James Hilaire, Nathan Smith, Brady Sillman, Hang Su,

Dhirender Singh, Andrea Skinner, Mary Banoub, Denise Cobb, Bhavesh Kevadiya, Vivek Agrahari, Monalisha Elango, and Ibrahim Ibrahim for their support and help.

I would like to thank all my friends and colleagues for their help and support in the past five years. I would like to thank Xin Wei, Gang Zhao, Hangting Hu, Yinnong Jia, Zhihao Mao, Yuning Zhang, Yang Peng, Yuliang Zhang, Tian Zhou, Zhiyi Lin for the lifelong friendship. Without them, life cannot be so valuable and memorable.

Finally, I would like to thank all my family. I would like to thank my husband Jian Zhang, who is always there for me with endless love and company; to my parents Jinwen Hao and Wenxiang Guo, who are continuously encouraging me without any condition; to my parents in law Suqin Xiao and Enjun Zhang, who are supporting me all the time; and to my daughter Nicole Zhang, whom I should work hard, never give up to become a good role model for.

Table of Contents

Table of Figures

Chapter I.

Introduction

1.1. HIV and AIDS

1.1.1. Epidemic

Human immunodeficiency virus infection and acquired immune deficiency syndrome (HIV/AIDS) is a spectrum of conditions caused by infection with the human immunodeficiency virus. Since its first discovery in 1981, HIV/AIDS has killed more than 25 million people worldwide. It has become a global pandemic. As of 2014, approximately 36.9 million people are living with HIV globally, and 1.18 million people died of HIV/AIDS. Due to the widespread infection of HIV there has been a determination for the discovery and use of medicinal agents that can inhibit the virus. HIV type-1 (HIV-1) displays extraordinary genetic variation and can be phylogenetically classified into three distinct groups and several subgroups across the globe. While HIV-1 clade C dominates the HIV-1 epidemic worldwide with more than 50% of the total viral infections, predominantly in Southern Africa, and other parts of Asia, HIV-1 subtype B is mainly found in Europe and America with about 10% of the total infections [1, 2].

1.1.2. Pathobiology

HIV is a member of the genus Lentivirus, belonging to the family Retrovirus. HIV is roughly spherical with a diameter of about 80 to 120 nm in diameter. It is transmitted as single-stranded, positive-sense, enveloped RNA virus. It is composed of 2,000 copies of the viral protein p24, which is tightly bound to nucleocapsid proteins and enzymes including reverse transcriptase, proteases, ribonuclease and integrase. The p24 protein is coated by capsid, which helps in ready adsorption onto the host cell surface and provides a protective shell for the nucleic acid core. A series of host cell proteins and viral specific glycoproteins including gp41 and gp120 are embedded in the phospholipid

bilayer. In addition to the viral core HIV has six regulatory genes (tat, rev, nef, vif, vpr and vpu) that affect its abilities to infect, replicate and assemble within the cell [3, 4].

HIV primarily infects components of the human immune system such as CD4+ T cells, monocytes, macrophages, glial cells, and dendritic cells. The HIV virion enters host cells by the adsorption of glycoproteins on its surface to receptors on the target cell followed by fusion of the viral envelope with the cell membranes and the release of the HIV capsid into the cell. Entry to the cell begins through interaction of the trimeric envelope gp160 spike with both CD4 and a chemokine receptor, either CXCR4 or CCR5. The virus will first attach to the host cell via the CD4 receptor through the CD4 binding domains of gp120. The envelope complex undergoes a structural change, exposing the chemokine binding domains of gp120 and allowing them to interact with the target chemokine receptor. Fusion peptide gp41 then can penetrate the cell membrane, causing the collapse of the extracellular portion of gp41 into a hairpin, fusion of the host cell membranes as well as subsequent entry of the viral capsid. The HIV RNA and various enzymes are injected into the cell. The viral single-strand RNA genome is transcribed into double-strand DNA and integrated into a host chromosome. Infection and ultimate destruction of CD4+ T cells heralds secondary immune deficiency and concomitant co-morbid conditions that include opportunistic infections and primary virus-induced metabolic changes that affect also the function of the central nervous system (CNS), gut and lymphoid tissues. Within days after primary infection HIV invades the nervous system through lymphocytes and macrophages that cross the blood brain barrier (BBB) and serve as Trojan Horses for viral dissemination [4, 5].

1.2. Macrophages and HIV reservoir

Mononuclear phagocyte including blood monocyte, tissue macrophages and dendritic cells are principal cells involved in the clearance and inactivation of the HIV. These cells act as the reservoirs and vehicles for the dissemination of this viral pathogen. After binding and uptake, the ability of HIV-1 to complete its replication cycle depends mainly on differentiation and activation of its target cell and on molecular determinants of the infecting viral strain. The viral infection is highly dependent on the state of macrophage differentiation and the role of macrophages is a reservoir for persistent lentiviral infection. It will decide whether viral infection is abortive, restricted, permissive, latent, or enhanced. Cellular differentiation parallels macrophage susceptibility to viral infection. The viral life cycle in monocytes and macrophages is regulated by physiological factors involved in differentiation from monocyte precursors to mature tissue macrophages [6-8].

The transmission of HIV occurs through exchange of body fluids and is mediated in large measure by cell-associated virus. HIV-1 in leukocytes of seminal and vaginal fluids, uterine cervix, and gastrointestinal lamina propria support a cell-mediated transmission of virus. After primary viral exposure, high levels of HIV replication ensue in the infected human host, which results in plasma viremia. Virus seeds tissue macrophages and continues to replicate during the long subclinical latency period. Viral replication is regulated by humoral and cellular immune factors. These viral-mediated immune regulatory factors are produced against a number of HIV gene products. Macrophage amplify production of a variety of immunoregulatory molecules such as complement, arachidonic acid metabolites, neutral proteases, various growth factors, and other cytokines including platelet-derived growth factor, tumor necrosis factor α (TNF- α), colony-stimulating factors (CSFs), the interleukins, and the interferons (IFN- α

and IFN-β). Many cytokines like interleukins (IL-1, -3, -4, and -6), macrophage and granulocyte-macrophage CSFs (M-CSF and GM-CSF), and TNF- α up-regulate HIV gene expression and thus play important roles in disease onset and progression. Some cytokines like IFN-α, -β, and –γ and IL-4 exert suppressive effects on HIV replication. The cytokine responses to viral infection complement immune-specific antiviral responses including antibody-dependent complement-mediated, neutralization, and cell-mediated immune responses.

Viral reservoir sites protect the virus from biological elimination pathways, immune response, and antiretroviral drugs. They allow viral dissemination throughout the body, and serve as a major source of viral rebound upon treatment failure, and contribute to the development of drug resistance. Resting CD4+ cells are known to be the main cellular reservoir for the latent HIV-1 infection due to their ability to persist for a long span. Although the pool of latently infected, resting CD4+ T cells has been the most extensively studied HIV reservoir to date and is widely recognized as one of the major obstacles to achieving eradication of virus, low levels of HIV replication may persist in infected individuals. The lack of consensus on the life span of the latent viral reservoir has sparked an intense debate regarding the possibility that low levels of HIV replication in subsets of CD4+ T cells in the lymphoid tissue may contribute to replenishment of infected CD4+ T cells. By this mechanism, the overall half-life of the viral reservoir could be indefinitely extended. In this regard, previous mathematical models have suggested that productively infected CD4+ T cells have a relatively short in-vivo half-life (<1 day) following initiation of ART. The data indicate that such cells should no longer be present in infected individuals who had been receiving clinically effective ART for extended periods. However, activated CD4+ T cells, enriched at high purity from the blood of a viremic individual receiving ART, carry HIV proviral DNA and are capable of spontaneously producing virions in culture. Furthermore, phylogenetic analyses of HIV

env provided evidence for virologic cross-talk between infected resting and activated CD4+ T cells in the absence of detectable plasma viremia. HIV replicates primarily in the lymphoid tissues with extremely high levels of viral replication and extensive destruction of CD4+ T cells in the gut-associated lymphoid tissue (GLAT) of infected animals or humans. The overall HIV burden is substantially higher in the GALT than in the blood of infected individuals receiving long-term treatment [9].

Besides, other cellular reservoirs including monocytes and macrophages are the most important reservoirs outside the blood stream, which have been described to play an important role in HIV persistence. Monocytes and macrophages are relatively long-lived cells since HIV has very low cytopathic effects on them, making them a persistent reservoir of HIV regardless of the presence of highly active antiretroviral therapy. Monocytes and macrophages express efflux transporters, which contribute to maintain subtherapeutic concentrations of antiretroviral medications in these cells and may explain why macrophages are sanctuaries for HIV. Macrophages are a major and crucial target of HIV-1 infection and, as potential long-term HIV reservoirs, infected cells must be selectively destroyed to achieve HIV-1 eradication. As macrophages function as potent antigen-presenting cells and mediators of both innate and acquired immunity, HIV-1-mediated macrophage deficiency is catastrophic to the global immune response. A significant obstacle in clearing virus from infected individuals is multiple latently infected viral sanctuaries. Latent HIV-1 can emerge with recrudescence as a productive infection later in disease progression and might also represent a source for the emergence of resistant HIV-1. Many regimens eventually fail, primarily because of lack of adherence to strict regimens, delayed toxicities and/or the emergence of drug-resistant HIV strains.

The function of macrophages in vivo presents a long-lived target for HIV-1 infection; the half-life ($t_{1/2}$) of macrophages is significantly longer than that of an activated

lymphocyte (weeks/years versus hours/days). More specifically, the life span of activated HIV-1-infected lymphocytes is relatively attenuated, with a $t_{1/2}$ of approximately 0.8–1.1 days, whereas productively infected macrophages maintain viability and virus production for at least 30 days. The latter study represents an in vitro assay and, although studies observing the $t_{1/2}$ of HIV-1 infected macrophages in vivo are lacking, existing studies define a distinct advantage for macrophages when observing their life span and virus production over time. Viral dynamics in vivo indicate that CCR5-using viruses predominate early during infection. As macrophages display high CCR5 expression levels, they represent an early target for the establishment of both chronic and latent infection. Macrophages interact with lymphocytes during antigen presentation, conferring direct infection to new CD4+ T lymphocytic targets. Macrophages have also been implicated as the causative agent in central nervous system (CNS) infection of HIV-1, which often manifests itself as HIV-associated dementia during the later stages in the progression to AIDS [9, 10].

Macrophages represent a crucial target for establishment and maintenance of chronic and latent HIV-1 infection. Various macrophage-like cells, including dendritic cells, alveolar macrophages, monocyte precursors and microglial cells, contribute to the complex interplay between systemic infection and administration of ART. Macrophages are found in every organ system and tissue, and, because of high CCR5 expression, represent a target for early establishment and maintenance of latent viral reservoirs.

1.3. Traditional antiretroviral therapies

The introduction of highly active antiretroviral therapy started from 1996, which has been a great medical success in terms of increasing survival and improving the quality of life of the HIV-infected patient population. Due to the steady advancements in HIV

research and drug discovery, HIV infected patients on current combination antiretroviral therapy (cART) can effectively maintain undetectable plasma virus levels for years. As the threat of HIV/AIDS persists to rise, effective drug treatments are required to treat the infected people. Antiretroviral therapy has markedly reduced HIV/AIDS related deaths and opportunistic infectious diseases. This has resulted in prolonged survival of individuals infected with HIV. Long-term medical care has significantly improved the patients' life expectancy and quality by suppression of plasma viral replication. Viral resistance to antiretroviral (ARV) drugs can be addressed with two or more drug combinations that target two to more drug targets within the same or different viral proteins. The drugs available for the treatment of HIV/AIDS are proven to be selective and effective with an acceptable safety to suppress plasma viral propagation. Alternate drug combinations will be utilized if drug resistant virus appears in clinics.

As the mechanisms and proteins essential for HIV replication are characterized, most of these viral proteins have been used as drug targets for inhibiting HIV replication. Potent inhibitors of viral entry, replications, intergration and maturation have been developed as therapeutic agents. These drugs are generally referred to as entry (CCR5/CD4), reverse transcriptase, integrase and protease inhibitors, respectively. Reverse transcriptase inhibitors have been elucidated in detail, which revealed two distinct classes of molecules that inhibit enzyme activity through unique mechanism. In combination, these reverse transcriptase inhibitors greatly reduce the risk of inducing drug-resistant virus. Nowadays, there are 26 or more drugs available for the treatment of HIV in the USA. Since single agent ART is no longer clinically relevant, the clinical use of combinations of drugs is more efficacious compared with HIV monotherapy. Clinically, therapeutic regimens often target multiple checkpoints in viral replication such as the combination of protease inhibitors with reverse transcriptase inhibitors. The development

of these agents for cART has been effective at suppressing plasma viral load and preventing drug resistance [11].

The efficacy of ART cellular pharmacology in macrophages has significant implications in disease progression. The interplay between ART cellular pharmacology in macrophages directly affects viral loads, selection of resistance mutations both within and between subsets of HIV-1 target cells, eradication of systemic virus and long-term patient survival. Eradication of systemic HIV-1 infection is not possible without clearance of latently infected cells. As macrophages are a sentinel target for HIV-1 infection and latency, understanding the cellular pharmacology of current antiretroviral therapy in macrophages is essential.

1.3.1. Entry inhibitors

Entry inhibitors inhibit entry of HIV-1 into host cells and there are two anti-HIV drugs approved by the US Federal Drug Administration (FDA): enfuvirtide and maraviroc. Enfuvirtide is a peptide derived from a repeat sequence of the transmembrane portion of HIV-1 envelope, gp41, and inhibits the hairpin formation necessary for virus-host cell fusion to occur. Enfuvirtide sensitivity was largely independent of the coreceptor usage, and its overall antiviral activity in macrophages correlated more closely with HIV-1 entry by CCR5 rather than with entry through CXCR4. It is demonstrated the downstream effects of enfuvirtide relative to CXCR4- versus CCR5-mediated signaling and provide a foundation for understanding the effect of entry inhibitors on multiple cellular events in macrophages. Maraviroc is a small molecule, which inhibits viral entry by binding to the CCR5 coreceptor and inhibiting the receptor-coreceptor viral entry interaction required for HIV-1 entry into the host cell. The median effective concentration (EC50) for maraviroc in primary macrophages is reported

to be 0.5 nM for a subtype B M-R5 virus versus 0.2–2.9 nM in activated lymphocytes for R5-using viruses across multiple subtypes [12-14].

1.3.2. Nucleoside reverse transcriptase inhibitors

Nucleoside reverse transcriptase inhibitors (NRTIs) have a well-established regulatory pathway and distinct clinical advantages. They are low plasma protein binding, sustained antiviral response and relative ease of chemical manufacture. There are about eight FDA approved NRTIs: zidovudine, didanosine, zalcitabine, stavudine, abacavir sulfate, lamivudine, entricitabine, and tonofovir disoproxil fumarate. The target of NRTIs in HIV-1 infection is the reversed transcriptase (RT), which is active early in the viral replication cycle. RT converts the genetic information of the virus stored at RNA into DNA by reverse transcription, which is a process necessary for continued viral replication. NRTIs are chiral small molecules that mimic natural nucleotides and require intracellular phosphyorylation to become functionally active against HIV-1 RT. In the triphosphate form, NRTIs compete with one of the four naturally occurring dNTP, namely, dCTP, dTTP, dATP or dGTP, for binding and DNA chain elongation near the active site of HIV-1 RT. As most NRTIs lack a 3′-hydroxyl terminus, incorporation of the analogue into the growing DNA strand results in termination of the DNA strand and the next phosphodiester bond is not formed. Because of these factors, both the concentration of cellular triphosphorylated drug and the levels of cellular dNTP pools play a key role in the efficacy of the NRTIs. Macrophages primarily remain in a resting G1 state and undergo limited DNA synthesis. Cellular dNTP levels are significantly lower in macrophages compared with activated cells. The EC50 for NRTIs ranges from 3 to 300 nM in macrophages for acute infection. By contrast, the EC50 is larger than 25 μM in chronically infected macrophages. The differences indicate that chronic HIV-1 infection alters the cellular milieu in a manner that modulates the ability of NRTI to

successfully become functionally active or subsequently inhibit viral reverse transcription [15, 16].

1.3.3. Non-nucleoside reverse transcriptase inhibitors

Non-nucleoside reverse transcriptase inhibitors (NNRTIs) make antiretroviral efficacy through interaction with binding pockets of HIV-1 RT and inhibiting its enzymatic activity by causing conformational changes at or near the active site. NNRTIs approved by FDA include etravirine, delavirdine, efavirenz and nevirapine. Although the cellular dNTP pool does not directly affect the mechanism of action of NNRTIs, the EC50 differs significantly for NNRTI against acute versus chronic infection in macrophages. The EC50 for inhibition of acute HIV-1 infection in macrophages ranges from 10 to 50 nM depending on the NNRTI; however, NNRTIs are not effective at inhibiting HIV-1 replication in chronically infected macrophages. To date, the mechanism responsible for ineffective inhibition of viral replication in macrophages by NNRTI is incompletely understood. If this mechanism were solely responsible for differential activity of NNRTI in chronically activated macrophages, significant antiviral activity would probably still be observed because establishment of new infection and subsequent p24 production would be terminated. Intracellular accumulation of NNRTI within macrophages might present with a significantly diminished intracellular bioavailability profile relative to lymphocytes, which could present a direct link between differential activities of NNRTI in macrophages versus lymphocytes [17].

1.3.4. Protease inhibitors

The HIV-1 protease is a member of the aspartic acid protease family and is structurally related to host aspartic acid proteases including renin, cathepsin D, gastrin, and pepsin. HIV-1 protease is a homodimer, composed of two noncovalently associated,

structurally identical polyprotein chains. The HIV genome is composed of three major genes including gag, pol and env. Transcription and translation of the gag and pol regions of the virus genome resultin the production of two large precursor polyproteins, p55 (gag) and a ribosomal frameshift product p160 (gag-pol). The enzyme active site contains well-defined subsites in which inhibitor or substrate side chains participate in tight binding interactions. HIV protease-mediated processing of the precursor polyproteins p55 and p160 occurs at different cleavage sites. Phe-Pro, Phe-Leu, and Phe-Thr are some of the scissile bonds, which can be used in the design of protease inhibitors. Protease inhibitors (PIs) have the ability to inhibit HIV-1 replication through competition for binding in the active site with the natural substrate. PIs can effectively inactivate the enzyme since it is not easily cleaved. Protease inhibitors are peptide-like chemicals that competitively inhibit the action of the virus aspatyl protease. They can affect the proteolytic cleavage of the polypeptide precursors into mature enzymes and structural proteins catalyzed by HIV protease. They can prevent proteolytic cleavage of HIV Gag and Pol polyproteins that include essential structural and enzymatic components of the virus, which prevents the conversion of HIV particles into their mature infectious form [18].

The widely used PIs with FDA approval are amprenavir, tipranavir, indinavir, saquinavir, lopinavir, ritonavir, darunavir, atazanavir, and nelfinavir. PIs display potent activity in both acutely and chronically infected macrophages. The EC50 in acutely infected macrophages ranged from 10 to 120 nM, whereas the EC50 in chronically infected macrophages ranged from 400 to 3.3×10^3 nM. Higher rates of viral RNA metabolism in macrophages is considered as a mechanism responsible for higher EC50 in macrophages. Plasma pharmacokinetics *in vivo* demonstrate inhibitory quotient values that are similar to the EC50 of PI *in vitro* for inhibition of chronic HIV-1 infection in macrophages. Macrophages are unique because they can be found in every tissue

compartment and organ systemically. Therefore, it is reasonable to suggest that many macrophages *in vivo* might be exposed to significantly lower levels of drug than those observed at inhibitory quotients in plasma in the circulating periphery [19].

1.3.5. Integrase inhibitors

Integrase inhibitors act to inhibit integration of HIV-1 proviral genome into host cell DNA. HIV-1 integrase presents a highly selective target for anti-HIV therapeutics. Raltegravir is a novel representative integrase inhibitor approved by FDA. Raltegravir targets integrase, an HIV enzyme that integrates the viral genetic material into human chromosomes, a critical step in the pathogenesis of HIV and is metabolized away via glucuronidation, which has exhibited potent and durable antiretroviral activity [20].

1.3.6. Other potential therapeutics

The elimination of virus cannot occur by a single mechanism, thus many new targets, including small interfering RNAs (siRNAs), carbohydrate-binding agents (CBAs), PI3K/Akt pathway inhibitors, and immunotoxins, are explored. The siRNAs could be useful for the induction of potent gene silencing by degradation of cognate RNA. The use of siRNA for HIV-1 infection presents a unique challenge because systemic or directed silencing of CXCR4 co-receptor would result in mortality, and silencing of CCR5 co-receptor could represent a selective pressure for emergence of highly pathogenic CXCR4-using virus. CBAs target the heavily glycosylated HIV-1 envelope, impairing the ability of macrophages or dendritic cells to recognize and perform antigen presentation to CD4+ T-lymphocytes, subsequently impairing transfer infection. The mechanism of CBAs is predominantly extracellular, which makes them efficacious when co-administered with other classes of drugs. The PI3K/Akt pathway is a cell survival pathway that is activated upon apoptotic stress and functions to activate downstream

modulators of cell survival. PI3K/Akt inhibitors were demonstrated to inhibit HIV-1 replication in acutely infected primary macrophages, and their antiviral activity was only observed when drugs were co-administered with a compound that positively modulates nitric oxide-induced cytotoxicity in HIV-1 infection. Immunotoxins might provide a mechanism for targeted elimination of HIV-1-infected cells, and both novel design of immunotoxin-based antiviral agents and their effect on macrophages remains an ongoing area of research. Inhibitors targeting HIV-1 accessory proteins provide a targeted approach for elimination of HIV-1 within infected cells. Vpu provides an attractive target because interference with Vpu acts post-integration to confer abnormal packaging of newly formed virions [21].

Even though combination antiretroviral therapy (cART) provides stable viral suppression, it is still not perfect due to the undesirable side effects, especially for people undergoing long-term treatment. Besides, the traditional therapies find their limitations in multidrug resistance, lack of viral replication-targeted therapy. Traditional therapy is not able to eradicate HIV from infected individuals. During the early stages of HIV infection, HIV establishes reservoirs within cells where HIV lies latent, and tissues, which are inaccessible to optimal levels of antiviral drugs, thus escaping the action of antiretroviral drugs. Therefore, eliminating or preventing viral infection in macrophages is a key element to achieve viral eradication, and new strategies to enhance penetration of antiviral therapeutics in macrophages are urgently needed. Eradication of systemic HIV-1 infection is not possible without clearance of latently infected cells. For these reasons, understanding dynamics of ART pharmacology in macrophages and subsequently eliminating productive infection in these cells, is critical to eliminating systemic HIV-1 infection.

1.4. Novel nanomedicine for antiretroviral therapy

Nanomedicine is one promising approach to target HIV in virus reservoir sites. Due to the introduction of highly active antiretroviral therapy (HAART) as well as the impact of preventive measures, the prevalence and incidence of HIV have declined globally over the last decade except for parts of Eastern Europe and Central Asia where a slight increase has been observed. However, although potent compounds have been developed to suppress virus replication into undetectable levels in the blood of HIV infected patients, it is still a challenge to completely cure patients from HIV/AIDS. Therefore, there is an urgent need to investigate the residual viral source, virologic and physiologic mechanisms that allow viral persistence, in order to develop targeted drug delivery strategies to eliminate residual virus in HIV infected patients.

To realize long-acting therapy, sustained dosage forms have had an extensive history and proven record of contribution to improve patient compliance. Formulation research and investigation has become indispensable in improving patients' life quality. For chronic treatments, converting multiple daily doses to once-a-day dosing with sustained release dosage form has shown light to enhance patient compliance. The application of nanoformulations has been proven to be an important area of pharmaceutical research and development.

Nanoparticles or nanomedicine refer to drug carrier particles and complexes in the range of 10-1000 nm. Nanoformulations include nanocrystals, colloids, nanoparticles, lipid vesicles, liposomes, biopolymers, and protein aggregates. These nanoformulations are intended to improve pharmaceutical properties and drug response by improving drug solubility, stability, biodistribution, pharmacokinetics, safety and efficacy.

Nanotechnology-based drug delivery systems could potentially enhance cellular uptake of antiretroviral drugs into HIV host and infected cells *in vitro* and improve the

pharmacokinetics, pharmacodynamics and biodistribution of ARV agents in various rodent models. It should be noted that most of these reports are in early stage and use only a single agent formulation, which is no longer acceptable clinical practice for HIV therapy. The potential of nanotechonology to modify tissue distribution and extend plasma half-life of HIV drugs was demonstrated. When the antiretroviral drug is encapsulated into a nanosystem, its absorption, metabolism and excretion is not exclusively governed by drug properties; rather, the nanosystem's physical-chemical properties, particularly surface-exposed molecules and electric charge, and size could modify the sustaining time and metabolic and elimination rates. Most current nanomedicine platforms for HIV treatment focus on drug delivery in the blood and on improving pharmacokinetic profiles. To reduce off-target effects and improve on-target drug distribution into tissues and cells that mediate or are linked to a clinical syndrome, an innovative nanoformulation must be stable both *in vitro* and *in vivo* for sufficient duration and exhibit physiochemical properties that allow distribution and localization of drug particles within the sites of interest, while minimizing peripheral toxicities [22, 23].

1.4.1. Polymeric nanoparticles

Polymeric nanoparticles have shown great potentials in HIV therapy since polymers are versatile and can be customized to allow for encapsulation and controlled release of therapeutic agents from the nanoparticles. They can also realize reservoir targeting through decoration with ligands that bind to receptors on the target site. Peptides, proteins and antibodies are most widely used targeting ligands, which have shown to promote binding and uptake of nanoparticles encapsulating the drugs. Biodegradable polymers, like polyethylene glycol-block-polylactide (PEG-PLA), polymethylmethacrylate (PMMA), and methylmethacrylate-sulfopropylmethacrylate (MMA-SPM), have been applied to encapsulate antiretroviral drugs. Polymeric

nanoparticle with small particle sizes were found to improve drug loading efficiency and uptake. Modification of the polymers with ligands that target receptors expressed at the surface of endothelial cells has greatly improved antiretroviral efficacy. This delivery system can also enhance drug encapsulation and subsequent intracellular delivery in macrophages [22, 23].

1.4.2. Micelles

Micelles are self-assembled colloidal systems consisting of amphiphilic molecules that spontaneously aggregate into particles at a concentration beyond the critical micelle concentration (CMC). A typical micelle has hydrophilic heads forming a shell structure, and the inner core structure serves as a reservoir for poorly water-soluble drugs. They have advantages including relatively small sizes (10-100 nm), ease of preparation, and prolonged *in vivo* circulation, which enable them to cross all kinds of physiological barriers. The application of Pluronic® copolymers inhibits efflux trasnporters, like P-glycoprotein (Pgp) and Multidrug Resistance Protein (MRP), consequently facilitate drug delivery of substrates. Pluronic® block copolymers contains one hydrophobic poly(propylene oxide) (PPO) as the core, and two hydrophilic poly(ethylene oxide) (PEO) termini. Using polarized monolayers of bovine endothelial cells, Batrakova et al. examined the influence of Pluronic® block copolymers on the permeability of drugs, including Pgp substrates, organic anion transporter substrates, and compounds with less specificity for efflux transporters. The results indicated a 1.3- to 20-fold enhancement in the permeability of all the compounds evaluated. It is also demonstrated Pluronic® P85 could enhance drug tissue drug permeability and facilitate antiretroviral efficacy in a severe combined immunodeficientcy (SCID) mouse model of viral encephalitis [24-26].

1.4.3. Liposomes

Liposomes are artificially constructed vesicles that consist of an aqueous core separated from the continuous aqueous solvent by one or more spherical, bilayer membranes of surfactant molecules. Liposomes are composed of phospholipids, and may contain small amounts of other molecules that serve as cellular recognition markers and cholesterol that regulates membrane fluidity and stability. As drug delivery systems, liposomes have the capability of encapsulating both hydrophobic as well as hydrophilic payloads. Liposomes have several other benefits, such as solubilization improvement, protection of cargoes from enzymatic degradation and enhancement of intracellular uptake. Liposomes have been used to deliver antiretroviral agents to cross tissue barriers through receptor-mediated transcytosis. Besides, cell-penetrating peptides (CPP) and antibody conjugation are alternative approaches for liposomes to penetrate HIV reservoir. Mononuclear phagocytic system is another liposomal delivery mechanism, which can significantly increase the drug half-life in the central nervous system (CNS). Surface-engineered liposomes have been developed to target the lymphoid virus reservoir by incorporating surface charge or site-specific targeting ligands. Liposomes with negative surface charge have shown higher accumulation in lymph nodes and spleen compared to particles with positive charge [27].

1.4.4. Nanosuspensions

Nanoformulated antiretroviral therapeutics (nanoART) was developed in our laboratory in the past decade. NanoART are polymer excipient coated drug nanosuspensions, which demonstrate high drug loading capacity, controllable size and charge, and tunable surface conjugation. Antiretroviral drugs could be formulated through high-pressure homogenization and wet milling for long-acting antiretroviral therapy. Mononuclear phagocyte targeted nanoART for delivery to HIV reservoirs was

developed with high drug loading, improved cell uptake and sustained drug retention. Drugs can be delivered into the target sites at levels above the effective therapeutic concentrations through mononuclear phagocytes. To improve pharmacokinetics and pharmacodynamics (PK/PD) of antiretroviral therapy, we further developed nanoART targeted to HIV reservoirs. Previous studies have shown that folate receptor (FOLR) is overexpressed on activated macrophages. Based on these findings, folate-decorated drug delivery systems have been developed to target macrophages for the treatment of inflammatory diseases with improved therapeutic efficacy. Folic acid was conjugated onto the coating excipient poloxamer 407 (P407) to generate folate-decorated nanoART for macrophage targeting. *In vitro* studies using a human MDM system, FA-nanoART showed a 2-fold increase in drug uptake, longer drug retention, and superior antiretroviral efficacy over non-targeted nanoART. *In vivo* PK/PD studies showed that FA-nanoART increased the plasma levels of ATV approximately 5-fold over that observed with non-targeted nanoART [28, 29].

1.4.5. Solid lipid nanoparticles

Solid lipid nanoparticles (SLNs) usually comprise biocompatible lipids, that are solid at room temperature or surfactants for emulsification. They are typically solid particles consisting of one or more biocompatible solid lipids, which are stabilized by emulsifiers. The particle size ranges from approximately 50 to 1000 nm. They possess advantages like long retention, superior biocompatibility and biodegradability, excellent stability and loading capability as well as ease of introduction of targeting ligands. SLNs for CNS delivery of ART were developed, and the permeability of stavudine, delavirdine, and saquinavir encapsulated in different nanocarriers, including polymer nanoparticles and SLN, were tested across an artificial BBB. There was increased permeability of SLN encapsulated drugs compared to free drugs. In addition, delavirdine and saquinavir

loaded SLN showed better permeability than those loaded into polymer nanoparticles [30].

1.4.6. Dendrimers

Dendrimers are a highly branched complex multiple repeating structures of a monomer. They are comprised of hydrophobic cores and highly branched surface functional groups that make them ideal for transport of drugs across biological barriers. The end groups of these molecules can be functionalized to generate dendrimers that can be used as drug carriers and targeting moieties can be attached that influence biodistribution and toxicity of the dendrimers. Poly(amido amide) (PAMAM), the most commonly used dendrimer has been shown to incorporate several anticancer drugs. However, no dendrimer-based delivery systems have been approved for anti-HIV treatment due to their high cellular toxicity [31].

1.4.7 Nanomedicine in antiretroviral therapy

Significant progress has been made to treat HIV/AIDS to improve the life quality of HIV infected people in the last decades. The utilization of nanomedicine in ART has successfully shifted rapidly progressive HIV infection to a disease with little detectable viral load in patients. It is still a big challenge so far to eradicate HIV due to the occurrence of drug resistance and viral reservoirs. Nanotechnology-based drug delivery systems can improve antiretroviral therapy by more precisely controlling drug concentrations in target cells and tissues, thus enhance uptake of antiretroviral agents into HIV-infected cell and tissue reservoirs and improve the pharmacokinetics, pharmacodynamics and biodistribution of antiretroviral agents using targeting ligands and improving drug delivery across tissue barriers. The goal of HIV eradication can be achieved through developing different nanomedicine platforms and decorating

nanomedicines with specific ligands to interact with receptors expressed on HIV infected cells.

Nanomedicine has provided new tools and rationales in the development for novel strategies for HIV/AIDS treatment. The rational design has provided new candidates against HIV with improved solubility, stability and pharmacokinetic and adherence properties. Most current nanomedicine platforms focus on drug delivery in the blood and on improving pharmacokinetic profiles. Nanosustained drug release formulations could maintain plasma drug concentrations for weeks and even months. Although there are benefits and advantages of applying the systems approach to novel nanoformulations, there are still challenges that need to be overcome in the future to translate academic research into the clinical setting. These include the biocompatibility of excipients, safety, stability and the scale-up procedure for large-scale preparations. Nanomedicine platforms should be explored to develop combination therapies for safe and effective long-acting HIV therapy to improve patient compliance and life quality.

1.5. Hypothesis and goals

This study focuses on developing long-acting antiretroviral prodrug with enhanced hydrophobicity and stability. A hydrophobic lamivudine (3TC) prodrug is successfully synthesized and incorporated into targeted and non-targeted nanocrystalline formulations to improve drug half-life, enhance macrophage uptake, and sustain antiretroviral efficacy. Folic acid targeted parenteral nanoformulations are prepared for improved pharmacokinetics and improved antiretroviral therapy. This long-acting antiretroviral drug delivery system can serve both as drug transporters and as facilitators of viral clearance. Macrophage loading capacities and intracellular compartments of nanoparticle depots are studied. Macrophage endosomal compartments can be

harnessed for particle storage, release and drug trafficking. NanoART is expected to provide increased drug uptake, retention in macrophages, which facilitates its long acting antiretroviral efficacy. Macrophage can act as drug transporters for improved clinical stability and bioavailability. Regulation of phagolysosomal endocytic pathway is also studied. The co-localization of nanoformulated atazanavir (ATV) at endosomal sites of viral assembly is expected to affect regulatory proteins and pathways that contribute to viral clearance. The cell targeted small magnetite ART (SMART) particles is developed to facilitate drug adherence and improve disease outcomes. Rapid noninvasive determination of drug biodistribution in virus-target tissues and reservoirs for nanoART can realize noninvasive assessments of antiretroviral drug tissue distribution through magnetic resonance imaging (MRI) techniques.

Chapter II.

Long-acting lamvudine prodrug design and formulation development

2.1. Abstract

The next generation of antiretroviral medicines will be characterized by infrequent parenteral administration, maintenance of continuous drug concentrations and viral reservoir-targeted drugs. This will enable reductions in toxicities, viral loads and resistance patterns while improving drug regimen adherence. Perhaps most importantly such advances would facilitate viral clearance in infectious reservoirs that include gut-associated lymphoid tissue, lymphoid nodes, the genitourinary system and the central nervous system. While such progress has been now realized for hydrophobic integrase and select nonnucleoside reverse transcriptase inhibitors, very limited success has been achieved with the more hydrophilic short-acting nucleosides. To overcome such limitations, we developed a two-step synthesis to create a long-acting lamivudine (2',3'-dideoxy-3'-thiacytidine, 3TC). A stable hydrophobic pro-drug crystal formulation was produced by poloxamer drug encasement. Conversion of the formerly hydrophilic 3TC significantly extended its bioavailability facilitated by chemical drug conjugation to a fatty acid and creating a myristoylated drug. A folate targeted poloxamer 407 coated a newly formed nanocrystalline pro-drug markedly improving cell uptake, bioavailability and pharmacokinetic profiles. Reduced cytotoxicity and robust antiretroviral activities were also observed. These findings bring the idea of long-acting antiretroviral medicines closer to the mainstay of clinical availability.

2.2. Introduction

The introduction of nanomedicine in antiretroviral therapeutic regimens has impacted the treatment of HIV infection. Long-acting nanoformulated antiretroviral therapy (nanoART) has the real potential to improve patient adherence, decrease systemic toxicities, and sustain viral suppression [32-37]. However, the remaining

challenge to bring nanoART to the forefront of antiretroviral therapy is to nanoformulate a broad range of hydrophilic drugs. While hydrophilic drugs are widely used in the clinic, their drawbacks include the need for frequent administration by rapid clearance, low intracellular absorption and suboptimal biodistribution. Cellular and tissue toxicities also reduce their clinical effectiveness. Ideal drug delivery systems and encapsulation strategies specifically for hydrophilic antiretroviral nucleoside reverse transcriptase inhibitors (NRTIs) are still under investigation.

NRTIs are the backbone of combination antiretroviral therapy in the treatment of HIV infection [38-40]. Lamivudine (3TC) by competing with an endogenous nucleotide transcriptase enzyme leads to viral DNA chain termination that follows incorporation of the active 3TC phosphorylated anabolite in place of endogenous cytidine triphosphate during reverse transcription. 3TC has potent antiviral effects on HIV-1, HIV-2, and hepatitis B virus [41-44]. However, the drug is < 36% protein bound and with a half-life of 5-7 hours and rapid renal elimination by tubular secretion is catalogued as a short-acting drug. These characteristics minimize its utility as a once daily fixed dose medicine.

Myristoyltransferase (NMT) effects myristoylation of proteins during the HIV life cycle [45-47]. Fatty acid analogues of myristic acid can inhibit NMT and can be used to convert a hydrophilic 3TC into a hydrophobic drug [48-50]. Myristolic 3TC (MTC) was encased into a nanoparticle with poloxamer 407 with well-distributed size and stable physical properties. Folic acid, the ligand for the folate receptor expressed on macrophages, attached to drug nanoparticles can facilitate drug uptake [51, 52]. Moreover, for nanoART macrophage uptake, the targeting ligand folic acid can facilitate drug uptake and retention in monocyte-macrophages [53]. We developed targeted MTC nanoformulations using folate as a targeting ligand, enabling it to affect cellular uptake, antiretroviral efficacy, and antiretroviral pharmacokinetic behavior. The

idea of formulating 3TC prodrug to improve therapeutic outcomes for patients receiving long-term antiretroviral treatment is novel and of significant potential utility.

2.3. Materials and methods

2.3.1. Reagents and antibodies.

3TC was acquired from GlaxoSmithKline Inc. (Research Triangle Park, NC, USA). Poloxamer 407 (P407) and CF488-succinimidyl ester (CF488) were obtained from Sigma-Aldrich (St. Louis, MO, USA). Sephadex LH-20 was obtained from GE Healthcare (Piscataway, NJ, USA). Pooled human serum was obtained from Innovative Biologics (Herndon, VA, USA). Macrophage colony-stimulating factor (M-CSF) was prepared from 5/9m alpha3-18 cells (ATCC; CRL-10154) cultured in ATCC complete growth medium as described previously [54]. Rabbit anti-human antibodies to Rab5, Rab7, Rab11, and Rab14 and Alexa Fluor 568 goat anti-rabbit IgG were purchased from Santa Cruz Biotechnology (Dallas, TX, USA). TRIzol reagent was obtained from Invitrogen (Grand Island, NY, USA).

2.3.2. Synthesis of hydrophobic 3TC derivative.

The hydrophobic 3TC derivative (MTC) was synthesized according to the scheme shown in Figure 2.1A. Briefly, 3TC (4 mmol) was dissolved in dimethylformamide (DMF, 6 mL) in an ice bath, imidazole (6 mmol) and tert-butyldimethylsilyl chloride (4.8 mmol) were added separately and the reaction mixture was stirred at room temperature (25 °C) overnight. After the completion of reaction, the reaction mixture was concentrated at reduced pressure and purified with silica gel column chromatography using dichloromethane and methanol (2-10%) as eluents. The yield compound was dissolved in dry pyridine (6 mL). A solution of 4,4'-dimethoxytrityl

chloride (DMTr-Cl, 8 mmol) was added to the reaction mixture dropwise at 0 °C. The temperature was raised to room temperature, and stirring was continued overnight. The reaction mixture was neutralized with saturated sodium bicarbonate solution (200 mL) and extracted with dichloromethane (200 mL) for three times. The organic layer was separated and concentrated *in vacuo*. The residue was purified with silica gel column chromatography using dichloromethane and methanol (2-10%) as eluents. The yield compound was dissolved in tetrahydrofuran (THF, 6 mL) and tetrabutylammonium fluoride (6.2 mL, 1.5 molar ratio) was added dropwise and stirred for 4 h. The reaction mixture was concentrated at reduced pressure, and the residue was purified with silica gel column chromatography using dichloromethane and methanol (2-10%) as eluents. The yield compound was dissolved in DMF (10 mL). Then myristic acid acid (945 mg, 2 molar ratio), 1-[Bis(dimethylamino)methylene]-1H-1,2,3-triazolo[4,5-b]pyridinium 3-oxid hexafluorophosphate (HATU, 1.72 g, 2.2 molar ratio) and N,N-diisopropylethylamine (DIEA, 1.5 mL, 3.4 molar ratio) were added to the mixture separately. The reaction mixture was concentrated at reduced pressure, and the residue was purified with silica gel column chromatography using dichloromethane with 2% methanol as eluents. Acetic acid (10 mL) was added to the yield compound and the reaction mixture was heated at 80 °C for 30 min. The reaction mixture was concentrated at reduced pressure, and the residue was purified with silica gel column chromatography using dichloromethane with 2% methanol as eluents. The chemical structure of final product was characterized by nuclear magnetic resonance spectrometry (^{1}H NMR) determined on a Varian Unity/Inova-500 NB (500 MHz; Varian Medical Systems Inc., Palo Alto, CA, USA). Chemical shifts are reported in parts per million (ppm). The structure of the final compound was analyzed by FTIR spectroscopy using a Spectrum Two FT-IR spectrometer,(PerkinElmer, Waltham, MA, USA) .

2.3.3. NanoMTC manufacture and characterization.

MTC nanoparticles were formulated by high-pressure homogenization (Avestin EmulsiFlex-C3; Avestin Inc., Ottawa, ON, Canada), using P407 and FA-P407 to encase the drug crystals. For the non-targeted MTC formulation (called NMTC), the suspension contained modified 3TC (1% [wt/vol]) and P407 (0.5% [wt/vol]) and for the targeted MTC formulation (called FA-NMTC), the suspension contained modified 3TC (1% [wt/vol]), P407 (0.3% [wt/vol]) and FA-P407 (0.2% [wt/vol]). The suspension was premixed overnight in 10mM HEPES buffer at room temperature and then homogenized at 20,000 PSI for about 360 passes until the desired particle size of about 350 nm was achieved. The size, zeta potential, and polydispersity (PDI) were determined by dynamic light scattering (DLS), using a Malvern Zetasizer Nano Series Nano-ZS (Malvern Instruments, Westborough, MA, USA). A minimum of 3 iterations were taken, which varied by < 2%. After reaching the desired size (around 300 nm), the sample was purified by centrifugation at 100 × g for 5 min to remove aggregated particles and then at 20,000 × g for 30 min to collect a purified particle pellet. The resulting particles were resuspended in 10 mM HEPES for further studies [55, 56].

2.3.4. Preparation of dye-labeled nanoMTC.

For preparation of CF488-labeled nanoMTC, CF488-P407 and P407 were dissolved in methanol at a weight ratio of 1:4. The solvent was evaporated, and the mixture was resuspended with 10 mM HEPES to yield a 0.5% surfactant solution. Modified 3TC was added at a 1% weight ratio. The suspension was premixed overnight in a light-protected environment at room temperature. The suspension was homogenized by high-pressure homogenization and purified by centrifugation as described above.

2.3.5. Human monocyte isolation and cultivation.

Human monocytes were obtained by leukapheresis from HIV-1-, HIV-2-, and hepatitis B-seronegative donors and then purified by countercurrent centrifugal elutriation. Cells were obtained following informed consent using a protocol approved by the University of Nebraska Medical Center Institutional Review Board. The recovered monocytes, >98% pure by Wright-stained cytosmears, were cultured in Dulbecco's modified Eagle's medium (DMEM) with 10% heat-inactivated pooled human serum, 1% glutamine, 50 μg/mL gentamicin, 10 μg/mL ciprofloxacin, and 1,000 U/mL recombinant human macrophage colony stimulating factor for 7 days, facilitating cell differentiation into macrophages (MDM) [57].

2.3.6. Nanoformulated MTC particle stability.

Formulated NMTC and FA-NMTC particles were dispersed in phosphate buffered saline (PBS) and placed into a 10 kDa dialysis tube in 2 L of PBS under stirring at 37°C. At 30 min and 1, 2, 3, 4, 6, 8 and 10 days, 100 μL of the suspension was collected. The supernatant was dissolved in 900 μL methanol [58]. The amount of MTC was measured by high-performance liquid chromatography (HPLC). HPLC analysis was as previously described [59]. Triplicate 20-μL samples were assessed by HPLC using a Synergi 4 μm Hydro-RP 80A C18 column (Phenomenex Inc., Torrance, CA). The mobile phase, consisting of 80% acetonitrile-20% 5 mM Na_2HPO_4, pH 9.0, was pumped at 1.0 mL/min with UV-visible (Vis) detection at 272 nm. MTC concentration was determined by peak area comparison to those of a standard curve generated with free MTC (0.049 to 50 μg/mL) [60].

2.3.7. Cytotoxicity studies.

Cytotoxicity of native drug, modified drugs and the different nanoformulations was evaluated by Cell Counting Kit-8 (CCK-8, Dojindo Molecular Technologies Inc, Rockville, MD, USA) [61]. Briefly, human monocytes were cultivated in a 96-well-plate at the density of 100,000 cells per well. After 7 days of differentiation, MDM were treated with native 3TC, MTC, NMTC, or FA-NMTC at a series of concentrations: 0.10, 0.33, 1.0, 3.3, 10.0, 33.3, and 100 mM. Four hours after treatment, 10 µL of CCK-8 was added to each well. The plate was incubated in a 5% CO_2 incubator for 2 h after which the absorbance was measured at 450 nm using a microplate reader. The cell survival rate was calculated based on the equation below:

$$Survival\ rate\ (\%) = \frac{Asample - Ab}{Ac - Ab} \times 100$$

$$Asample: sample\ absorbance, Ab: blank, Ac: negative\ control$$

2.3.8. Nanoformulated MTC particle cell uptake.

Human monocytes were cultivated in a 12-well-plate at the density of 1.5 million cells per well. After 7 days of differentiation, MDM were treated with 100 µM nanoformulated MTC. Uptake of nanoMTC was assessed without medium changes for 8 h. Adherent MDMs were collected by scraping into PBS, at 1, 2, 4 and 8 h after treatment. Cells were pelleted by centrifugation at 1000 × g for 8 min at 4°C. Cell pellets were briefly sonicated in 200 µL of methanol and centrifuged at 20,000 × g for 10 min at 4°C. The MTC content in the cells was determined by HPLC.

2.3.9. Antiretroviral activities.

Antiretroviral efficacy was determined by HIV-1 reverse transcriptase (RT) activity [62, 63]. Briefly, MDM were treated with 100 μM native 3TC, MTC or nanoformulated MTC for 4 h. Following treatment, cells were washed with PBS for three times and cultivated with fresh medium. At 0, 5, 10 and 15 days after treatment, cells were challenged with HIV-1_{ADA} at a multiplicity of infection (MOI) of 0.1 infectious particles per cell. Following viral infection, the cells were cultured for another 7 days with half-medium exchanges every other day. Medium samples were collected on days 7 for measurement of progeny virion production, as determined by RT activity. For assessment of RT activity, 10 μL medium samples were mixed with 10 μL of a solution containing 100 mM Tris-HCl (pH 7.9), 300 mM KCl, 100 mM dithiothreitol, 0.1% NP-40, and water in a 96-well plate. The reaction mixture was incubated at 37°C for 15 min, and 25 μL of a solution containing 50 mM Tris-HCl (pH 7.9), 150 mM KCl, 5 mM dithiothreitol, 15 mM $MgCl_2$, 0.05% NP-40, 10 μL/mL poly(A), 0.25 U/mL oligo, and 10 μCi/mL [^{3}H]dTTP was added to each well; the plates were incubated at 37°C for 18 h. Following incubation, 50 μL of cold 10% trichloroacetic acid was added to each well, the wells were harvested onto glass fiber filters, and the filters were assessed for [^{3}H]dTTP incorporation by beta-scintillation spectroscopy using a TopCount NXT (PerkinElmer Inc., Waltham, MA, USA).

2.3.10. Immunocytochemistry and confocal microscopy.

For immunofluorescence staining, cells were washed three times with PBS and fixed with 4% paraformaldehyde (PFA) at room temperature for 30 min. The cells were treated with blocking/permeabilizing solution (0.1% Triton, 5% BSA in PBS) and quenched with 50 mM NH_4Cl for 15 min. The cells were washed once with 0.1% Triton in PBS and sequentially incubated with primary and secondary antibodies at room

temperature. Slides were covered in ProLong Gold AntiFade reagent with DAPI (4',6-diamidino-2-phenylindole) and imaged using a 63× oil lens on an LSM 510 confocal microscope (Carl Zeiss Microimaging, Inc., Dublin, CA, USA) [28]. The immunofluorescence was quantitated, and the percent overlap was determined using ImageJ software, the JACoP plug-in for percent overlap, and Zeiss LSM 510 Image browser AIM software version 4.2 for determining the number of pixels and the mean intensity of each channel, as previously described [55]. The results are represented as means ± standard errors of the mean.

2.3.11. HIV-1 p24 staining.

Cells in different treatment groups were fixed with 4% phosphate-buffered PFA for 15 min at room temperature. The fixed cells were blocked with 10% BSA in PBS containing1%Triton X-100 for 30 min at room temperature and incubated with mouse monoclonal antibodies to HIV-1 p24 (1:100; Dako, Carpinteria, CA, USA) for 3 h at room temperature. Binding of HIV-1 p24 antibody was detected using a Dako EnVision+ System, HRP-labeled polymer anti-mouse secondary antibody, and diaminobenzidine staining. Cell nuclei were counterstained with hematoxylin for 60 s. Images were taken using a Nikon TE300 microscope with a 40× objective [55, 64].

2.3.12. Pharmacokinetic studies.

All animal studies were conducted humanely according to a protocol for animal experiments approved by the University of Nebraska Medical Center Institutional Animal Care and Use Committee. Male Balb/cJ mice (Jackson Labs, Bar Harbor, ME, USA) were maintained on a folate-deficient diet (Harlan Teklad TD.00434; Harlan Laboratories, Inc., Indianapolis, IN, USA) beginning 2 weeks prior to drug administration. Mice were injected with native 3TC, MTC, NMTC, FA-NMTC (50 mg/kg

based upon 3TC) or PBS intramuscularly (IM). Plasma was collected at 8 h, 1, 3, 5, 7, 10 and 14 days after drug administration. Tissues (liver, kidney, brain, spleen, gut, lymph node and muscle) were collected after sacrifice on day 14. 3TC and MTC from plasma and tissues were extracted using acetonitrile and assayed by UPLC-MS/MS. In preparation for drug analysis, 3TC and MTC were extracted from plasma (20 µL) using 1 mL of acetonitrile. Internal standard was added to each sample (10 µL) and consisted of 1.33 µg/mL deuterated-3 isotope of lamivudine (3TC), 0.665 µg/mL deuterated-4 isotope of ABC, and 0.5 µg/mL lopinavir. Samples were dried using a ThermoScientific Savant Speed Vacuum (ThermoScientific, Waltham, MA, USA), and reconstituted in 80% v/v methanol in Optima grade water. Standards were prepared with initial 3TC concentrations (ng/ml) of: 13,300; 5,320; 2,660; 1,330; 532; 266, 133; 53.2; 26.6, 13.3; 5.32; 2.66; and 1.33 for final 3TC concentrations (ng/mL) of: 500, 200, 100, 50, 20, 10, 5, 2, 1, 0.5, 0.2, 0.1 and 0.05. MTC standards had initial concentrations of (ng/mL): 5000, 2000, 1000, 500, 200, 100, 50, 20, 10, 5, 2, 1, and 0.5 and the same final concentrations as the 3TC standards. Plasma standards were prepared by extracting 20 µL of blank plasma from control Balb/cJ mice (BioreclamationIVT, Hicksville, NY, USA) into 1 mL of acetonitrile. The same internal standard was added to each standard.

For tissue preparation, 50-100 mg of liver, spleen and lymph node were homogenized in 4 volumes of an esterase inhibitor mixture (12.5 mg/mL sodium fluoride and 3.75 mg/mL EDTA solution in Optima grade water) and 2.5 µL of a protease inhibitor (10 mM PMSF in HPLC grade isopropanol). Tissue homogenate (100 µL) was mixed with 10 µL of internal standard (5 µg/mL deuterated-3 isotope of lamivudine (3TC), 2.5 µg/mL deuterated-4 isotope of ABC, and 2 µg/mL lopinavir) and extracted in 300 µL methanol. Supernatant was used directly for MTC analysis or mixed with water for 3TC analysis. Standards were prepared with initial 3TC

concentrations (ng/mL) of: 50,000; 20,000; 10,000; 5,000; 2,000; 1,000; 500; 200; 100; 50; 20; 10; and 5 for final 3TC concentrations (ng/mL) of: 500, 200, 100, 50, 20, 10, 5, 2, 1, 0.5, 0.2, 0.1 and 0.05. MTC standards had initial concentrations of (ng/mL): 20,000, 8,000, 4,000, 2,000, 800, 400, 200, 80, 40, 20, 8, 4, and 2 and the same final concentrations as the 3TC standards. Tissue standards were prepared by homogenizing 50-100 mg of blank liver, spleen or lymph node from control Balb/cJ mice in 4 volumes of the same esterase and protease inhibitor mixtures as the samples. The same internal standard was added to each standard then extracted in 300 µL of methanol. Drug quantitation was completed using a Waters ACQUITY H-class UPLC system (Waters, Milford, MA, USA) connected to a Waters Xevo TQS-micro mass spectrometer with an electrospray ionization (ESI) source.

Chromatographic separation of 10 µL 3TC sample injections was achieved using an ACQUITY UPLC CSH C18 column (1.7 µm, 2.1 mm x 100 mm) using a 13 min gradient of mobile phase A (7.5 mM ammonium bicarbonate in Optima grade water and adjusted to pH 7 using glacial acetic acid) and mobile phase B (100% Optima grade methanol) at a flow rate of 0.25 mL/min. Initial mobile phase conditions of 90% A were held for 2.5 min, decreased to 5% A over 6.5 min, held at 5% A for 1.3 min, then increased to 90% A over 0.45 min and held for 2.25 min. MTC chromatographic separation was achieved using the same CSH column and mobile phases, but with a 16 min isocratic method using 19% mobile phase A and flow rate of 0.3 mL/min. Drug was detected in the ESI positive mode with a cone voltage of 4 V and a collision energy of 10 V. Multiple reaction monitoring (MRM) transitions used for 3TC and MTC were 230.23 > 111.97 and 440.10 > 111.97 respectively. The deuterium-4 isotope of 3TC was used as the internal standard for 3TC quantitation and had an MRM transition of 233.23 > 114.97. Lopinavir was used as the internal standard for MTC quantitation and had an MRM transition of 629.18 > 447.20. Spectra were analyzed

and quantified by MassLynx software version 4.1. All calculations were made using analyte peak area to internal standard peak area ratios.

2.13. Statistics.

All the data were analyzed by one-way analysis of variance (ANOVA) and Tukey's multiple-comparison test using GraphPad Prism software (GraphPad Software, Inc., La Jolla, CA). All the cellular based experiments were replicated three times and the animal experiment was replicated twice. The sample size was determined according to published guidelines with a minimum of 5 animals per group (n=5). No outliers from animal or cell experiments were excluded. Differences were considered significant at a P value of <0.05.

2.4. Results

2.4.1. Characterization of chemically modified 3TC.

A hydrophobic 3TC derivative (MTC) was synthesized successfully, as illustrated by the ^{1}H NMR and FT-IR spectrum in Figure 2.1B and 1C. In the ^{1}H NMR spectrum, chemical shifts of 0.9 and 1.3 ppm represented the 1° ($RC\mathbf{H}_3$) and 2° ($R_2C\mathbf{H}_2$) aliphatic protons derived from the fatty acid chain. The protons connected to the ester ($-\mathbf{H}_2C$-COOR) contributed to the peak at 2.4 ppm. In the FT-IR spectrum, the wavenumbers of 2917 and 2850 cm^{-1} were attributed to the C-H stretch, which belonged to the alkyl derivative derived from the fatty acid chain conjugated to the native 3TC; the wavenumber of 1692 cm^{-1} was attributed to the C=O stretch from the ester bond. The solubility of the hydrophobic MTC was determined to be 100 µg/mL in water, compared to 70 mg/mL water solubility of native 3TC.

2.4.2. Characterization of nanoformulated MTC.

The nanoformulations were manufactured by high-pressure homogenization. Particle size, charge and PdI for all formulations were determined by dynamic light scattering (DLS). The schematic diagram of the targeted MTC particles was illustrated in Figure 2.1D and the characteristics of different formulations are summarized in Figure 2.2A. For FA-NMTC nanoparticles, a 40% FA-P407/60% P407 polymer solution was used to formulate the MTC. Both NMTC and FA-NMTC showed equivalent physicochemical characteristics. For NMTC nanoparticles, the particle size was 375 ± 21 nm with a PdI of 0.21; while the FA-NMTC showed a slightly larger particle size of 433 ± 23 nm with a PdI of 0.25. The zeta-potential for FA-NMTC decreased to -19.7 ± 1.3 mV compared with -21.0 ± 0.8 mV for NMTC. The changes in size and zeta-potential can be attributed to the FA conjugated to the P407 polymer. High drug loading (75.0% for NMTC, 76.9% for FA-NMTC) and encapsulation efficiency (96.3% for NMTC, 98.4% for FA-NMTC) were found for both formulations.

2.4.3. Nanoformulated MTC particle stability.

The stability of NMTC and FA-NMTC nanoformulations is illustrated in Figure 2.2B. There was no significant burst release in the first 8 h and sustained MTC concentrations were seen over 12 days. The cumulative MTC release reached 70.0% on day 3 and 94.8% on day 12 for NMTC, and 76.4% on day 3 and 96.7% on day 12 for FA-NMTC.

2.4.4. Cytotoxicity of nanoformulated MTC.

Cytotoxicity of native 3TC, MTC and both nanoformulations was evaluated by Cell Counting Kit-8. MDM were treated with native 3TC, MTC, NMTC, or FA-NMTC at different concentrations for 4 h and cytotoxicity is shown in Figure 2.2C. Native 3TC

showed strong cytotoxicity when the drug concentration increased to above 1 mM and the cell survival rate decreased to 9.6% at 3.3 mM. Compared with native 3TC, MTC shower much lower cytotoxicity. The cell survival rate was 95.9% at 3.3 mM and slightly decreased with the increment of drug concentration. The cytotoxicity for both nanoformulations was between native 3TC and MTC and no significant difference was observed between these two formulations.

2.4.5. Macrophage uptake.

MDM uptake of nanoformulated MTC was assessed and MTC levels were quantified by HPLC. Cells were exposed to nanoMTC for 8 h at 100 μM (42.7 g/mL) for both NMTC and FA-NMTC treatment. As shown in Figure 2.2D, the uptake of nanoMTC was increased over the first 2 h, and maximum uptake was observed at 2 h for both nanoformulations. At 2 h, the uptake of FA-NMTC was 24.88 μg/10^6 cells, which was more than 2 times higher than that of NMTC (10.45 μg/10^6 cells). After 2 h, cell drug levels began to decrease, and drug levels of MTC for NMTC and FA-NMTC at 8 h were 2.06 and 2.85 μg/10^6 cells, respectively.

2.4.6. Antiretroviral activities of nanoformulated MTC.

To assess the antiretroviral activity of nanoMTC treatment HIV-1 RT activity was determined in HIV-1-infected MDM treated with native 3TC, NMTC or FA-NMTC. Cells were treated with 100 μM of native 3TC or nanoformulated MTC for 4 hours. At this time the medium was removed, cells were washed 3 times with PBS and fresh medium without drug was added prior to HIV-1_{ADA} challenge at days 0, 5 and 10 after treatment. Infected cells were cultured for an additional 7 days and RT activity in the culture medium was determined. Significant differences were found between cells treated with native 3TC or nanoformulated MTC. For native 3TC treated cells, RT

activity was suppressed only in the day 0 infection group. After day 5, the RT activity for the 3TC treated group increased dramatically over time, and no viral suppression was observed at day 15. In contrast, for nanoformulation treated groups, sustained antiretroviral activities were observed. The RT activities were suppressed to a relatively low level (< 25%) during the first 10 days. At day 15, the RT levels for NMTC and FA-NMTC were 59.8% and 68.5%, respectively, compared with 110.0% for the native 3TC group. Significant differences were observed between NMTC and FA-NMTC during the first 10 days ($p<0.05$) and FA-NMTC showed greater antiretroviral activity compared with NMTC, however, the difference was not significant at day 15 (Figure 2.3A). These results were confirmed by HIV-1 p24 staining (Figure 2.3B). NMTC and FA-NMTC showed greater antiretroviral efficacy compared with native 3TC, and much less p24 staining was observed in these two groups. FA-NMTC shower greater suppression of viral replication especially in the first 10 days, little to no p24 antigen was detected in MDM treated with FA-NMTC.

2.4.7. Immunocytochemistry and confocal microscopy.

To assess subcellular behavior of the nanoformulated MTC particles, fluorescently-labeled nanoparticles were used to visualize if co-localization of endolysosomal proteins and nanoMTC occured. CF488-labeled nanoMTC was prepared and Rab 5, 7, 11, 14 and LAMP 1 were selected as targeted proteins. Immunostaining was performed 4 h after particle incubation for visualization of endocytic compartments and nanoMTC co-localization. As observed nanoMTC distributed in a punctate pattern throughout the cytoplasm and perinuclear cell regions (Figure 2.4). NanoMTC was found predominantly in late (Rab 7) and recycling (Rab 11 and 14) endosomes [51], and this immunofluorescence co-localization demonstrated that nanoMTC was taken and stored in macrophages through the endolysosomal pathways. Our previous

studies have demonstrated that the HIV reservoir exists mainly in late and recycling endosomes, and HIV-1 and nanoformulations deregulated cellular proteins in an opposing manner [56], supporting the idea of subcellular-targeted nanoparticles for long acting antiretroviral therapy.

2.4.8. Pharmacokinetics.

Balb/cJ mice were administered nanoformulated MTC at 50 mg/kg based on 3TC concentration to determine the pharmacokinetic parameters for both NMTC and FA-NMTC as the scheme shown in Figure 2.5A. Plasma drug concentrations following formulation treatment were analyzed by UPLC-MS/MS and data are presented in Figure 2.5B and C. At each time point, very little MTC was detected, which indicated the complete conversion of MTC to 3TC. Higher and more sustained drug levels were observed for MTC nanoformulation treated groups and plasma drug levels were maintained over 10 days for both nanoformulations. At day 1, no drug could be detected in plasma from the native 3TC treated group; the drug levels for MTC, NMTC and FA-NMTC groups were 58.65 ± 6.94, 349.25 ± 12.51, and 383.24 ± 13.77 ng/mL, respectively. At day 3, little drug was detected in plasma from the MTC treated group, whereas plasma drug levels for NMTC and FA-NMTC groups were 131.30 ± 18.09 and 151.63 ± 23.16 ng/mL, respectively. Compared with NMTC, FA targeted nanoformulation showed prolonged drug release and plasma drug levels were more than 2 fold higher than these of NMTC from day 5 to day 14. At day 14, the plasma drug level for FA-NMTC was 22.66 ± 12.53 ng/mL and that for NMTC was at the limit of quantitation (< 0.5 ng/mL). Tissue drug levels are shown in Figure 2.5D; no 3TC was detected in tissues for mice treated with native 3TC or MTC after 14 days. Drug levels for the FA-NMTC treated group were greater than 2-fold higher than these for the NMTC group in liver, spleen and lymph nodes.

2.5. Discussion

Reverse-transcriptase inhibitors are a class of antiretroviral drugs used to treat HIV/AIDS and hepatitis B. RTIs inhibit activity of reverse transcriptase, a viral DNA polymerase that is required for replication of HIV and other retroviruses. Lamivudine (3TC) is a typical nucleoside analog reverse-transcriptase inhibitor (NRTI). Its favorable safety profile, low potential for drug interaction, good tolerability, and high resistance barrier makes it one of the preferred choices for HIV/AIDS therapy in multiple clinical scenarios. However, the low protein bound, short half-life and fast clearance of 3TC limit its clinical application. In this paper, we describe development of a nanoformulated 3TC prodrug in order to improve its clinical potential.

Myristic acid was used to synthesize the hydrophobic MTC. This 14-carbon alkyl chain could significantly decrease the water solubility of native 3TC and improve the drug-protein, drug-membrane interactions during systemic circulation. In the presence of NMT, HIV-1 viral proteins are covalently attached to myristic acid, which exposes them to the antiretroviral drug sufficiently. It has been reported that NMT is a crucial enzyme involved in catalyzing the myristoylation of capsid protein p17, $Pr160^{gag\text{-}pol}$, and $Pr55^{gag}$, which are involved in the life cycle of HIV-1 [46]. Myristic acid has been shown to inhibit NMT [65-67]. HIV-1 replication could, consequently, be inhibited by the myristoylated 3TC. An ester bond was formed after chemical conjugation, which did not affect the antiretroviral efficacy of the prodrug, since the ester bond could be easily hydrolyzed in the presence of intracellular esterases, including lysosomal acid lipase, phospholipase, acetylhydrolase, nucleases and lipoprotein lipase, which are localized mainly in lysosomes. These enzymes catalyze the breakdown of acyl groups and hydrolyze compounds taken into lysosomes. In our study, the hydrophobic MTC presumably diffused through the cell membrane into different cell compartments. The

prodrug was transported into lysosomes, degraded by the esterases, and released the native 3TC to provide antiretroviral activity. Interestingly, MTC particles exhibited comparable antiretroviral efficacy to native 3TC as shown in day 0 RT result. Relatively low RT levels were observed in cells treated with both MTC formulations, which indicates that the myristoylation did not alter the antiretroviral efficacy of native 3TC. Myristoylated 3TC demonstrated reduced cytotoxicity compared with native 3TC, which could be attributed to the increased molecular weight; the enhanced hydrophobicity can also explain the reduced cytotoxicity since the solubility of MTC decreased dramatically. Compared to MTC, water-soluble 3TC, which is easily ionized in solution, can be cationized, influencing its complexation with the cell membrane, leading to higher cytotoxicity [68].

Nanocrystals are extraordinary drug delivery carriers and are useful because of their high drug loading capacity, improved stability and bioavailability [63, 69]. Nanosize drug crystals can be coated with surfactant for enhanced cellular uptake and sustained cellular maintenance for long-acting efficacy. For drugs with a short half-life, like 3TC, the therapeutic index is limited due to the low bioavailability, therefore nanocrystals are ideal platforms for increasing drug retention and improving systemic circulation. P407 was used as a coating surfactant in order to provide stable nanosuspensions, improve nanoparticle dispersity, and realize long-term drug release. Both FA-targeted and non-targeted MTC nanoparticles were prepared with well-distributed particle size and PdI. FA-NMTC exhibited a slightly larger size compared with NMTC due to the longer chain of FA-P407 coating polymer, but otherwise no significant difference was observed based on the characterization of the these two formulations. Both nanoformulations were stable in PBS and sustained drug release was observed *in vitro*, which demonstrated that this platform could be utilized to

manufacture particles with stable physiochemical properties and a sustained release profile.

The FA-NMTC nanoparticles showed better cell uptake by macrophages, especially in the first 2 hours. These particles were expected to be taken through both phagocytosis and receptor-mediated endocytosis. Folate derivatives are internalized mainly through the reduced folate carrier (RFC), which binds to the reduced form of vitamin B_9; and the folate receptor (FR), which has a high affinity for folic acid [70]. There are several different isoforms of FR including FR-α and FR-β, which are glycosylphosphatidylinositol-anchored proteins (GPI-AP) receptors. We have demonstrated in previous studies that FA coated nanoparticles are taken up by macrophages mainly through FR-β due to its overexpression in activated macrophages during myelopoiesis [53]. Especially for HIV-1 infected patients, FR-β will be highly expressed since the immune cells are activated [71, 72]. Meanwhile, nanoparticles can directly activate macrophages and more FR-β could be stimulated and overexpressed on the cell membrane of macrophages [53]. Both folate targeted and non-targeted MTC formulations can be taken up by macrophages through clathrin mediated endocytosis. Particles undergo recognition in the blood stream through opsonization and the opsonized particles attach to the cell membrane and are ingested into phagosomes [73]. The folate conjugated MTC nanoparticles are internalized by macrophages preferentially through a clathrin-independent pathway by the effect of FR-β. Folate attached to the MTC particles binds to GPI-anchored folate receptor, FR-β, which is overexpressed on the macrophage surface [74]. This process facilitates the internalization of the MTC particles, which can explain the 2-fold difference after 2 h treatment and the enhanced antiretroviral activity compared with the non-targeted nanoformulation. Due to the enhanced cell uptake, FA-NMTC exhibited greater

antiretroviral activity than non-targeted NMTC as confirmed by RT assay and HIV-1 p24 staining. Greater protection against HIV-1 was observed for targeted nanoparticles and the significant differences lasted for 10 days. Equivalent antiretroviral efficacy for both formulations by day 15 could be because most of the drug had been released by that time; however, both formulations showed greater antiretroviral efficacy compared with native 3TC.

It has been proved that endolysosomes can be affected by HIV-1 infection through Rab protein expression, and endosomes are sites of active viral assembly, where a great amount of virions accumulate during productive infection [55, 56]. Endolysosomal pathways are vital to the transport antimicrobial drugs since they enable the drug particles to re-locate at specific sites where virus produces and duplicates. We investigated the intracellular localization of non-targeted MTC particles in macrophages. We found they predominantly co-localized in late (Rab 7) and recycling (Rab 11 and 14) endosomes and lysosomes (LAMP1), which it demonstrated that nanoMTC was taken up and stored in macrophages through the endolysosomal pathways. MTC particles contained within endocytic compartments would provide a protected environment to facilitate drug release with steady antiretroviral efficacy. This not only provides effective drug delivery to HIV-1 action sites for improved therapeutic efficacy, but also protects the particles from intracellular degradation.

To investigate the *in vivo* pharmacokinetic parameters of nanoformulated MTC, we treated the mice with 50 mg/kg 3TC equivalents based as native 3TC, pro-drug MTC or nanoformulated MTC. Nanoformulated MTC exhibited sustained drug release and the folate coated MTC formulation exhibited 2-fold enhanced plasma and tissue drug levels compared with non-coated formulation in. Even after two weeks, the plasma level for FA-NMTC was still greater than three times higher than the half maximal effective concentration (EC_{50}) of 3TC (about 6.9 ng/mL). These studies also

demonstrated that the targeted MTC particles were more effectively stored in the macrophage depots after injection, as evidenced by their localization in reticuloendothelia tissues and lymph nodes. NanoMTC were taken by monocytes in blood, and redistributed during systemic circulation to reticuloendothelial tissues. In macrophages, MTC was gradually released into the endosomal compartments and converted to native 3TC by hydrolases. In vivo MTC was efficiently converted to 3TC since little MTC was detected in plasma and tissues. Due to effective binding to the FR on macrophages, more FA-NMTC particles could be taken up by monocyte/macrophages, distributed into different cellular compartments, and avoid degradation by lysosomes, all of which would explain the higher *in vitro* uptake and more sustained *in vivo* pharmacokinetic behavior for FA targeted MTC particles.

2.6. Conclusions

A hydrophobic 3TC prodrug was successfully synthesized through myristoylation and incorporated into targeted and non-targeted nanocrystalline formulation to improve drug half-life and reduce cytotoxicity. Nanoformulated MTC exhibited enhanced cellular uptake and sustained antiretroviral efficacy. Folate targeted MTC nanoparticles exhibited improved pharmacokinetics and this novel drug delivery system has showed great potentials in the clinical application.

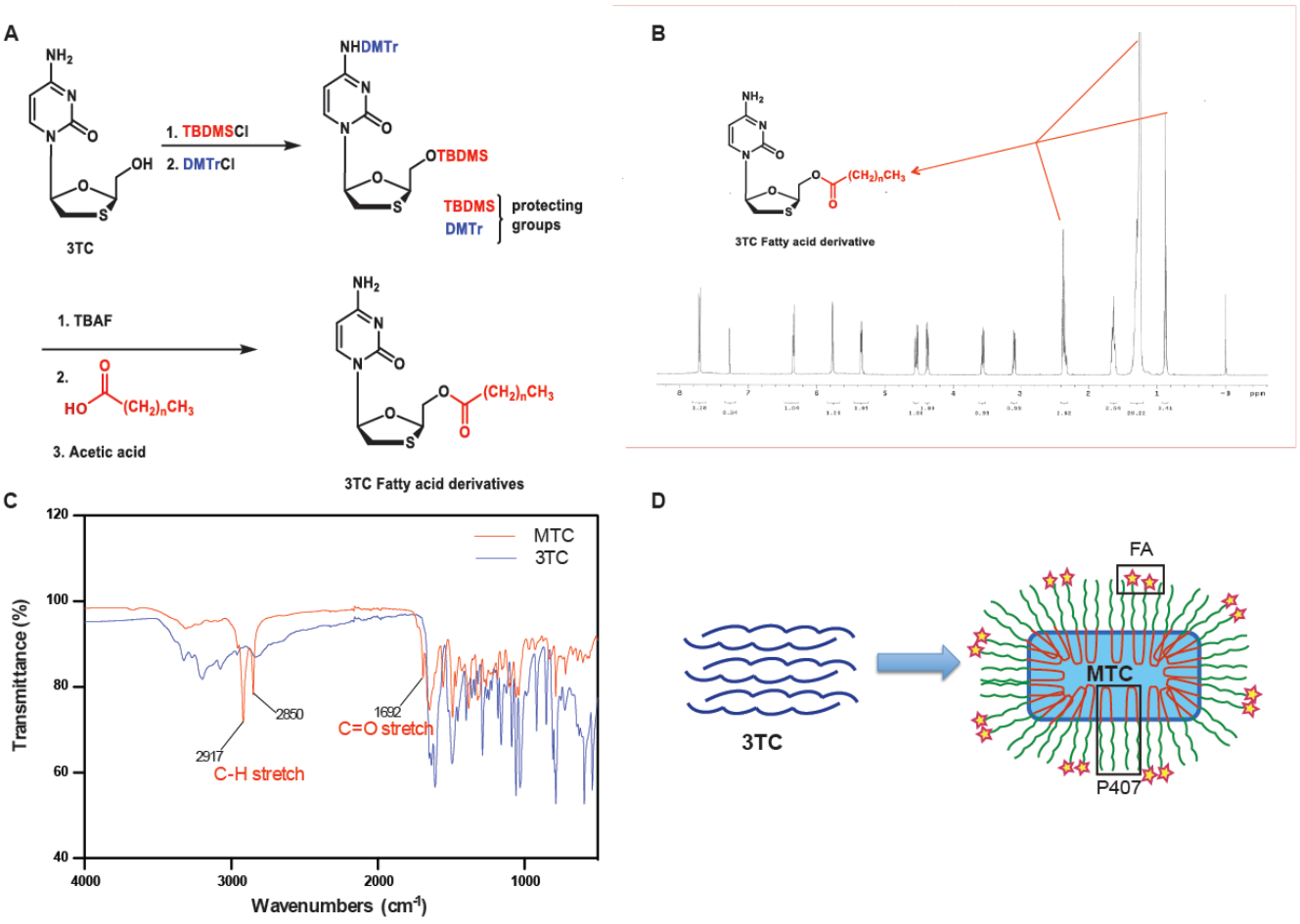

Figure 2.1. Characterization of myristoylated 3TC.

(A) Synthesis of myristoylated 3TC (MTC) derivative. (B) The ^{1}H NMR spectrum of MTC. MTC was dissolved in Dichloromethane-d_2 and characterized by nuclear magnetic resonance spectrometry (^{1}H NMR) determined on a Varian Unity/Inova-500 NB. Chemical shifts are reported in parts per millions (ppm). (C) FT-IR spectra of MTC and native 3TC. MTC and 3TC powder was analyzed by Spectrum Two FT-IR Spectroscopy to detect the structure of the final compounds. (D). Schematic diagram of the FA-NMTC formulation. Hydrophilic 3TC was myristoylated into hydrophobic MTC, and FA-P407/P407 polymer solution was used to encase MTC into FA-NMTC.

A

Formulation	NMTC	FA-NMTC
Size	375 ± 21 nm	433 ± 23 nm
PdI	0.21 ± 0.03	0.25 ± 0.03
Zeta-potential	-21.0 ± 0.8 mV	-19.7 ± 1.3 mV
Drug loading	75.0%	76.9%
Encapsulation efficiency	96.3%	98.4%
FA-P407	0	40%

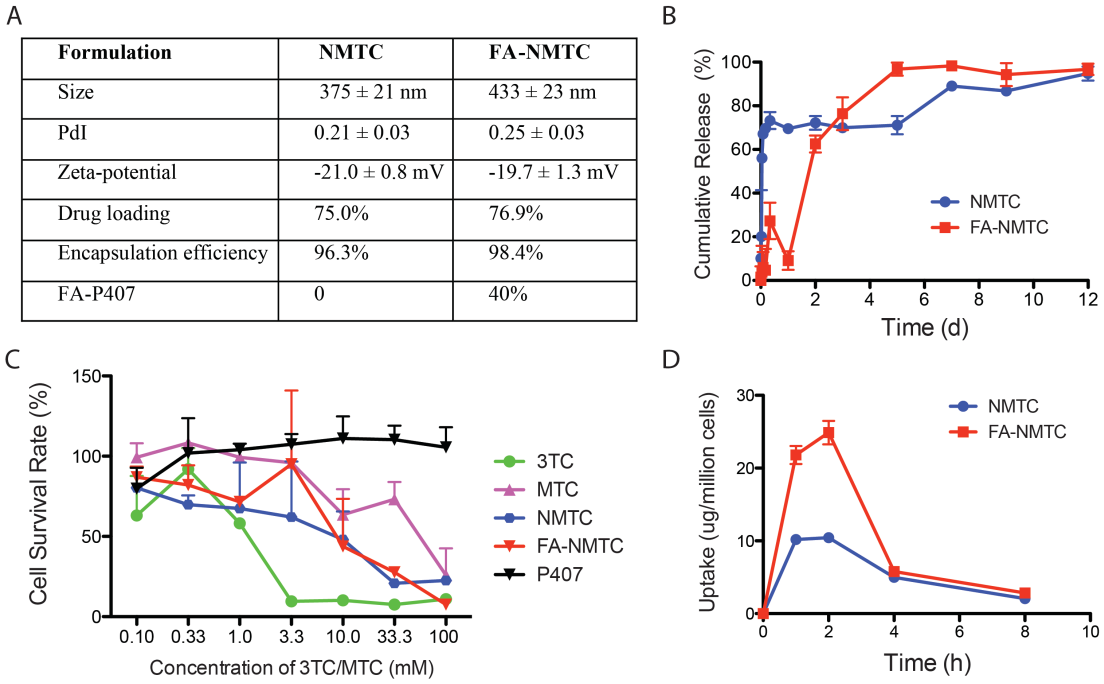

Figure 2.2. Characterization of MTC formulations

(A) Characteristics of MTC nanoformulations. (B) Cumulative release of MTC in isotonic solution. (C) Cytotoxicity of nanoformulated MTC. Cytotoxicity of native 3TC, MTC and both formulations was evaluated by Cell Counting Kit-8. MDM were treated with native 3TC, MTC, NMTC, or FA-NMTC at different concentrations for 4 h and cytotoxicity was determined. The difference between 3TC and MTC at concentrations 1.0, 3.3, 10.0, 33.3, and 100 mM are significant ($P < 0.05$). (D) Time course of uptake of MTC formulations in human MDM.. MDM were treated with 100 μM nanoformulations (based on MTC content) for 1, 2, 4 and 8 h. The cell lysates at indicated times were analyzed by HPLC for MTC quantification. Data represent the mean ± standard error of the mean (n = 3), for each time point.

A

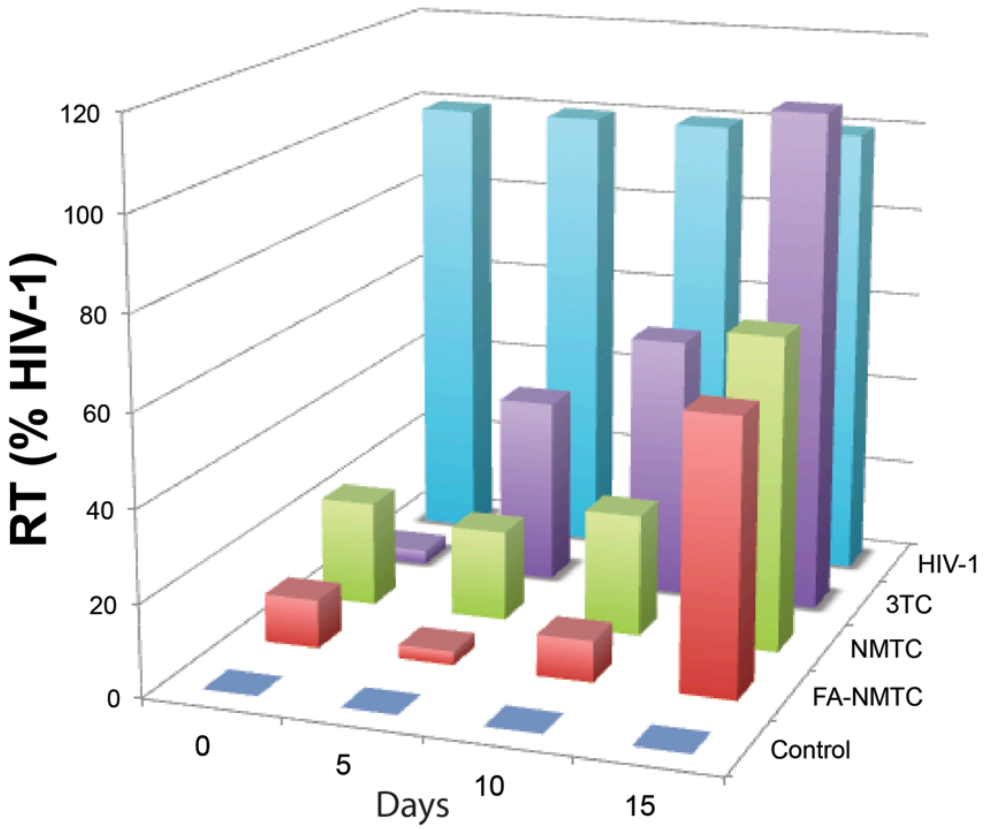
RT (% HIV-1)
120
100
80
60
40
20
0
0
5
10
15
Days
HIV-1
3TC
NMTC
FA-NMTC
Control

B

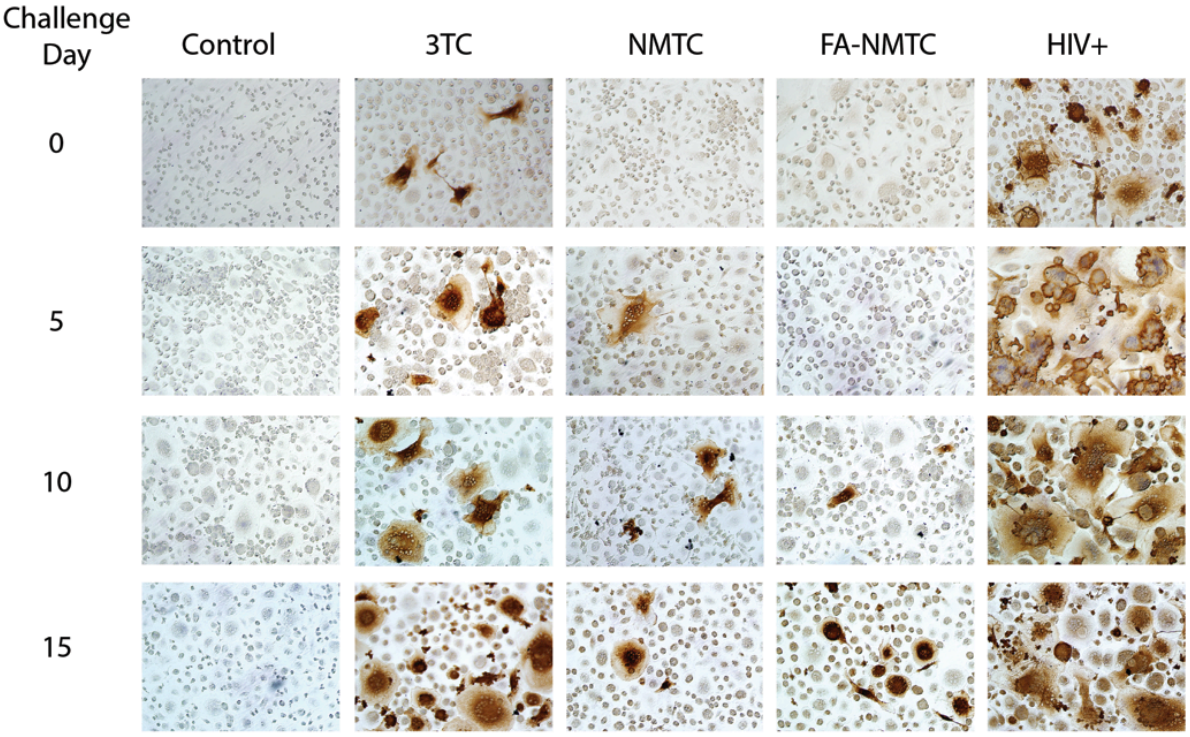
Challenge Day
Control
3TC
NMTC
FA-NMTC
HIV+
0
5
10
15

Figure 2.3. Antiretroviral efficacy of MTC nanoformulations.

(A) HIV-1 RT activity of native 3TC and nanoformulated MTC. (B) HIV-1 p24 staining of virus-infected MDM pretreated with native 3TC or nanoformulated MTC. MDM were treated with 100 μM native 3TC or nanoMTC for 4 h. At days 0, 5, 10, or 15, MDM were infected with HIV-1 for 4 h. Uninfected cells without treatment served as a negative control; HIV-1 infected cells without treatment served as a positive control for the RT assay. All the samples were collected after 7 days of viral infections for RT assay and HIV-1 p24 staining. For RT activity, results are shown as the mean of 5 replicates. The differences between 3TC and nanoMTCs (NMTC and FA-NMTC) at days 5, 10 and 15 are significant ($P < 0.05$). The differences between NMTC and FA-NMTC are significant at days 0, 5, and 10 ($P < 0.05$).

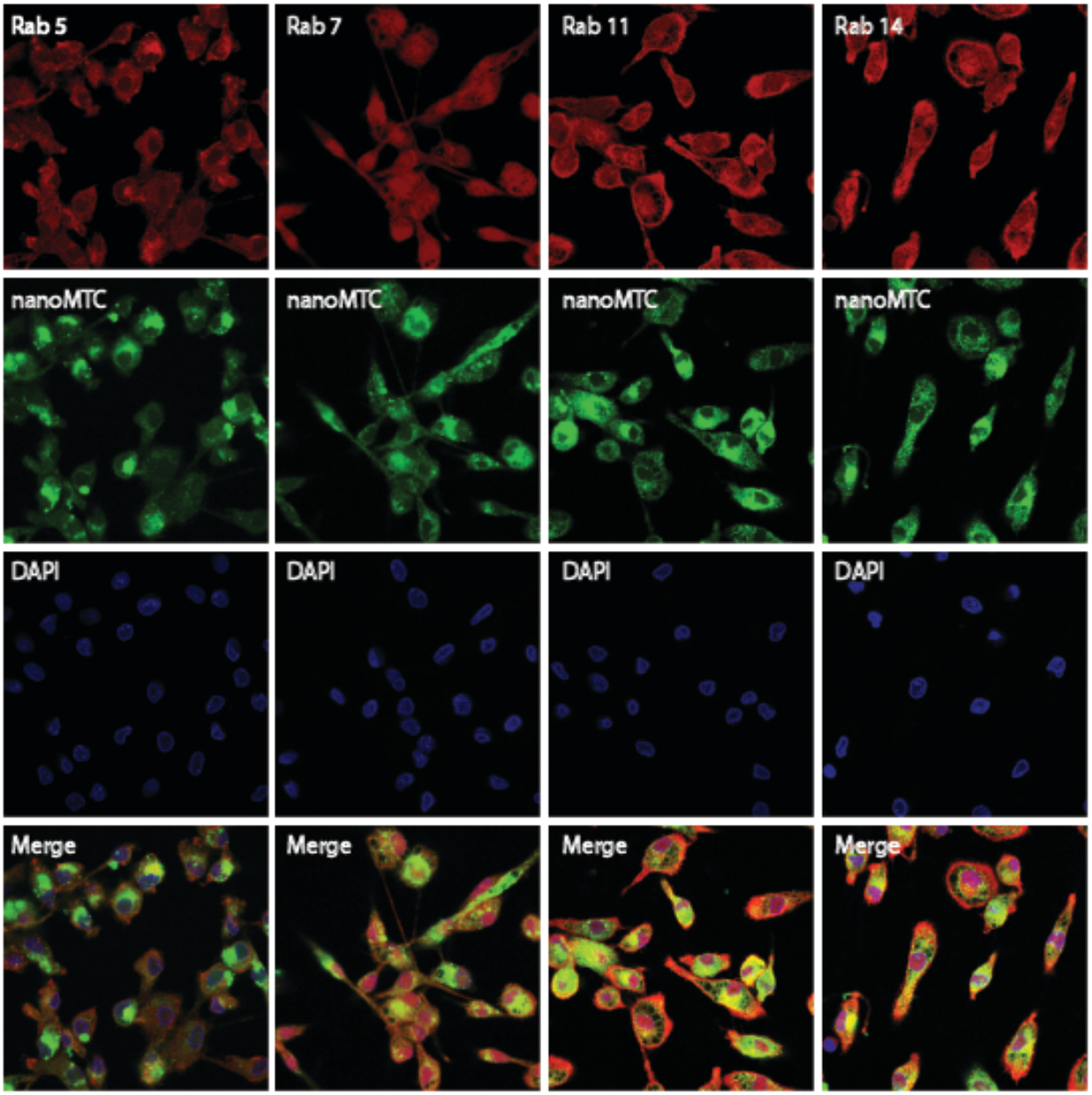

Figure 2.4. Subcellular localization of nanoformulated MTC in MDM.

MDM were cultured for 7 days and treated with 100 μM CF488-labeled NMTC for 4 h. The cells were stained with Rab 5, 7, 11, or 14 primary antibodies and AlexaFluor 568-labeled secondary antibodies to visualize the corresponding cell compartments using confocal microscopy. Nanoparticles are shown in green, cell compartments in red, and nuclei in blue.

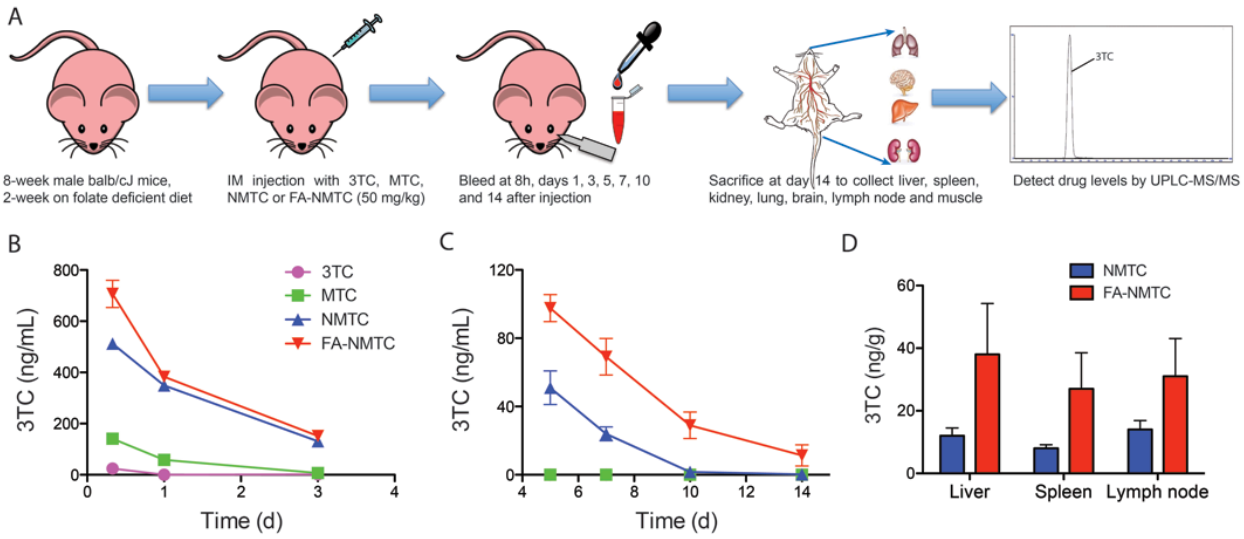

Figure 2.5. Plasma drug levels of nanoformulated MTC in Balb/C mice.

(A) Scheme of the pharmacokinetic study design. (B) Plasma drug levels from 8h to day 3. (C) Plasma drug levels from day 5 to 14. (D) Drug levels in liver, spleen and lymph node with formulations treated mice at day 14. Mice were administered intramuscularly (IM) 50 mg /kg equivalents of 3TC using native 3TC, MTC or MTC nanoformulations. Plasma was collected into acetonitrile for drug analysis at 8 h, and days 1, 3, 5, 7, 10 and 14 after treatment and tissues were collected at day 14 after sacrifice. 3TC levels were determined by UPLC-MS/MS. Data are expressed as mean ± SEM. Statistical differences were determined using one-way ANOVA among groups.

Chapter III.

Endolysosomal trafficking of nanoformulated antiretroviral therapy

3.1. Abstract

Limitations in antiretroviral therapy (ART) include poor patient adherence, drug toxicities, viral resistance and failures to penetrate viral reservoirs. Recent developments of nanoformulated ART (nanoART) could overcome such limitations. To this end, we now report a novel effect of nanoART that facilitates drug depots within intracellular compartments at sites at or adjacent to the viral replication cycle. Poloxamer 407 coated nanocrystals containing the protease inhibitor atazanavir (ATV) were prepared by high-pressure homogenization. These drug particles readily accumulated in human monocyte-derived macrophages (MDM). NanoATV concentrations were ~1,000 times higher in cells than what could be achieved by native drug. ATV particles in late and recycling endosome compartments were seen following pull down by immunoaffinity chromatography with Rab-specific antibodies conjugated to magnetic beads. Confocal microscopy provided cross validation by immunofluorescent staining of compartments. Mathematical modeling validated drug-endosomal interactions. Measures of reverse transcriptase activity and HIV-1p24 levels in culture media and cells showed that such endosomal drug concentrations enhanced antiviral responses up to 1,000 fold. We conclude that late and recycling endosomes can serve as depots for nanoATV. The co-localization of nanoATV at endosomal sites of viral assembly and its slow release sped antiretroviral activities. Long acting nanoART can serve as a drug carrier in both cells and subcellular compartments and as such facilitate viral clearance. The need for long acting ART is significant and highlighted by limitations in drug access, toxicity, adherence and reservoir penetrance. We propose that targeting nanoformulated drugs to infected tissues, cells and subcellular sites of viral replication may improve clinical

outcomes. Endosomes are sites for human immunodeficiency virus assembly and increasing ART concentration to such sites enhances viral clearance. The current work uncovers a new mechanism for why nanoART can enhance viral clearance over native drug formulations.

3.2. Introduction

Long-acting nanoformulated antiretroviral therapy (nanoART) can result in improved patient adherence, decreased systemic toxicities and sustained viral suppression. This is seen through nanoART's abilities to maintain consistent plasma and tissue drug levels [75-78]. Nonetheless, to facilitate clearance of the human immunodeficiency virus type one (HIV-1), antiretroviral drugs need be effectively delivered to viral sanctuaries [62]. This can target persistent or restricted infection [53, 79, 80]. With this in mind, our laboratories pioneered the use of monocytes and monocyte-derived macrophages (MDM) as nanoART carriers and drug depots. Macrophages can increase drug stability by preventing drug metabolic degradation and because of their highly mobile nature, they may also be used for delivery of ART to and from lymphocytes and other viral reservoirs [81-83]. How drug nanoparticles remain sequestered in macrophages for extended periods is incompletely understood. What is known is that nanoART can be delivered to endosomal organelles through clathrin-endosome pathways and remain inside the cell for extended time periods [81]. However, the virologic consequences of such a cell delivery system have not yet been elucidated. Investigations of nanoparticle interactions at the subcellular level remain of vital importance to the fields of long-acting antiretroviral pharmacokinetics and pharmacodynamics.

We reasoned that such mechanisms could be elucidated through investigations of nanoformulated viral protease inhibitors (PI). PI are substrate analogs for the HIV

aspartyl protease enzyme, involved in processing viral proteins by cleaving precursor proteins into smaller fragments and enabling the release of mature viral particles from infected cells. Once bound to the active site, they block the viral protease and in turn inhibit viral maturation, which blocks the formation of replication competent virions [84, 85]. Atazanavir (ATV), a United States Food and Drug Administration-approved PI for the treatment of HIV-1 infection can selectively inhibit virus-specific processing of gag-pol polyproteins. As a consequence PIs block viral assembly at action sites [86].

It is well known that subcellular organelles are utilized for HIV-1 assembly in mononuclear phagocytes (MP; monocytes and tissue macrophages) [87, 88]. Indeed, large caches of infectious HIV-1 released from MDM are produced in late endosomes [89]. We thus reasoned that if nanoART can improve drug delivery to tissues and cells and affect viral clearance, its effects could be amplified if the PI is delivered to the late endosomal sites operative for viral assembly. Herein, we demonstrate that nanoART enhances its antiretroviral efficacy by being delivered to subcellular sites of active viral replication. By tracking endosomal nanoART transport, sequential immunoaffinity separations of cellular compartments and by developing computer assisted mathematical models we were able to track the antiretroviral drug activities inside macrophages. Antiretroviral responses as measured by reverse transcriptase (RT) activityand HIV-1p24 antigen provided evidence for the co-localization of nanoART and progeny virus. Mathematical modeling uncovered the pathways for nanoparticle trafficking through endosomal compartments [90]. Previous combinations of experimental and computational studies were limited by the inherent complexity of integrating simulated modals with experimental results [91]. The nanoparticle-subcellular compartment modeling supports the idea that nanoformulations can facilitate the use of macrophages as drug carriers for ART and thus facilitate the establishment of drug depots and speed of viral clearance.

3.3. Materials and methods

3.3.1. Reagents & antibodies

ATV sulfate purchased from Longshem Co (Shanghai, China) was free-based with triethylamine. Poloxamer 407 (P407) and CF568-succinimidyl ester (CF568) were obtained from Sigma-Aldrich (St. Louis, MO, USA). Sephadex LH-20 was obtained from GE HealthCare (Piscataway, NJ, USA). Pooled human serum was obtained from Innovative Biologics (Herndon, VA, USA). Macrophage colony stimulating factor (MCSF) was prepared from 5/9m alpha3-18 cells (ATCC®, CRL-10154TM) cultured in ATCC complete growth medium as described [20]. Rabbit anti-human antibodies to Rab5, Rab7, Rab11 and Rab14, and Alexa Fluor 488 goat anti-rabbit IgG were purchased from Santa Cruz Biotechnology (Dallas, TX, USA). Protein A/G mix magnetic beads were purchased from Millipore (Billerica, MA, USA). TRIzol reagent was obtained from Invitrogen (Grand Island, NY, USA).

3.3.2. NanoATV manufacture and characterization

ATV nanoparticles were formulated by high-pressure homogenization (Avestin EmulsiFlex-C3, Avestin Inc., Ottawa, ON, Canada) using P407 to encase the drug crystals. The suspension containing free-based ATV (1%, w/v) and P407 (0.5%, w/v) in 10 mM HEPES buffer was premixed overnight at room temperature then homogenized at 20,000 psi for ~30 passes until the desired particle size of <300 nm was achieved. Size, zeta-potential and polydispersity (PDI) were determined by dynamic light scattering (DLS) using a Malvern Zetasizer Nano Series Nano-ZS (Malvern Instruments, Westborough, MA, USA). A minimum of four iterations were taken and these varied by < 2%. After reaching the desired size (< 300 nm) the sample was purified by centrifugation at 500 × g for 5 min to remove aggregated particles, then at 10,000 × g for 30 min to

collect a purified particle pellet. The resulting particles were resuspended in a 0.2% (w/v) P407 surfactant solution for cell studies.

3.3.3. Synthesis of dye-labeled nanoATV

For preparation of CF568-labeled nanoATV, CF568-P407 and P407 were dissolved in methanol at a weight ratio of 1:4 [6]. The solvent was evaporated and the mixture resuspended with 10mM HEPES to yield a 0.5% surfactant solution. Free-based ATV was added at a 1% weight ratio. The suspension was premixed overnight in a light protected environment at room temperature. The suspension was homogenized by high-pressure homogenization and purified by centrifugation [10].

3.3.4. Human monocyte isolation and cultivation

Human monocytes were obtained by leukapheresis from HIV-1,2 and hepatitis B seronegative donors then purified by counter-current centrifugal elutriation. The recovered monocytes, >98% pure by Wright stained cytosmears, were cultured in Dulbecco's Modified Eagle's Media (DMEM) with 10% heat-inactivated pooled human serum, 1% glutamine, 50 µg/mL gentamicin, 10 µg/mL ciprofloxacin and 1000 U/mL recombinant human MCSF for seven days facilitating cell differentiation into macrophages (MDM) [57].

3.3.5. Native and nanoformulated ATV cell uptake and retention

MDM were treated with native ATV or nanoATV at 30 or 70 µg/ml. Uptake of drug was assessed without media change for 24h. Cell collection occurred at serial time points. After 24 h drug exposure, drug retention in MDM was evaluated. Adherent MDM were collected by washing 3X with 1 mL of phosphate buffered saline (PBS), followed by scraping cells into 1 mL PBS. Samples were centrifuged at 950 × g for 10 min and supernatant removed. The cell pellets were resuspended in 200 µL methanol and

sonicated with a probe sonicator. The methanol extracts were centrifuged at 20,000 × g for 10 min prior to high performance liquid chromatography (HPLC) analysis as previously described [63]. Triplicate 20 µL samples of cells were assessed by HPLC using a YMC Pack Octyl C8 column (Waters Inc., Millford, MA) with a C8 guard cartridge. Mobile phase consisting of 47% acetonitrile/53% 25mM KH_2PO_4, pH 4.15, was pumped at 0.4 mL/min with UV/Vis detection at 212 nm. ATV levels in cells were determined by peak area comparisons to those of a standard curve generated with free drug (0.025-50 µg/mL).

3.3.6. Immune isolation of endocytic subcellular compartments

Immune isolation of endocytic compartments was performed as previously described [81]. Briefly, MDM were treated with native or nanoATV for 16 h. Cells were washed 3X in PBS to remove extracellular drug and then scraped in homogenization buffer (10 mM HEPS-KOH, pH 7.2, 250 mM sucrose, 1 mM EDTA, and 1 mM $Mg(OAc)_2$). Cells were then disrupted by 15 strokes in a dounce homogenizer. Nuclei and unbroken cells were removed by centrifugation at 400 × g for 10 min at 4^0C. Twenty µL of slurry protein A/G paramagnetic beads conjugated to Rab 5, 7, 11 or 14 antibodies (binding in 10% BSA in PBS for 12 h at 4^0C) were incubated with cell supernatants. Following a 24 h incubation at 4^0C, Rab 5, 7, 11, and 14^+ endocytic compartments were washed with PBS then collected on a magnetic separator. The drug content of each compartment was determined by HPLC [81].

3.3.7. Detection of HIV-1 integration by polymerase chain reaction (PCR)

To estimate the HIV integration, a modified method of that developed by O'Diherty and colleagues was employed [92]. After seven days of culture, MDM were treated with 100 µM native or nanoATV for 16 h then challenged with HIV-1_{ADA} at a multiplicity of infection

(MOI) of 0.1 infectious viral particles/cell. Following viral infection for 4 h, cells were cultured for an additional 14 days with half media exchanges every other day before the cells were scraped for collection. TRIzol Reagent was used to isolate DNA and RNA samples. The number of proviruses/cell was determined by a kinetic PCR assay. The standard curve was derived by running the nested PCR protocol on several dilutions of the integrated standard nucleic acid samples [93]. The concentrations of human genomes in the isolated sample DNA (or RNA) were determined by $OD_{260/280}$.

3.3.8. Antiretroviral activities

Antiretroviral efficacy was determined by HIV-1 RT activity [57, 94]. Briefly, MDM were treated with 100 μM native- or nano-ATV for 16 h and then challenged with HIV-1_{ADA} at a MOI of 0.1. Following viral infection, cells were cultured for 14 days with half media exchanges every other day. Medium samples were collected on days 2, 4, 6, 8, 10, 12 and 14 for measurement of progeny virion production as assayed by RT activity. Here, 10 μL media samples were mixed with 10 μL of a solution containing 100 mM Tris-HCl (pH 7.9), 300 mM KCl, 100 mM dithiothreitol, 0.1% nonyl phenoxylpolyethoxylethanol-40 (NP-40) and water in a 96-well plate. The reaction mixture was incubated at 37^0C for 15 min and 25 μL of a solution containing 50 mM Tris-HCl (pH 7.9), 150 mM KCl, 5 mM dithiothreitol, 15 mM $MgCl_2$, 0.05% NP-40, 10 μL/mL poly(A), 0.25 U/mL oligo d(T), and 10 μCi/mL ^{3}H-thymidine triphosphate was added to each well; plates were incubated at 37^0C for 18 h. Following incubation, 50 μL of cold 10% TCA was added to each well, the wells were harvested onto glass fiber filters, and the filters were assessed for ^{3}H-thymidine triphosphate incorporation by beta-scintillation spectroscopy using a TopCount NXT (PerkinElmer Inc., Waltham, MA, USA).

3.3.9. Immunocytochemistry and confocal microscopy

For immunofluorescence staining, cells were washed three times with PBS and fixed with 4% paraformaldehyde (PFA) at room temperature for 30 min. Cells were treated with blocking/permeabilizing solution (0.1% Triton, 5% bovine serum albumin (BSA) in PBS) and quenched with 50 mM NH_4Cl for 15 min. Cells were washed once with 0.1% Triton in PBS and sequentially incubated with primary and secondary antibody at room temperature. Slides were covered in ProLong Gold anti-fading reagent with DAPI and imaged using a 63× oil lens in a LSM 510 confocal microscope (Carl Zeiss Microimaging, Inc., Dublin, CA, USA) [28].

3.3.10. HIV-1p24 staining

Cells in different treatment groups were fixed with 4% phosphate-buffered PFA for 15 min at room temperature. Fixed cells were blocked with 10% BSA in PBS containing 1% Triton X-100 for 30 min at room temperature and incubated with mouse monoclonal antibodies to HIV-1p24 (1:100; Dako, Carpinteria, CA, USA) for 3 h at room temperature. Binding of HIV-1p24 antibody was detected using a Dako EnVision+ System-HRP labeled polymer anti-mouse secondary antibody and diaminobenzidine staining. Cell nuclei were counter stained with hematoxylin for 60 s. Images were taken using a Nikon TE300 microscope with a 40 × objective. Quantitation of immunostaining was performed by densitometry using ImagePro Plus, v. 4.0 [95].

3.4. Results

3.4.1. NanoART characterization

The nanoATV particles were formulated as a nanosized drug crystal from free-base ATV and P407. Physical properties including size, PDI and zeta potential were

measured by DLS. The particle size was 371.7 nm with a PDI of 0.194, which indicated the majority of nanoATV particles were homogeneous. The zeta potential was -28.9 mV, and the negative charge was contributed by P407. Scanning electron microscopy revealed smooth rod-like morphologies for the nanoATV particles and confirmed size measurements and distribution, which was consistent with our previous studies [81, 82].

3.4.2. Native and nanoATV cell uptake and retention

MDM uptake and retention of drug were assessed by HPLC. Cells were exposed to native ATV or nanoATV for 24 h and two treatment concentrations (30 and 70 μg/mL) were used. Significant differences were observed in rate and extent of drug uptake between native and nanoATV treatment groups (Figure 3.1A). The uptake of nanoATV was found to increase with time and the maximum uptake was observed at 16 h for 70 μg/mL treatment group (53.5 μg ATV/10^6 cells) and 24 h for 30 μg/mL (23.7 μg ATV/10^6 cells). However, uptake of less than 0.1 μg ATV/10^6 cells was observed at 24 h for both native ATV treatment groups, and this was not time-dependent. Drug retention in MDM was determined 24 h after treatment. In MDM treated with nanoATV, drug levels of 28.5 μg/10^6 cells and 14.0 μg/10^6 cells in 70 and 30 μg/mL treatment groups, respectively, were sustained over 24 h. Sustained release was expected for up to 15 days with nanoparticle treatment based on previous studies [53, 82]. Much less ATV was detected 24 h following treatment with native ATV.

3.4.3. Antiretroviral activities of native and nanoATV

To estimate the level of HIV-1 DNA and RNA PCR amplification assays were employed. After seven days of cultivation, MDM were treated with 100 μM native or nanoATV for 16 h then challenged with HIV-1_{ADA} at a MOI of 0.1. Following infection, cells were cultured for 14 days with half media exchanges every other day before cell collections. Isolated

total cell DNA or RNA were quantitated by kinetic PCR and nucleic acid levels calculated using standard curves made by the linear regression analyses. These data are shown in Figure 3.1C and D. At day 14 after HIV-1 challenge, 1.15×10^4 and 1.05×10^4 viral copies/10^3 MDM of viral DNA and RNA, respectively were determined in infected samples. Viral copies paralleled the concentrations of native ATV where 1 μM of ATV failed to show significant antiretroviral activity. In contrast for nanoATV treated groups, viral DNA and RNA was effectively suppressed at 1 μM. Viral copies were 29.59 and 36.09/10^3 MDM for HIV-1 DNA and RNA, respectively. This was seen following 100 μM nanoATV treatment, which effectively suppressed viral replication.

To determine the levels of progeny virus produced in native and nanoATV treated cultures we treated MDM with native or nanoATV in increasing drug concentrations of 0.01, 0.1, 1, 10, and 100 μM. Treatment was for 16 h with subsequent HIV-1_{ADA} challenge at a MOI of 0.1. The same formulation used for cell uptake and retention was tested for antiretroviral activities to ensure that the results were comparable. Infected cells were cultured for 14 days with half media change every other day. Culture supernatants were collected at days 2, 4, 6, 8, 10, 12, and 14 for determination of progeny virion production assayed by RT activity. A dose-dependent effect on RT activity for native and nanoATV at all time points was observed (Figure 3.1E and F). Significant differences between native and nanoATV were seen. For native ATV treated cells, suppression of RT activity was maintained over time only at 100 μM, and most of the other native drug concentrations failed to show significant viral suppression compared to untreated controls. In contrast, nanoATV reduced RT activity effectively starting at 1 μM. A two-log increase in viral suppression was seen with nanoATV as compared to native ATV.

3.4.4. NanoATV effects on HIV-1 p24 antigen

Cross validation of the results shown above was made through evaluation of viral antigen expression following native and nanoATV treatments for infected cell cultures. The expression of HIV-1 p24 antigen was used to determine antiretroviral activity in MDM that were treated with native or nanoATV and subsequently challenged with HIV-1 at a MOI of 0.1. Evaluation of p24 expression by infected MDM treated with native or nanoATV showed a concentration-response effect on the HIV-1 p24 expression at day 14 following viral exposure (Figure 3.2). Higher treatment concentrations resulted in lower p24 expression for both treatment groups. Formation of multinucleated giant cells was also observed. Significant differences between the native and nanoATV were seen at all concentrations. The expression of HIV-1 p24 antigen decreased slightly in cells treated with 1 or 10 μM native ATV, but an 89.4% decrease was found in cells treated with 100 μM native ATV (data not shown). HIV-1 p24 expression in cells was reduced with all concentrations of nanoATV. Viral suppression was to nearly asymptomatic levels with nanoATV treatment; i.e. 90.9, 94.2 and 95.7% for 1, 10 and 100 μM nanoATV treatment, respectively (data not shown).

3.4.5. NanoATV subcellular distributions

Confocal microscopy enabled both visualization and quantitation of the subcellular nanoATV distribution in early (Rab 5), late (Rab 7) and recycling (Rab 11, 14) endocytic compartments [96]. In these experiments, MDM were treated with 100 μM nanoATV fluorescently labeled with CF568. Immunostaining was performed 16 h after particle incubation for visualization of endocytic compartments and nanoATV co-localization. These experiments showed nanoATV distribution in a punctate pattern throughout the cytoplasm and perinuclear cell regions. NanoATV was found predominantly in late and recycling endosomes of uninfected macrophages (Figure 3.3A). Quantitation of the

fluorophore labeled Rab species in endosomes with CF568 (fluorescent)-labeled nanoATV was made by adapting Pearson's correlation coefficient to measure only positive co-localization coefficients (i.e. M1 and M2) of the two fluorophores at different emission wavelengths. Based on this, we showed significant accumulation ($p< 0.001$) of nanoATV within Rab 5- (35.4 ± 5%), Rab 7- (65.1 ± 7%), Rab 11- (70.3 ± 11%) and Rab 14- (56.9 ± 12%), positive compartments. To assess subcellular co-localization of nanoATV with assembled HIV-1 virions, MDM were treated with 100μM CF568-labeled nanoATV for 16 h following 14 days of HIV-1_{ADA} infection. Identical Rab-specific antibodies were employed to immunostain endocytic compartments in multinucleated giant cells. Quantitation of fluorophore in Rab compartments showed clear co-localization between virus and the nanoparticles (Figure 3.3B and 3D). The greatest amount of dual co-localization was found in Rab 7-immunopositive late endosomes. These data indicated that after HIV-1 infection, nanoATV persists in late endosomal compartments, the site of active viral assembly, but at half the level present in recycling endosomes of uninfected macrophages (3.3C vs. 3.3D).

3.4.6. NanoATV trafficking in endosomal subcellular comparments

To assess the locale of nanoATV at the subcellular level we analyzed individual endosomal compartments within MDM by immunoaffinity techniques. MDM exposed to nanoATV were mechanically disrupted at specific time points, and subcellular compartments including early, late and recycling endosomes were immunoisolated using A/G paramagnetic beads conjugated to Rab 5, 7, 11 or 14 antibodies. Endocytic compartments bound to beads were collected by magnetic separation, digitally imaged and then analyzed by HPLC for drug content. Time dependent endocytic uptake was observed in all labeled endosomes and the data was used to generate 48 h subcellular uptake curves (Figure 3.4A). At 48 h, the maximum nanoATV uptake was 10.6 ± 1.4

μg/10^6 cells in Rab 14 (early recycling endosomes) compartments, followed by 8.3 ± 0.7 μg/million cells in Rab 11 (late recycling endosomes) compartments. The lowest nanoATV concentration was found in Rab 5 compartments, representing early endosomes, regardless of HIV-1 infection, which was consistent with the co-localization confocal microscopy tests.

3.4.7. Simulation of nanoATV at the subcellular level

Mathematical means to simulate drug particle uptake and retention at both the cellular and subcellular levels were developed based upon our results. These models demonstrated that trafficking of nanoformulated particles in endosomal cell compartments provided an accurate and reliable view of their behavior in real time. The drug levels in specific compartments at different time points together with the confirmation that more nanoATV than native ATV could accumulate in late and recycling endosomes proved these to be the major subcellular depots for nanoATV. The modeled flow of nanoparticles is presented in Figure 3.4C where outside of the cell and the specific subcellular compartments involved in trafficking of the majority of nanoATV are represented as the graph nodes: 'Out' – the outside of the cell, 'Rab5', 'Rab7', 'Rab11', and 'Rab14' – denoting the compartments identified by the respective Rab proteins. The instantaneous concentration of nanoATV outside the cell, Q_1, is associated with the node 'Out', and the instantaneous concentrations of respective Rab proteins, Q_2, …, Q_5, are associated with the nodes 'Rab5', 'Rab7', 'Rab11', and 'Rab14'. It has been noticed that the total number of the observed nanoATV/fluorescent labeled particles in the experiment decreases over time. This has been taken to account in the model as an open path marked δ in the graph of Figure 3.4C.

Based on the graph topology, the time changes of the concentrations in the model are controlled by the set of 5 difference equations:

$$Q_1^{(i)} = Q_1^{(i-1)} - V_1^{(i-1)}\Delta T + V_6^{(i-1)}\Delta T + V_7^{(i-1)}\Delta T$$

$$Q_2^{(i)} = Q_2^{(i-1)} + V_1^{(i-1)}\Delta T - V_2^{(i-1)}\Delta T - V_3^{(i-1)}\Delta T - V_4^{(i-1)}\Delta T$$

$$Q_3^{(i)} = Q_3^{(i-1)} + V_3^{(i-1)}\Delta T - V_6^{(i-1)}\Delta T$$

$$Q_4^{(i)} = Q_4^{(i-1)} + V_2^{(i-1)}\Delta T - V_5^{(i-1)}\Delta T$$

$$Q_5^{(i)} = Q_5^{(i-1)} + V_4^{(i-1)}\Delta T + V_5^{(i-1)}\Delta T - V_7^{(i-1)}\Delta T - V_8^{(i-1)}\Delta T$$

where ΔT denotes the time increment in simulations, and $(\cdot)^{(j)}$ denotes the value of (·) at jth step of simulation.

Based on the experimental results, using multiple linear regression, and curve fitting methods implemented as standard MATLAB functions, the following relationships between the concentrations Q_1, …, Q_5, and the rates of changes V_1, …, V_8 were established:

$$V_1 = 0.04269Q_1 + 0.7778$$

$$V_2 = 0.1000Q_2 - 0.085Q_3 + 0.0814$$

$$V_3 = 0.0367Q_2 - 0.2714Q_4 + 2.238$$

$$V_4 = 0.003Q_1 + 0.0367Q_2 - 0.155Q_3 - 0.1263Q_5 + 0.7366$$

$$V_5 = -0.003Q_1 + 0.155Q_3 - 0.33$$

$$V_6 = -0.0031Q_1 + 0.2344Q_4 - 0.22$$

$$V_7 = -0.0031Q_1 + 0.01785Q_5 - 0.112$$

$$V_8 = 0.01\exp(0.01t)Q_5$$

where *t* is time from the experiment start. The units for all the rates are μg/10^6 cells/h and μg/10^6 cells for concentrations. The simulation model based on the set of difference equations was implemented in MATLAB using similar technique as applied in [97].

3.4.8. Subcellular antiretroviral activity

To determine in which compartments the virus persists and the antiretroviral efficacy of our nanoATV at a subcellular level, MDMs were challenged with HIV-1_{ADA} for 4 h at a MOI of 0.1, then treated with 100 μM native ATV or nanoATV for 16 h. MDM were mechanically disrupted at days 7 and 14, and subcellular compartments were immunoisolated using A/G paramagnetic beads conjugated to Rab 5, 7, 11 or 14 antibodies. Endocytic compartments bound to beads were collected by magnetic separation for the RT assay. The highest RT activity was found in Rab 11 compartments, representing recycling endosomes, and Rab 7 compartments, representing late endosomes, in non-treated cells after 7 and 14 days of HIV-1 challenge (Figure 3.5B), respectively, which suggested that virus located mainly in these endosomal compartments. NanoATV and native ATV at 100 μM both exhibited antiretroviral efficacy, while nanoATV more effectively decreased RT activity in all endosome compartments, especially Rab 7 and 11 fractions. Based on the confocal results, greater overlap of nanoATV and cellular compartments was found in late and recycling endosomes, which could explain why nanoATV was more effective in suppressing HIV-1 virus in these compartments.

3.5. Discussion

Nanocrystals are broadly used for drug delivery due to their high drug loading capacity, increased dissolution in solution and enhanced bioavailability [98-101]. Herein, we report the manufacture of P407 coated nanocrystal ATV (nanoATV) by homogenization and show that its physical properties, including size and surface charge, facilitate macrophage particle uptake and drug stability. Indeed, nanoATV was readily internalized by macrophages and produced sustained drug release. This serves to improve drug

efficacy by increasing subcellular bioavailability. Nanosized drug crystals coated with surfactant exhibit enhanced cellular uptake and facilitate the cellular maintenance of drug particles for prolonged time periods. Particle coating serves to increase intracellular drug stability. Notably, nanoATV leads to effective inhibition of HIV-1 replication for prolonged time periods. In contrast to native ATV, nanoATV shows weeks of viral suppression linked to its abilities to increase drug delivery to subcellular macrophage compartments. This is facilitated by sustained antiretroviral drug release rates.

Interestingly, HIV-1 infection affects the size and or number of endosomes as reflective of Rab protein expression (G. Zhang, preliminary communication). We posit that such virus-induced alterations in endosomes are biologically relevant to sustain viral growth. Indeed, endosomes are sites of active viral assembly and are the cellular substructures where large numbers of virions accumulate during productive infection [89]. Such a function has added strategic advantages for the nanoformulated antiretroviral drug as it enables the drug particle to reside in the identical site where viral maturation occurs in the cell. Taken together, such events certainly facilitate antiretroviral drug activities. This may also be operative for a broad number of endosomal compartments that affect “transport” of anti-microbial drugs and is likely a common pathway for macrophage scavenging functions. Notwithstanding we also accept that the pathways for endosomal trafficking and HIV are not perfectly congruent. Further investigations will determine the mechanisms behind each trafficking scheme. Such observations, nonetheless, open the means to improve antimicrobial therapies beyond what is being reported in the current study.

Over the past decade our laboratory has pioneered the development of long-acting nanoART. NanoATV serves as a model for macrophage-based nanoparticle drug delivery as descriptions of cell uptake and intracellular localization of ART content parallel one another. To better understand formulation trafficking at the cellular and

subcellular levels, we developed a mathematical means to simulate endosomal trafficking [90]. The model is simple to implement and can provide assessment of "putative" drug activities based on changes in concentration of nanoATV and/or Rab proteins in real time. Based on the model, divergent behaviors between native and nanoATV were readily observed. NanoATV was taken up efficiently into macrophages and effected sustained drug release while native ATV was minimally internalized. This helps to explain why nanoATV possesses distinct long-acting antiretroviral efficacy. Through our subcellular uptake simulation model, nanoATV subcellular distributions were visualized, and late and recycling endosomes were considered as the nanoATV depots. Indeed, large amounts of nanoATV were deposited in these endocytic compartments. However, it is also noted that differences exist between HIV-1 and nanoparticle drug subcellular accumulation including recycling endosomes. Whether this is a clever means of virus altering the "transport" properties of nanoparticles or a compensatory host mechanism in attempts to contain virus is not yet known. Further studies are certainly needed to assess the unique transport properties of the virus and the drug-laden particle.

Harnessing macrophage transport properties for drug delivery can improve clinical drug responses. Indeed, cell-based nanocarriers have been developed for not only cancer chemotherapy but also a wide range of microbial infections [102-104]. Macrophage-based nanomedicine delivery schemes may have several advantages over more conventional drug delivery including enhanced cure rates, reduced side effects, increased drug stability and effective subcellular targeting [28, 95, 105, 106]. Using the macrophages as a nanocarriage vehicle can permit investigations of nanoATV entry, intracellular trafficking and drug release kinetics.

NanoATV contained within endocytic compartments provide a protected environment to facilitate drug release with unaltered antiretroviral activities. Both late and

recycling endosomes were able to retain a large number of the nanoparticles. Macrophages likely play a vital role in HIV pathogenesis as they are among the first cells infected [107, 108]. Within an infected macrophage, virions are formed in a temporally and spatially coordinated manner wherein the components that make up the virus assemble in association with a specific cellular membrane from which the viral envelope is derived [89]. HIV-1 virions bud directly into late endosomes and thereby acquire late endosomal membrane proteins, such as Rab 7, LAMP-1 and CD63 [88]. Macrophages secrete virions from virus-containing intracellular vacuoles [109]. Late endosomes are principal locales for HIV assembly [110-114]. Importantly, nanoATV retains full antiretroviral activity in late endosomes, as RT activity was significantly decreased in Rab 7 and Rab 11 vesicles.

In summary our results demonstrate that nanoATV and HIV target overlapping subcellular compartments. Entry of virus and particles inside macrophages tis facilitated through clathrin-mediated pathways [115-118]. NanoATV particles are stored within late endosomes or recycling compartments, which serves to minimize intracellular degradation. For release, nanoATV are slowly recycled to the plasma membrane [119-122]. This provides a means for escape from phagolysosomal degradation and effective delivery of drug to action sites, which in the end has a net effect of improved therapeutic efficacy.

3.6. Conclusions

NanoATV is now demonstrated to effect increases in cellular drug uptake and retention in macrophages. The long acting antiretroviral efficacy of crystalline nanoformulated drugs is significantly enhanced over its native counterparts. Macrophages act as carriers of nanoATV to improve drug bioavailability. Computer assisted mathematical modeling

can simulate subcellular trafficking of nanoATV to late and recycling endosomes that serve as drug particle depots. Overall, nanoATV and HIV utilize similar subcellular pathways. Delivery of drug through subcellular compartments increases its antiretroviral responses.

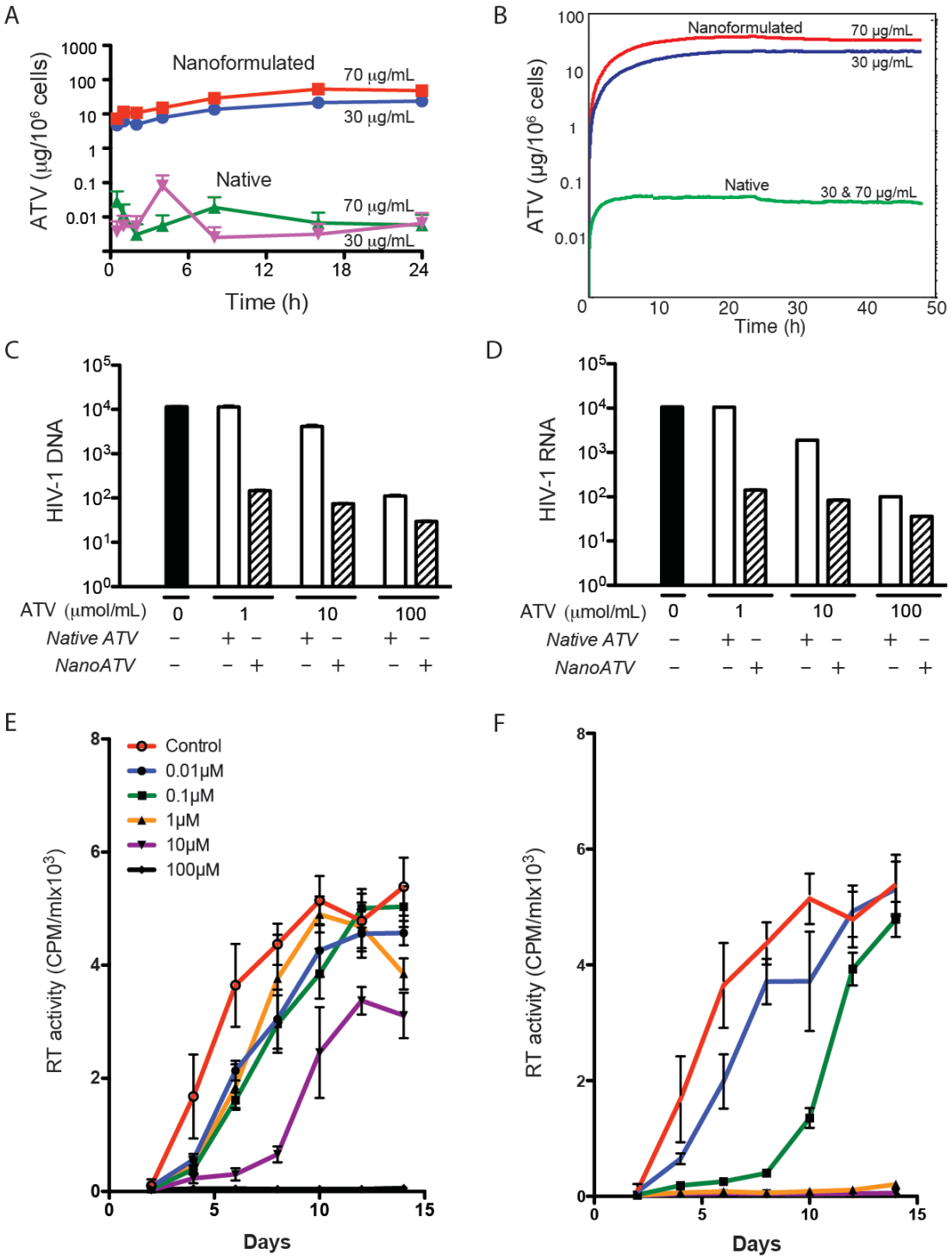

Figure 3.1. Comparisons of native and nanoATV cellular drug uptake and antiretroviral activity.

(A) Time course for monocyte-derived macrophage (MDM) uptake of native or nanoATV are illustrated. MDM cultures were treated with native or nanoATV for 24 h. (B) Computational simulation of the time course of MDM drug uptake and retention. After 24 h treatment with native or nanoATV, cells were washed with PBS and treated with fresh medium for 24 h. HIV-1 (C) DNA and (D) RNA levels were quantitated 14 days after infection in MDM treated with various concentrations of native or nanoATV. The units for viral DNA and RNA are copies/10^3 cells and copies/cell, separately. HIV reverse transcriptase (RT) activity 14 days after HIV-1 infection in MDM treated with various concentrations of (E) native- or (F) nanoATV. Data are expressed as average +/- SEM for N=5 replicates.

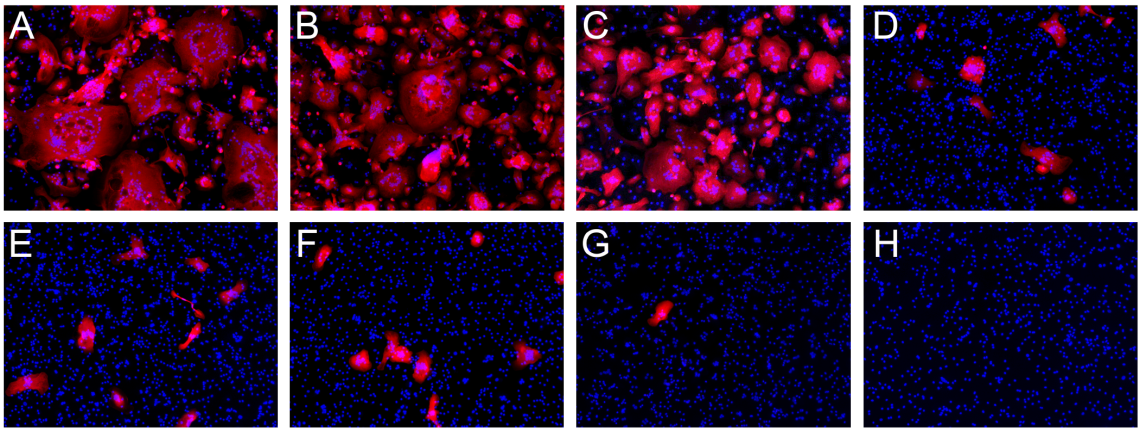

Figure 3.2. HIV-1p24 staining of virus-infected MDM pre-treated with native or nanoATV.

MDM were treated with native or nanoATV for 16 h then challenged with HIV-1 at a MOI of 0.1. Infection was allowed to continue for 14 days. The treatment groups included: (A) HIV-1 infected controls; (B-D) 1, 10 and 100 μM native ATV, respectively; (E-G) 1, 10 and 100 μM nanoATV, respectively; (H) uninfected MDM.

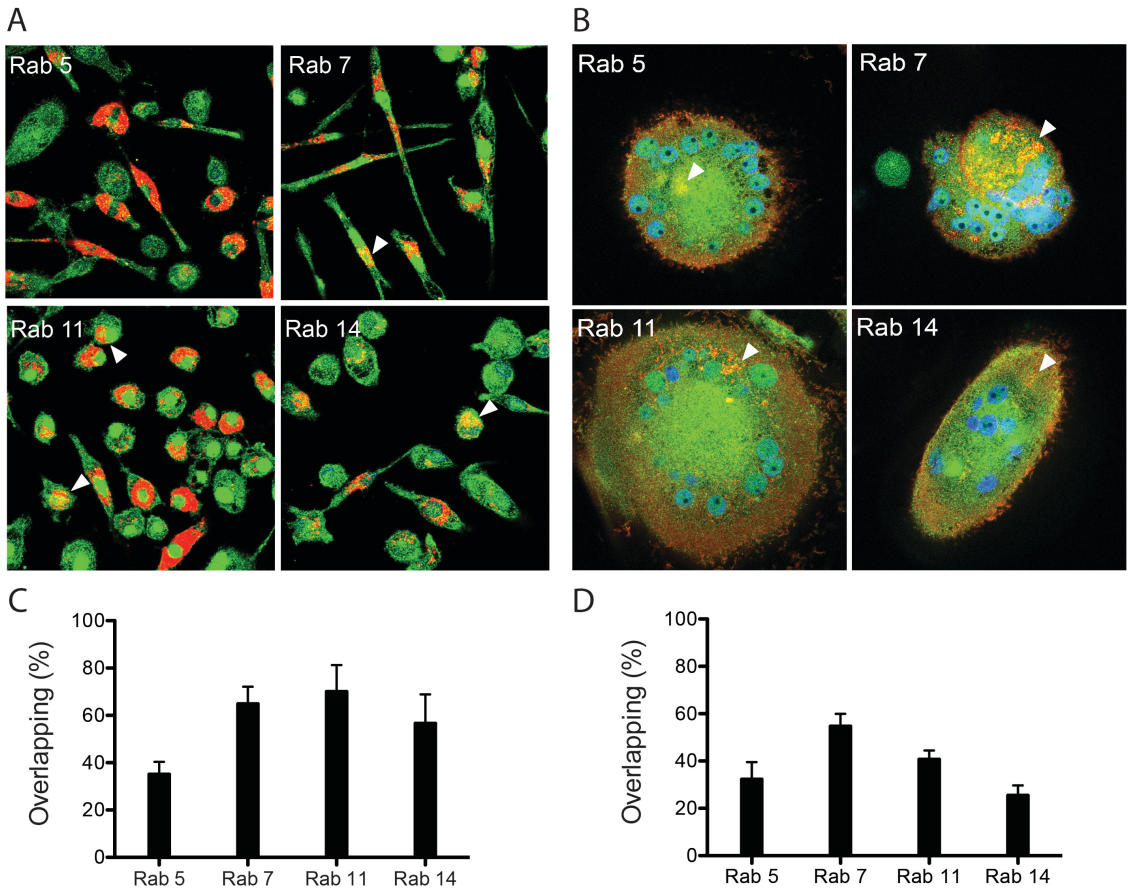

Figure 3.3. NanoATV subcellular distribution.

(A) Uninfected MDM and (B) HIV-1 infected MDM were treated with 100 μM, dye-labeled nanoATV for 16 h then immunostained with Rab 5, 7, 11 or 14 antibodies and AlexaFluor 488-labeled secondary antibody (green) to visualize particle and organelle co-registration. Quantitation of the overlap of nanoATV and Rab proteins in (C) uninfected and (D) HIV-1 infected MDM are shown. Data are expressed as the average +/- SEM of N=10 replicates.

A

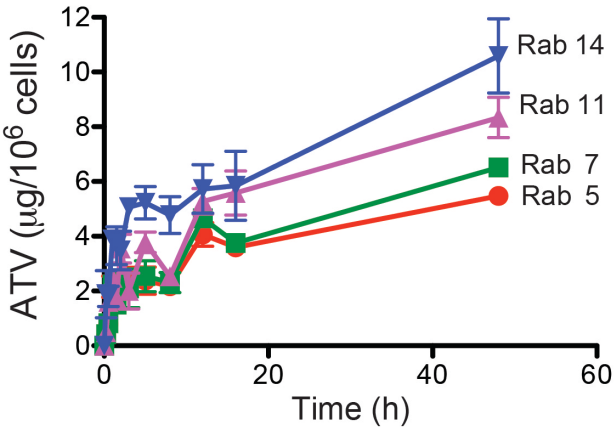
ATV (μg/10^6 cells)
Time (h)
Rab 14
Rab 11
Rab 7
Rab 5

B

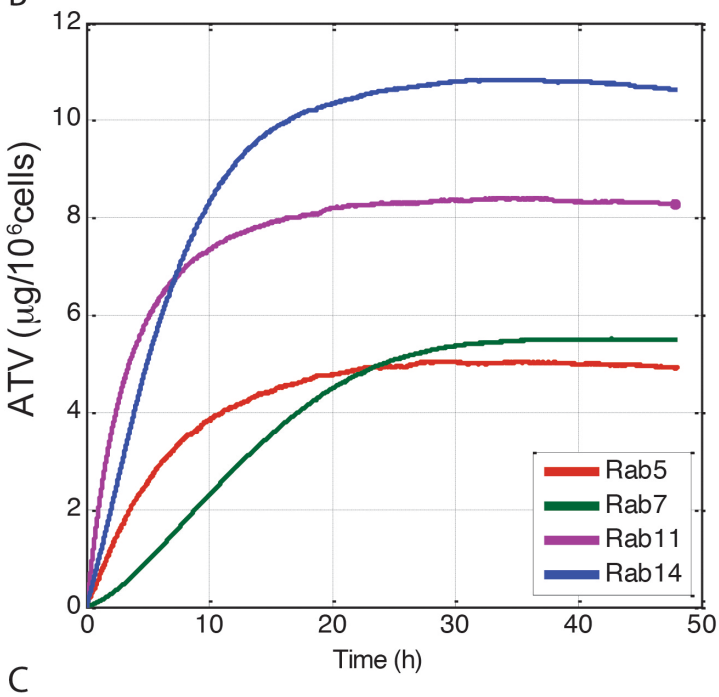
ATV (μg/10^6cells)
Time (h)
Rab5
Rab7
Rab11
Rab14

C

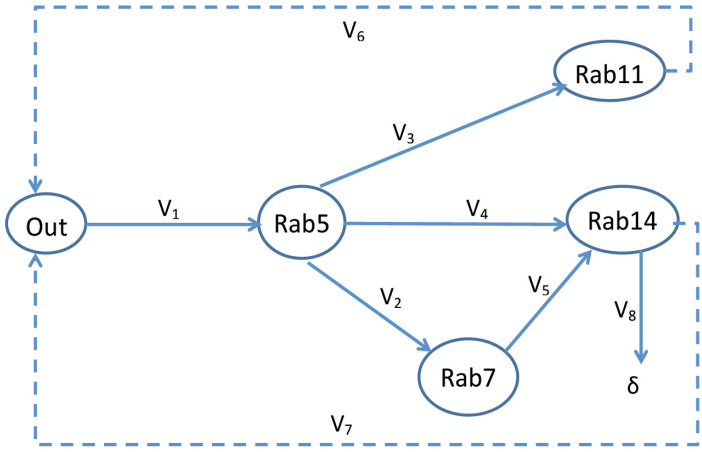
V6
Rab11
V3
Out
V1
Rab5
V4
Rab14
V2
V5
V8
Rab7
δ
V7

Figure 3.4. Kinetics of particle trafficking in subcellular endosomes.

(A) Subcellular uptake in different compartments in MDM treated with 100 μM nanoATV over 48 h. (B) Simulated subcellular nanoATV uptake activity in different compartments over the same time frame. (C) Simulated subcellular nanoATV uptake pathways. Data are expressed as average +/- SEM of N=3 replicates.

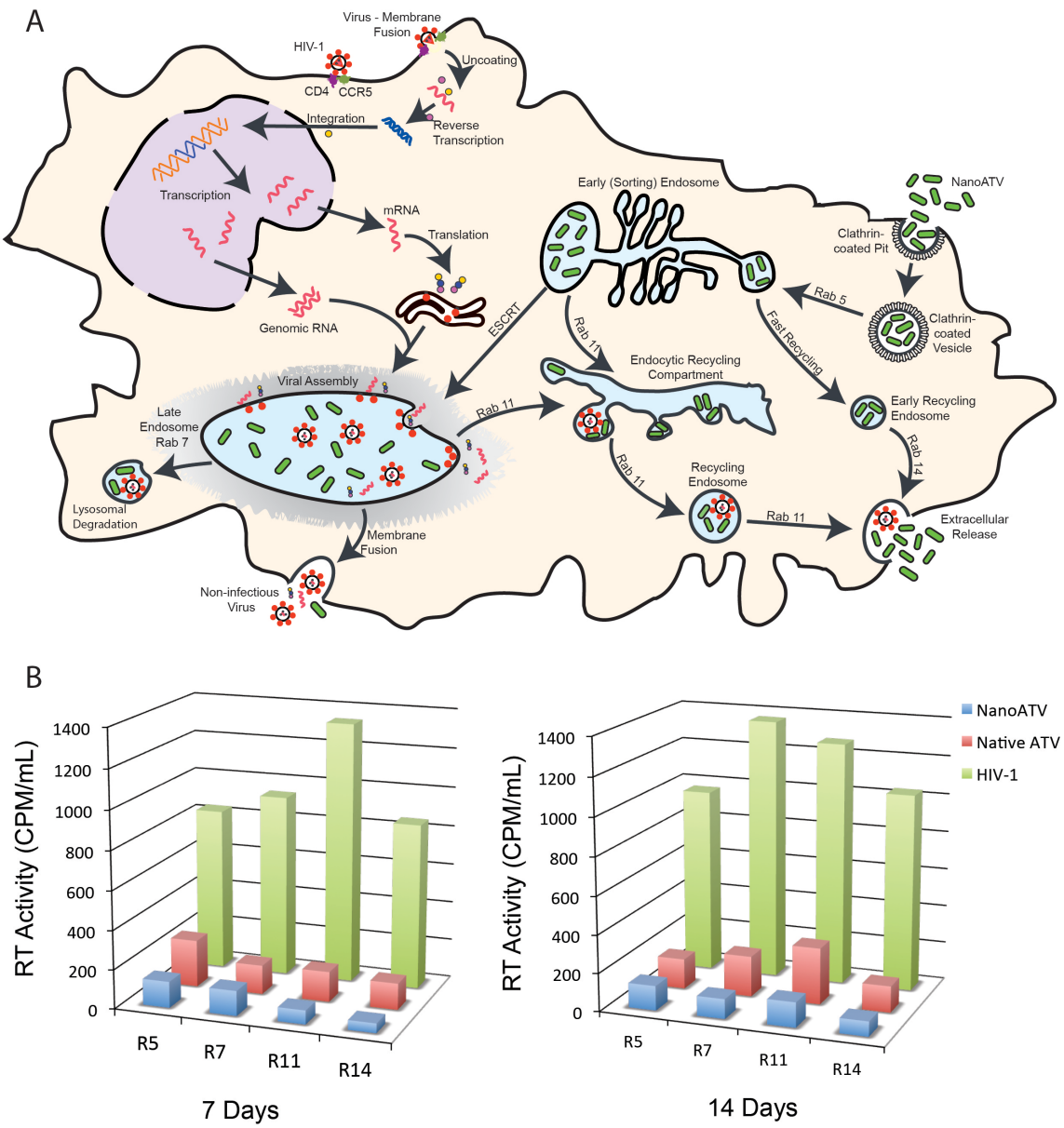

Figure 3.5. Intracellular pathways for HIV-1 progeny virion production and nanoATV trafficking.

(A) Schematic diagram for HIV-1 and nanoATV trafficking. HIV reverse transcriptase (RT) activity in subcellular endosomal compartments is shown. MDM were infected with HIV-1 for 4 h then treated with 100 μM native or nanoATV for 16 h. Endosomal compartments were isolated using specific Rab antibody-coated magnetic beads and RT activity was measured in endosomal compartments on (B) day 7 and (C) day 14 after infection. R5,

R7, R11, R14: Rab 5, 7, 11 and 14, respectively. Data are expressed as the average of N=5 replicates.

Chapter IV.

Opposing regulation of endolysosomal pathways by long-acting nanoformulated antiretroviral therapy

4.1. Abstract

Long-acting nanoformulated antiretroviral therapy (nanoART) is designed to improve subject regimen adherence, reduce systemic drug toxicities, and facilitate clearance of human immunodeficiency virus type one (HIV-1) infections. While nanoART establishes drug depots within recycling and late monocyte-macrophage endosomes, whether or not this provides a strategic advantage to eliminate the virus is not been completely elucidated. To this end, we applied quantitative SWATH-MS proteomics and cell profiling to nanoparticle atazanavir (nanoATV)-treated and HIV-1 infected human monocyte-derived macrophages (MDM). Native ATV and uninfected cells served as controls. Surprisingly, both HIV-1 and nanoATV engaged the endolysosomal trafficking for their assembly and depot formation, respectively. Notably, the pathways were deregulated in opposing manners by the virus and the nanoATV likely by viral clearance. Paired-sample z-scores, of the proteomic data sets, showed up- and down- regulation of Rab-linked endolysosomal proteins. NanoART and native ATV treated uninfected cells showed limited effects. The data was confirmed by Western blot. DAVID and KEGG bioinformatics tools showed relationships between secretory, mobility and phagocytic cell cell functions and virus and particle trafficking. We posit that modulation of endolysosomal pathways by antiretroviral nanoparticles provides strategic path to combat HIV infection.

4.2. Introduction

Long acting nanoformulated antiretroviral therapy (nanoART) is emerging as an important part of the *treatment* armamentarium for human immunodeficiency virus type one (HIV-1) infection [123-126]. While our prior studies defined both a platform for drug delivery and the trafficking mechanisms operative for nanoART in monocyte-

macrophages, how these cells can be harnessed as drug depots for improved antiretroviral responses has not been realized [55, 62, 63, 95, 127]. Indeed, human monocyte-derived macrophages (MDM) serve as nanoART carriers extending ART half-life and drug stability [35, 81]. Such cell-based drug delivery strategies may also decrease systemic drug toxicities [53, 128]. We posit that endolysosomal pathways can serve as Trojan horses for viral persistence or as vehicles for its elimination. If correct, facilitated viral replication and the means to eliminate it may occur at identical subcellular locales. The operative nanoART response would facilitate drug delivery by bringing the medicine to the site of action within mononuclear phagocytes (MP; monocytes, macrophages and dendritic cells). To investigate a seemingly mechanistic paradox, functional proteomic tests were employed to uncover how drug particles affect the HIV-1 replication cycle beyond nanoART activity.

The intracellular trafficking pathways held by the virus and nanoART were investigated by Sequential Windowed data independent Acquisition of the Total High-resolution Mass Spectra (SWATH-MS) profiling. This technique was applied to obtain a broader picture of complex nanoART-HIV interactions. The method was previously employed in our and other laboratories to identify and quantify cellular peptides on a larger scale [129-133]. While past transcriptomic and proteomic analyses were applied to study virus-cell interactions [130-133], they have failed to uncover key proteins affected by targeted antiretroviral treatments. Herein, we identified deregulated cellular proteins affected by nanoatazanavir (nanoATV) in HIV-1-infected MDM. Comparison was made between formulated and native ATV by the effect of HIV-1. Common cellular proteins with coordinated molecular, biochemical and biological functions were altered in virus-infected and nanoATV treated cells. These were linked to phagosome signalling pathways specifically associated with the endosomal and lysosomal compartments. Specifically, opposing expressions of Rab7 and -11 and LAMP1 were seen in HIV-1

infected and nanoATV-treated cells. Notably, the downregulation of late and recycling endosomes and LAMP1, indicated that pathways that could be employed, in measure, for viral assembly and nanoparticle lysosomal degradation were affected. Through cross validation of proteomics, cell biology and protein chemistry, our data provide novel insights into how nanoART facilitates viral clearance while establishing long-lived cell-based depots different from native drug. These works represent a previously unknown mechanism for how long-acting nanoART provides a strategic advantage to combat viral infection.

4.3. Materials and methods

4.3.1. Reagents and Antibodies

ATV sulfate (Gyma Laboratories of America Inc., Westbury, NY, USA) was free based with triethylamine. Poloxamer 407 (P407) and CF568-succinimidyl ester (CF568) were purchased from Sigma-Aldrich (St. Louis, MO, USA). Human serum was obtained from Innovative Biologics (Herndon, VA, USA). Macrophage colony-stimulating factor (MCSF) was prepared from 5/9m alpha3-18 cells (ATCC; CRL-10154) [54]. Rabbit anti-human Rab 5, -7, -11, LAMP1 and β-actin antibodies were purchased from Santa Cruz Biotechnology, Dallas, TX, USA. Alexa Fluor 594 goat anti-rabbit IgG and Alexa Fluor 647 donkey anti-mouse IgG were obtained from Life Technologies (Eugene, OR, USA)

4.3.2. NanoATV manufacture and particle characterization

P407-ATV was prepared by high-pressure homogenization using an Avestin Emulsiflex C3 homogenizer (Avestin Inc; Ottawa, ON, Canada) [63, 82]. CF568-labeled P407-ATV was prepared as described previously [53] using a 1: 4 (w/w) ratio of CF568-P407 and P407. Drug content of the nanosuspensions were determined by reverse phase high-

performance liquid chromatography (HPLC) [105]. Particle size, polydispersity and zeta potential for the nanoparticles were determined by dynamic light scattering using a Malvern Zetasizer Nano-ZS instrument (Malvern Instruments Inc.; Westborough, MA, USA).

4.3.3. Monocyte isolation, cultivation and HIV-1 Infection

Human peripheral blood monocytes were obtained by leukapheresis from HIV-1,2 and hepatitis B seronegative donors and plated at a density of 1 x 10^6 cells/mL in Dulbecco's modified Eagle's medium supplemented with 10% heat-inactivated human serum, 1% glutamine, 50 µg/ml gentamicin, 10 µg/ml ciprofloxacin and 1,000 U/ml MCSF. After seven days of cell differentiation, MDM were infected with HIV-1_{ADA} at a MOI of 0.1 infectious viral particles per cell. After 4 hours the medium was removed and cells were treated with 100 µM P407-ATV. Following 16 hours of drug treatment, the media was replaced with drug-free fluids and cells were incubated for an additional seven days [57, 62].

4.3.4. SWATH-MS

MDM samples for mass spectrometry were collected seven days after infection and drug treatment. Cells were washed with ice-cold PBS, scraped, pelleted, and stored at −80°C until processed. Cell samples from four donors were processed simultaneously. Cell pellets were re-suspended in cell lysis buffer containing 4% (w/v) SDS, 0.1 M dithiothreitol (DTT) and 0.1 M Tris-HCl. Lysates were vortexed at room temperature for 10 min and then boiled at 95°C for 5 min to denature proteins. Protein quantification was performed using the Pierce 660 nm protein assay (Thermo Scientific; Wilmington, DE, USA) following the manufacturer's protocol. On the basis of protein quantifications, 100-200 µg of each sample was processed using filter aided sample preparation (FASP)

[134-136]. Samples were denatured with urea exchange buffer (8 M urea, 0.1 Tris-HCl, pH 8.5) placed into filter cartridges (10 kDa), centrifuged and then treated with 50 mM iodoacetamide (Sigma-Aldrich). Trypsin (Promega; Madison, WI, USA) was added (2 µg/100 µg protein) and incubated at 37°C overnight on the cartridge. Eluted peptides were dried via vacuum centrifugation. Peptides were cleaned using an Oasis mixed cation exchange cartridge following manufacturer's protocols (Waters Inc.; Milford, MA, USA) and then dried under vacuum. After processing through mixed cation exchange, peptides were subjected to further clean up using C18 Zip-Tips (EMD Millipore; Billerica, MA, USA) and dried under vacuum. Peptides were resuspended in 0.1% formic acid (Honeywell Burdick & Jackson; Muskegon, MI, USA) and quantified using NanoDrop2000 (Thermo Scientific). One µg of peptide was then prepared for SWATH-MS quantitative proteomics analysis, as previously described [129, 137]. Samples used to generate the SWATH-MS spectral library were subjected to traditional, data-dependent acquisition (DDA).

4.3.5. Bioinformatics

Each SWATH-MS condition (per each donor) was transformed independently of other conditions and comparisons between control condition and experimental conditions were calculated. Extracted raw data transformation was performed as described by Haverland et al. [129] The raw intensity for each protein was transformed by taking the natural log (ln) of the intensity followed by assignment of *z*-score. The *p*-value for the computed *z*-score was assigned using standard normal distribution. Functional analysis and signalling pathway representation were performed using an array of complementary, open-access bioinformatic tools. Functional annotation of the proteins differentially expressed was performed using the Database for Annotation, Visualization and Integrated Discovery (DAVID) Bioinformatics Resources (6.7) and the Protein Analysis

Through Evolutionary Relationships (PANTHER) Classification System (9.0), by entering the UniProt sequence feature. The gene ontology (GO) annotations showed proteins according to Biological Processes, Molecular Functions and Cellular Components. Protein Class functional analysis was obtained by PANTHER. Protein–protein interactions among all identified transcription regulators were investigated using Search Tool for the Retrieval of Interacting Genes/Proteins (STRING) (9.1) considering a confidence of greater than 0.4 (medium confidence). Unconnected proteins (orphan proteins) and unconnected satellite networks (networks which were detached from the largest network) were removed.

The complementary pathway analysis, Kyoto Encyclopedia of Genes and Genomes (KEGG) was used to determine significant pathways between experimental conditions. The KEGG pathway (71.0) for the phagosome was coloured using the KEGG mapper colour pathway tool. Green represents all proteins confidently identified and red and blue colours are assigned to up- or down-regulated proteins, respectively.

4.3.6. Antiretroviral activities

HIV-1 reverse transcriptase (RT) activity was measured to assess antiretroviral efficacy in HIV-1 infected MDM. MDM were treated with 10, 100 or 250 μM native- or nanoATV for 16 hours then infected with HIV-1_{ADA} for 4 hours at a MOI of 0.1 immediately and five and 10 days after drug treatment. Following viral infection, cells were cultured for an additional seven days at which time cell media were collected for measurement of RT activity. Briefly, in a 96-well plate, 10 μL of sample supernatants were mixed with 10 μL of solution containing 100 mM Tris-HCl (pH 7.9), 300 mM KCl, 100 mM dithiothreitol, 0.1% NP-40 and water. The reaction mixture was incubated at 37˚C for 15 min and 25 μL of a solution containing 50 mM Tris-HCl (pH 7.9), 150 mM KCl, 5 mM DTT, 15 mM $MgCl_2$, 0.05% NP-40, 10 μL/mL poly(A), 0.25 U/mL oligo d(T) and 10 μCi/mL ^{3}H-

thymidine triphosphate was added to each well; plates were incubated at 37˚C for 18 hours. Following incubation, 50 µL of cold 10% TCA was added to each well, the wells were harvested onto glass microfiber filters and the filters were assessed for ^{3}H-thymidine triphosphate incorporation by b-scintillation spectroscopy using a TopCount NXT (Perkin Elmer Inc.; Waltham, MA, USA) [55, 62].

4.3.7. Western Blots

Protein expressions of Rab 5, 7 and 11, LAMP-1 and Actin were detected by Western blot assays. MDM were treated with native drug or nanoATV and infected with HIV-1_{ADA} as described. Seven days after infection cells were collected and lysed using CellLytic M Cell Lysis Reagent (Sigma-Aldrich). Protein content was quantitated using the Pierce 660-nm protein assay. Ten µg of protein was separated by electrophoresis using a NuPAGE Novex 4-12% Bis-Tris gel (Life Technologies-Novex; Grand Island, NY, USA). After electrophoresis, the proteins were transferred to a PVDF membrane (BioRad Laboratories, Hercules, CA, USA) and then blocked with 5% non-fat dry milk in PBS and 0.1% Tween-20 (PBST). Membranes were probed with primary antibodies for Rab5, Rab7, Rab11 or LAMP-1 and β-actin (Santa Cruz Biotechnology) followed by horseradish peroxidase-conjugated secondary antibody (Life Technologies-Novex). Proteins were detected using the SuperSignal West Pico Chemiluminescent substrate kit (Thermo Scientific) [55, 81, 138].

4.3.8. Immunofluorescence and confocal microscopy

For immunofluorescence staining, cells were washed three times with PBS and fixed with 4% paraformaldehyde (PFA) at room temperature for 30 min. Fixed cells were permeabilized with 0.1% Triton in PBS and then blocked with 5% bovine serum albumin (BSA) in PBS for 30 min. Cells were washed with 5% BSA in PBS and sequentially

incubated with primary antibody against HIV-1 p24 (Dako; Carpinteria, CA, USA) and either Rab5, -7, -11 or LAMP-1 (Santa Cruz Biotechnology) for 1 hour then washed 3 times with PBS. Secondary antibodies conjugated with Alexa594 or Alexa647 dyes (Life Technologies-Molecular Probes) were applied against the primary antibody isotype and incubated at room temperature for 1 hour then washed 3 times with PBS. Slides were covered in ProLong Gold AntiFade reagent with DAPI (Life Technologies-Molecular Probes) and imaged using a 40X oil lens on a LSM 510 confocal microscope (Carl Zeiss Microimaging, Inc.; Dublin, CA, USA) [55, 139].

4.3.9. Cytokine Bead Array

MDM were infected with HIV-1_{ADA} for 4 hours at a MOI of 0.1 then treated with 100 μM native- or nanoATV for 16 hours immediately. 24 hours after drug treatment, 50 μL cell culture media from treated and infected MDM were tested to determine the concentrations of inflammatory cytokines measured by a cytokine bead array (CBA) detection kit (Becton Dickinson Biosciences; Mississauga, ON, USA) and performed according to instructions of the manufacturer. Monoclonal antibodies specific to interleukin-12 (IL-12), tumor necrosis factor (TNF), IL-10, IL-6, IL-1b and IL-8 were added to the samples in a 96 well plate. A serial dilution of known cytokines generated the standard curve. Following three hours of incubation, all samples were acquired and analysed on a FACSArray. The standard curve was determined using a parameter logistics model and analysed with FCAP Array software. Cytokine levels are expressed as pg/mL [140].

4.4. Results

4.4.1. Proteomics analyses of HIV-1 infected MDM

HIV-1 infection engages a spectrum of cellular proteins seen in specialized cell populations that support its replication [109]. The effect of nanoART on cell protein expression has not yet been defined, in its target macrophage. To such ends, we applied quantitative SWATH-MS proteomics followed by bioinformatics to uncover proteins deregulated by free ATV or nanoATV with or without HIV-1 cell exposures. For these experiments MDM were first infected with HIV-1_{ADA} and four hours later medium was removed and cells were treated with 100 μM P407-ATV. Following 16 hours of drug treatment, the media was replaced with drug-free fluids and cells harvested for proteomic tests after an additional seven days This experimental paradigm was followed to assess the role that the antiretroviral delivery system had on macrophage proteome during spreading viral infection. In attempts to separate the effects of the antiretroviral drug, the nanoparticle and viral infection both separate and combined analyses of each of these were required. Following biological assessments, cells samples were collected and we assessed how nanoATV and free ATV could modulate virus-induced protein changes. MDM were infected with HIV-1 at a multiplicity of infection (MOI) of 0.1 then treated with 100 μM free or nanoATV. After seven days, cells were harvested and SWATH-MS was performed on whole cell lysates [129]. Based on the expansive proteomic data sets based on the biological response variables amongst the cell treatments for nanoATV, ATV and HIV-1 illustrations of the data sets were divided into replicate files and two independent figures. The first identified differnces between HIV-1 infected with or without nanoART and the second (with and without native ATV. Quantitative profiling identified 527 significantly changed MDM proteins following HIV-1 infection. These were up- or down-regulated ($p<0.05$) assessed by paired-samples z-

scores. The numbers of proteins exhibiting changed expression in HIV-1-infected cells were greater than in replicate infected cells treated with nanoATV, 527 *versus* 376 respectively (Figure 4.1A). Up- and down- regulated proteins in HIV-1 infected cells were 41 and 59% of total (n=216 and 311, respectively). In contrast for nanoATV-treated HIV-1-infected MDM, up- and down-regulated proteins were 59 and 41% of total (n=222 and 154, respectively). Uninfected cells treated with nanoATV had fewer deregulated proteins (n=195) compared to the other groups. The proteins uncovered engaged the PANTHER database which sorted the deregulated proteins by classes. This illustrated the relative numbers of proteins in each class for the HIV-1-infected and infected and nanoATV-treated cells (Figure 4.1B). This showed that the number of deregulated proteins in HIV-1-infected *versus* infected and nanoATV-treated cells was greater for each of classes (nucleic acid binding, hydrolase, transferase, protease, signalling molecule, transporter, transcription factors and ligases). These results demonstrate that the deregulation of cellular proteins by HIV-1 infection can be altered by nanoATV treatment. To uncover the function classes of proteins deregulated by HIV infection we examined the functional categories by PANTHER classification. These data are based on Gene Ontology annotations (GO molecular function, GO biological processes and GO cellular component). Figure 4.2A shows the proteins sorted according to molecular function with the percentages of total deregulated proteins classified for subgroups. Common proteins were separated based on binding (28 to 31%), enzyme regulator (5%) and transporter (3-4%) activities between the nanoATV, HIV-1 and HIV-1 and nanoATV MDM. Proteins included Rab5, 7 (GDP/GTP and protein binding) and LAMP1 (enzyme and protein binding) were joined. The classification revealed enrichment for metabolic, cellular, localization, regulation and cellular organizational cellular processes. These were the principal categories or protein sets (Figure 4.2B). The relative ratios for the proteins were similar amongst groups. GO for cellular component showed that

deregulated proteins sorted by cell organelle and macromolecular complex (Figure 4.2C). Note that such groupings were common to HIV-1 and HIV-1 and nanoATV cells. The data, demonstrated that HIV-1 and HIV-1 and nanoATV affect similar cellular processes. However, the numbers of proteins in each were reduced following infection and nanoATV treatment.

4.4.2. KEGG pathway analyses for HIV-infected MDM

The proteins relative to functional pathways were further investigated using the KEGG database, which, indicated phagosomes as one of the main pathways related to HIV-1 infection and nanoATV treatment. *First* we identified the role of HIV-1 infection as compared to HIV-1 infected nanoART-treated MDM on the phagosome network (Figure 4.3A and B, respectively). Few numbers of proteins were deregulated with nanoATV treatment. However, proteins were deregulated during HIV-1 infection and treatment groups. Notably, there was an opposite regulation for proteins within the phagosome and endosomal compartment between HIV-1-infected and HIV-1-infected and nanoATV-treated MDM. Up-regulation of Rab 5 and -7 proteins was observed in HIV-1 infected cells; in contrast these same proteins were down-regulated in nanoATV-treated HIV-1 infected cells, pink = increased expression, blue = decreased expression). A similar pattern for LAMP1 was also observed. Moreover, DAVID functional enrichment clustering gave similar enrichment results for lysosomes in HIV-1-infected and HIV-1-infected and nanoATV-treated cells by filtering the data sets at a *P* value <0.01. There was a down-regulation of endosomal and lysosomal proteins in the group of uninfected cells treated with native ATV (Figure 4.4A) or nanoATV. The latter showed few down-regulated in parallel endosomal compartments (Figure 4.4B). HIV-1 infected MDM treated with native ATV showed few altered proteins (data not shown). A composite of these protein network changes are summarized in Table 4.1.

4.4.3. Protein-protein interaction networks

To elucidate the operative and dynamic biological processes, methods depicting changes of protein interaction networks are needed. Here we used our data from SWATH-MS and applied it to the STRING bioinformatics tool to determine the dynamics of the protein interaction after HIV-1-infection with or without nanoATV treatment. Differentially expressed proteins in infected or infected and treated MDM were identified using a P-value <0.05, and protein-protein interaction [141] networks were constructed. The results of the networking reproduced a consistently high number of altered cellular proteins by HIV-1 (Figure 4.5A). The complex changes and interactions during HIV-1 infection are clearly visualized and, more importantly, the reduced complexity is clear when the infected cells are treated with nanoATV (Figure 4.5B). These dynamic changes following HIV-1 infection and nanoATV treatment provide evidence of the importance of antiretroviral therapy to control protein-protein interaction networks.

4.4.4. Antiretroviral activities of native and nanoformulated ATV

To confirm the antiretroviral activity of the nanoATV treatment the HIV-1 RT activity was determined in native- or nanoATV-treated HIV-1-infected MDM. Cells were treated with 10,100 or 250 μM of native drug or nanoATV for 16 hours, followed by HIV-1_{ADA} challenge at an MOI of 0.1 at days 0, 5 and 10 after treatment. Infected cells were cultured for an additional 7 days and RT activity in the culture medium was determined. Significant differences were found between cells treated with native- or nanoATV. For native ATV treated cells, RT activity was suppressed only in the day 0 infection group, at all treatment concentrations. At 10 and 100 μM little antiviral suppression was observed in the day 5 and 10 infection groups. In contrast, for cells treated with nanoATV, RT activity was suppressed to less than 20% HIV-1 positive control with all treatment concentrations and at all infection days (Figure 4.6)

4.4.5. Endolysosomal proteins deregulated HIV-1 and nanoATV

We selected the proteins from the KEGG pathway related to phagosome and endosomal compartment which were oppositely regulated by HIV-1 and HIV-1/nanoATV, (Rab 5, -7, -11 and LAMP 1), for validation of the proteomics analysis. Protein expression of Rab 5, -7, -11 and LAMP1 was determined by Western blot. As shown in Figure 4.7, there was a down-regulation in Rab 5, -7, -11 and LAMP1 protein expression in nanoATV-treated infected cells group. This effect was greater than that seen with native ATV treatment, validating the KEGG analyses, and was time dependent, highlighting the dynamic nature of endosomal trafficking based on macrophage differentiation, viral infection and nanoparticle treatments. Notably, assay of Rab protein levels, at multiple days following of HIV-1 infection and antiretroviral treatment revealed that nanoATV while inducing a significant down-regulation of endosomal and lysosomal proteins the effects paralleled what was observed in uninfected cells. Moreover, the downregulation was significant as it was sustained over 10 days. To better assess the potential relationships between the virus, Rab protein and nanoART we used immunofluorescence to visualize if co-localization of Rab7 or LAMP1, HIV-1 p24 and nanoATV could occur. Immunofluorescence co-localization (Figure 4.8) demonstrated that HIV-1 p24 (yellow), Rab7 or LAMP1 cellular proteins and nanoATV were in the identical cellular locale. These results highlight the fact that the endosomal trafficking routes taken by the virus and the nanoparticles are identical. Most importantly the results support the idea that HIV-1 and nanoATV while present in the identical subcellular locale influence endosomal trafficking in opposite ways.

4.4.6. Cytokine profile for HIV-1 and nanoATV

To assess the activation state of the MDM, cytokine production was determined in HIV-1 infected cells with or without nanoATV treatment. Cell culture media from

nanoATV treated and untreated HIV-1 infected and uninfected MDM were incubated with capture beads for IL-12, TNF, IL-10, IL-6, IL-1b and IL-8 and a detection fluorochromo. Acquisition was performed by FACSArray cytometry. IL-12 and TNF were increased in HIV-1 infected MDM. However, when the infected cells were treated with nanoATV cytokine levels were reduced (Figure 4.9), implying a positive correlation with endosomal and lysosomal proteins expression in our analysis mentioned above. NanoATV treated infected macrophages also expressed higher levels of IL-6 and IL-8, compared to infected and uninfected cells. There were no significant changes for IL-10 and IL-1b (data not shown). These results showed a negative correlation in the expression of IL-12 and TNF between treated and untreated HIV-1 infected MDM, suggesting a role for nanoATV as a regulator of pro-inflammatory cytokines.

4.5. Discussion

While it is well known that HIV-1 alters cellular nucleic acid binding and regulatory protein functions affecting its transcription and translation [129, 142-144] how such virus-host cell interactions are altered by nanoART is not understood [81]. To this end, we used functional proteomics, cell biology and protein chemistry to investigate potential interactions between the virus, the host cell and nanoART to elucidate how common endocytic trafficking pathways can be engaged to both support viral replication and, at the same time, affect its elimination. Endolysosomal pathways were uncovered and found to be antagonistic in HIV-1 infected cells with nanoATV treatment. Notably, the results highlight how the cell can be manipulated to either facilitate or inhibit viral growth.

The data also serves to highlight unique cellular processes engaged in both the viral replication cycle and the means to attenuate it. Within an infected cell, virions are formed in association with the cellular membrane. Initial investigations of HIV-1 assembly in

macrophages were done through electron microscopy studies and suggested that new virions were formed from the limiting membrane of a late endosomal compartment that was linked to vesicle formations as is known to occur in multi-vesicular bodies (MVB) but not at the plasma membrane known to be operative in T cells [113]. The linkage between Endosomal Sorting Complex Required for Transport (ESCRT), MVB biogenesis and viral budding is well known. In past years it was thought that HIV-1 budding is linked to ESCRT through the presence of late endosomal markers associated with macrophage-derived virions. However, the model has now been re-examined with several recent reports show that the viral compartment has a neutral pH and can be connected to the plasma membrane by micro-channels. [145-150]. We posit that the virion trafficking and viral budding can be two independent but not mutually exclusive pathways. Both are likely operative. *First*, we now show through cross validations of proteomic, cell biology and protein chemistry is that the endolysosomal machinery is significantly deregulated by HIV-1 infection and in opposite manner by nanoART treatment. *Second*, there is a close association between endosomal-linked pathways that include Rab5, -7 and -11 and viral infection. *Third*, the fact that this pathway is conversely down regulated by HIV-1 infection likely reflects that the ability of the virus to hijack ESCRT is augmented by the drug nanoparticles. Such a theory was previously put forward in our own past works [81]. In regards to assembly and intracellular accumulation of progeny HIV-1 we need not discount the elegant work performed by immunofluorescence microscopy and immunoelectron microscopy that the organelles are of an internally sequestered plasma membrane domain divergent from endosomes. Both pathways can be operative in this scenario and are not mutually exclusive from one another. Nonetheless, there is little question that virions are endosomal-associated. Progeny virions are pulled down associated with these proteins and reverse transcriptase activities are reduced significantly in parallel structures. While we did not

study the tetraspanins CD81, CD9, and CD53, their regulation in phagocytosis or intracellular trafficking is appreciated [151]. It is noted that CD81 is linked to activation of mononuclear phagocytes, notably microglia [152]. Moreover, they are also involved in the formulation of multinucleated giant cells [153] an additional major feature of viral infection in macrophages. Rab proteins function to evade degradation and direct transport to intracellular locations and utilize host vesicles to affect a stable intracellular niche for microbial stability and longevity [154]. Thus, it is not surprising that HIV-1 would induce these pathways. While the uninfected macrophages, the proteins are at the cell surface and in intracellular vacuole-like structures with a complex content of vesicles and interconnected membranes these compartments are in a dynamic state within the cell and strongly regulated by HIV-1. While we acknowledge that endosome markers could be recruited to the viral structures and incorporated into virions the dynamic process of the virus and the macrophage transcends progeny virion assembly and includes viral trafficking and transport mechanisms. Such observations combined with a broader theory of the complexity of virus-cell interactions in the infected macrophages heralds the notion that multiple events are operative for virion assembly and persistence [155].

NanoART enters the macrophages primarily through clathrin-mediated pathways and is then stored in endocytic compartments. This provides a protected environment for release of the drug to sites of viral growth. Compared with nanoART, the non-fromulated native drug didn’t show similar trafficking behavior since less endolysosomal proteins were found related to native drug treatment. On the one hand, amorphous native drug can hardly be taken or stored by macrophage; on the other hand, native drug cannot be internalized or carried by subcellular compartments for intracellular transportation. Subcellular distribution of nanoformulated ART is in late and recycling endosomal compartments. These same compartments serve as drug depots. Since late endosomes

are sites of viral assembly, nanoART stored within such compartments can retain significant antiretroviral activity. This was clearly demonstrated by the significant reductions in HIV-1 RT activity previously observed in isolated endosomal compartments in nanoATV treated HIV-1 infected MDM.

All together, the current studies suggest a mechanism whereby the endolysosomal pathway is harnessed for HIV-1 viral replication and this same pathway may provide a means for its elimination. Indeed, while it is known that HIV-1 traffics through Rab5, -7, and -11 endosomal compartments how such early, late, and recycling endosomal pools regulate stages of the viral life cycle are not understood [156]. Such an intersection though is believed critical to the viral life cycle as the functions of the compartments serve to maintain cell homeostasis and protein transport [157]. It has been reported that Rab5 regulates clathrin-mediated endocytosis from the plasma membrane to early endosome pools serve as an intersection point for proteins sorted to undergo degradation through Rab7-dependent late endosome and lysosomal routes or be sorted back to the plasma membrane through Rab11-dependent recycling pathways [156]. The ability of the macrophage to overcome such degradation events at the subcellular level underlie its abilities to persistent in its macrophage reservoir [156]. Moreover, it is well known and accepted that Rab proteins function to evade degradation and direct transport to intracellular locations and utilize host vesicles to affect a stable intracellular niche for microbial stability and longevity. Similar mechanisms certainly parallel the persistence of nanoART and sustained drug depots for extended time periods. Notably, while proteomic tests revealed a large number of proteins deregulated by HIV-1 infection and these were the same protein sets also affected by nanoART. The protein sets included those affecting nucleic acid binding, hydrolase and enzyme activities, oxidoreductase responses, and the cellular cytoskeletal backbone. These were all characterized by GO molecular function that placed Rab5 and -7 proteins as those

engaged in GTP catabolic processes, endocytosis and small GTPase-mediated signal transduction pathways. The molecular functions for both endosomal-linked proteins are GDP/GTPase activity and protein binding [158]. LAMP1 is associated with autophagy, the establishment of protein localization to cell organelles, golgi to lysosome transport, protein transport along microtubules and regulation of natural killer cell degranulation cytotoxic activities. For the cellular component GO classification, LAMP1 is located at the late endosome, lysosome, multivesicular body and vesicular exosome. It is included in the group of enzyme and protein binding molecular function protein sets. Indeed, as GO information, Rab family members are small, RAS-related GTP-binding proteins that regulate vesicular transport. Each Rab targets multiple proteins that act in exocytic and endocytic pathways.

An important finding in the current study was that Rab5, -7 and -11 and LAMP1 were significantly upregulated in expression following HIV-1 infection. HIV-1 could induce those proteins linked to endosomes. While endosome markers could be recruited to the viral structures and incorporated into virions the dynamic process of the virus and the macrophage transcends progeny virion assembly but also viral trafficking and transport mechanisms also strongly affected during the dynamic course of viral infection. Interestingly, Rab 5, -7, -11 and LAMP1 deregulation in infected MDM was reversed, in part, by nanoATV. The extent of protein deregulation in infected MDM was reduced by nanoATV. As shown in some studies, Rab5 has a role in endocytosis and post-endocytic trafficking [159]. Its activation promotes focal adhesion disassembly, migration and invasiveness in tumor cells [160] and its knockdown decreases cell motility and invasion by an integrin-mediated signaling pathway [161]. Moreover, it has been indicated that Rab5, -7 and -11, affect RGS4 trafficking through plasma membrane recycling or endosomes [158] and are used by the drug particles and the virus in a coordinated manner. This was seen for other viral infections such as hepatitis B virus, which can

affect Rab5 and -7 expression and use pathways for viral transport from early to mature endosomes. This is a required step in the viral life cycle [162]. Similarly, in our study, following endocytosis HIV-1 travels through the complex endocytic pathway networks to reach the nucleus and initiate its replication and as such support the notion that endosomal proteins play a critical role in the viral life cycle.

Interestingly, Rab5, -7 and -11 and LAMP1 were down-regulated in HIV-1 and nanoATV-treated cells. This opposite regulation between HIV-1 and nanoATV in regulation of endosomal proteins is likely important in that cellular trafficking pathways and may also be involved in the release of infectious progeny virus. As such late endosome-associated Rab7A is known to be required for HIV-1 propagation, regulation of Env processing and the incorporation of mature Env glycoproteins into viral particle [163]. In addition Rab7A promotes Vpu interaction with BST2/tetherin to facilitate HIV-1 release [164]. This may also be operative for nanoparticle viral interactions and suggests that in the present study nanoATV may disrupt mechanisms of critical cellular protein-protein interactions harnessed during the viral life cycles to perpetuate its growth. In other studies, silencing the expression of Rab9 inhibited HIV-replication [141] and silencing the endogenous Rab11a GTPase expression could destabilize HIV-1 Gag and reduce virion production both *in vitro* and in NOD/SCID/gc-/- mice [165]. It has been well documented that Rab11 is located on pericentriolar recycling endosomes and plays a key role in regulating vesicle trafficking through recycling endosomes to the plasma membrane as well as in exocytosis [81, 114, 166]. Therefore, down regulation of Rab11, as shown in our study, could destabilize HIV-1 proteins that would fail to traffic through the endosomal compartments and could be redirected for degradation at the lysosomal site.

The deregulation of endosomal proteins suggests a new mechanism for viral suppression by nanoART. This includes altered expression of endosomal proteins resulting in parallel reductions in viral assembly sites. In addition, reduction of LAMP1 following nanoART treatment could reduce degradation of the nanoparticles and therefore extend the half-life of ART. Our data is corroborated by studies demonstrating co-localization of HIV-1 and endosomal and lysosomal proteins (Rab7 and LAMP1) [81, 167, 168]. Moreover, differences in cytokine profile expressions in untreated and nanoATV treated infected HIV-1 macrophages suggest that nanoATV down regulated the expression of pro-inflammatory cytokines. HIV-1 has been linked to the up-regulation of cytokines and in fact HIV-1 Tat upregulates IL-12 and TNF-α and -β expression in monocyte-derived dendritic cells [169, 170], suggesting an advantage of nanoATV in the regulation of pro-inflammatory cytokines during HIV-1 infection. In contrast with nanoATV, the effect of native ATV was relatively lower. Moreover, it has been reported that IL-12 up-regulates Rab7 and induces lysosomal transport. Others have reported that Rab proteins are regulated by cytokines and affect TNF secretion by activated macrophages [171-173]. These findings provide further support to link Rab, IL-12 and TNF expression. As HIV-1 virions assemble at the plasma membrane and recruit endosomes to enable particle release, nanoATV depletes endosomal/lysosomal proteins and deregulates pro-inflammatory cytokines thus controlling viral growth. Although a mechanism is now forged to bridge nanoATV activities and endosomal signaling pathways this study serves as only an entry to future investigations.

To this end, we are currently examining the possible signaling pathways deregulated by nanoATV. Altogether, we found that SWATH-MS proteomics, bioinformatics analyses and cell biology showed that nanoATV treatment of HIV-infected MDM can down-regulate the endocytic proteins in HIV-1 infected cells and thus

decrease the subcellular space available for viral assembly. Through this mechanism, nanoATV has unique but real potential towards improving virus clearance. Our work articulates commonly used pathways that are engaged in common macrophage functions such as phagocytosis and vesicular trafficking that are used both by the virus and the anti-virus.

4.6. Conclusions

HIV-1 and nanoATV deregulate cellular proteins in opposing manners. The common pathways are linked to viral assembly and are endolysosomal-linked. Rab5, 7, 11 and LAMP1 serve to coordinate molecular and biological functions of the virus and the antivirus in subcellular compartments. Alterations made by HIV-1 and nanoATV indicate that specific organelles are action sites for both. These findings provide novel insights into the role played by long acting subcellular targeted nanotherapies for combating HIV-1 infection.

A

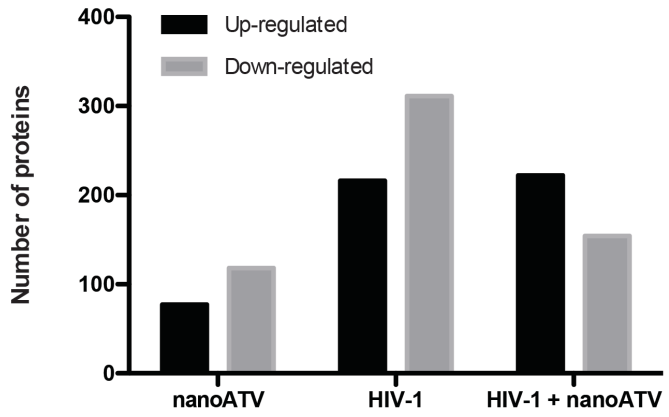

B

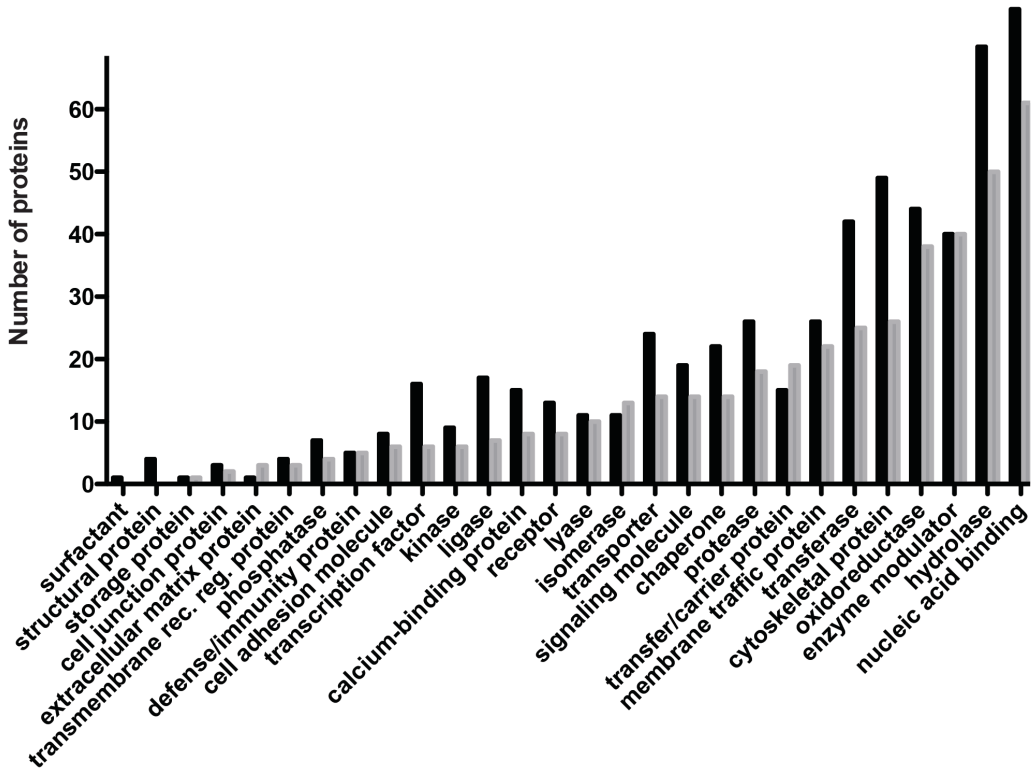

Figure 4.1. Deregulated proteins during HIV-1 infection and nanoATV treatment. Uninfected and HIV-1 infected MDM were treated with or without nanoATV. The cells were then collected for peptide identification. (A) Numbers of significantly up- or down-regulated proteins were identified by mass-spectrometry based proteomics (SWATH-

MS) and compared to uninfected and untreated MDM used as controls. (B) Numbers of proteins changed by PANTHER were classified according to protein class. These were represented by 28 independent clusters ($p<0.05$).

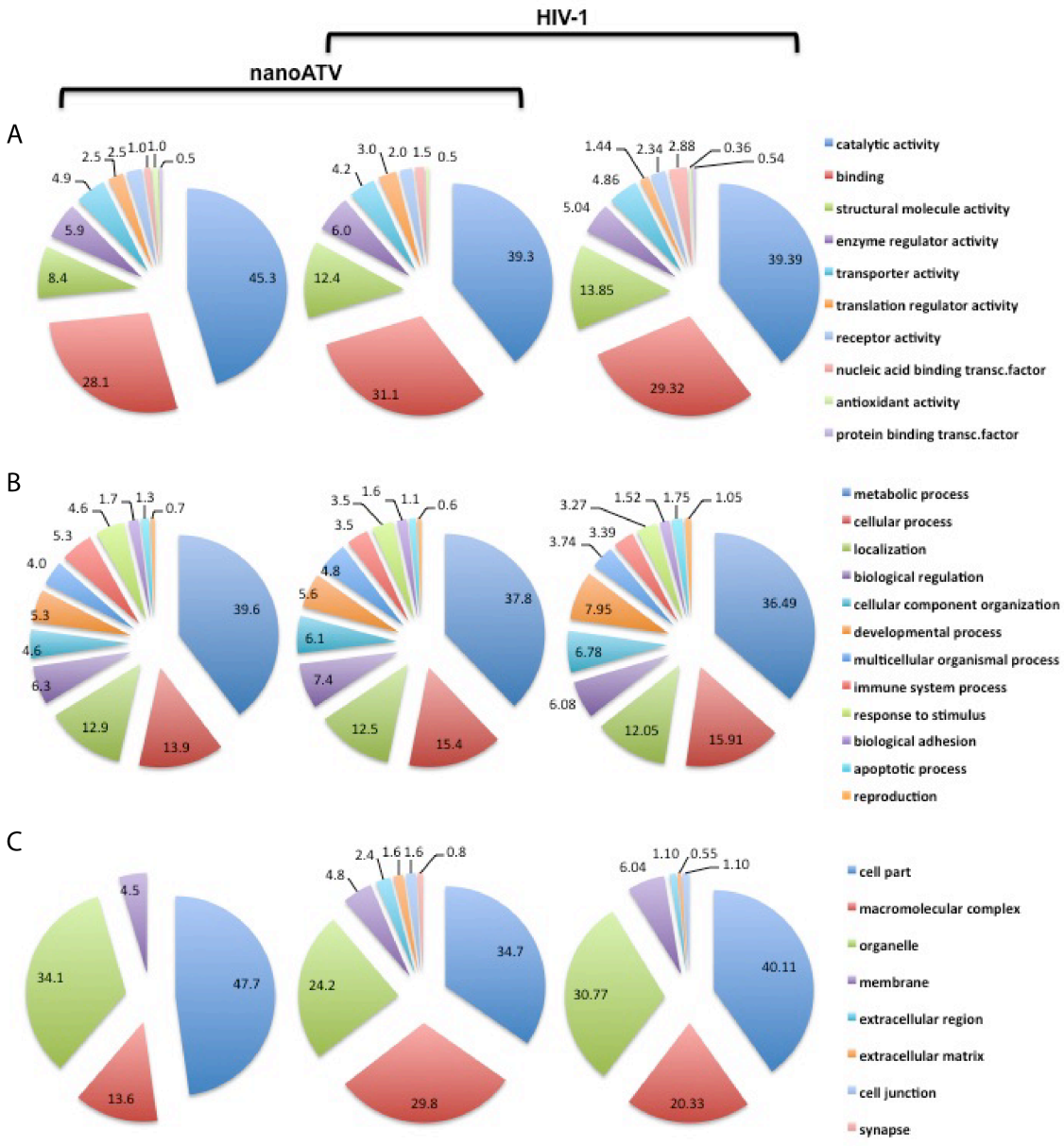

Figure 4.2. Functional characterization of significant deregulated proteins between uninfected and HIV-1-infected and nanoATV treated MDM.

Proteins were compared to uninfected/untreated control cells ($p<0.05$) then bioinformatics analysis was performed. The Gene Ontology molecular function (A), biological processes (B) and cellular component distribution (C) were obtained from the analysis using the Protein Analysis Through Evolutionary Relationships (PANTHER) classification system.

A. HIV-1

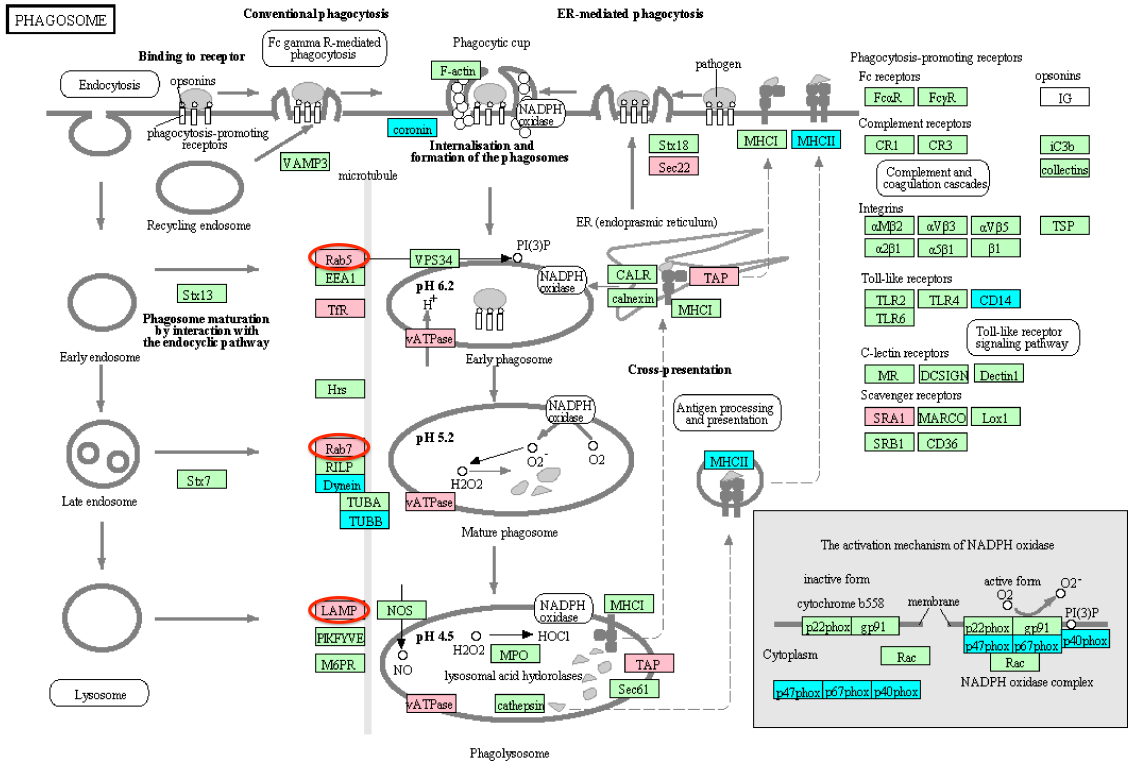

B. HIV-1 + nanoATV

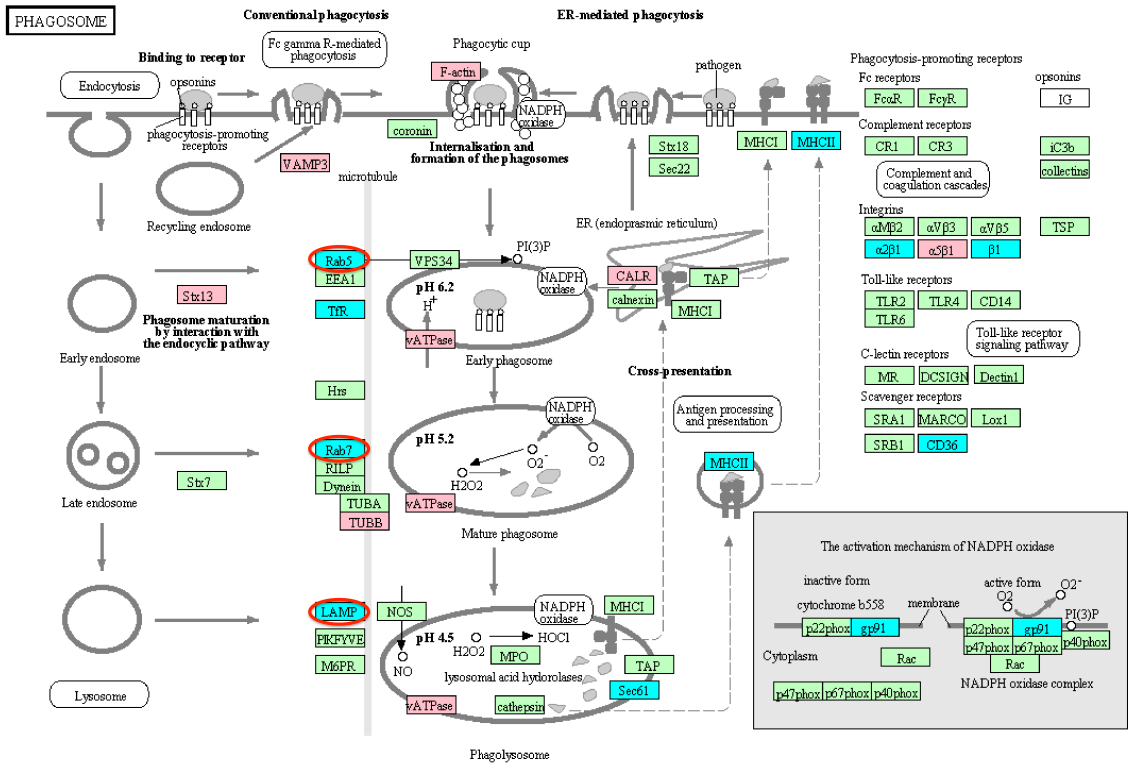

Figure 4.3. Schematic representation of the MDM phagosome network identified in HIV-1-infected (A) and HIV-1-infected and nanoATV treated cells (B).

Proteins identified were compared against control uninfected MDM cultures ($p<0.05$). The acquired profiles were analyzed through the bioinformatics program using a comprehensive set of functional annotation tools to uncover biological data sets behind the uncovered list of genes. This tool is titled Data for Annotation, Visualization and Integrated Discovery (DAVID) facilitated the linked sets of enriched functional-related protein groups. This tool was employed to identify enriched biological processes among the expressed proteins. Gene Ontology terms were used to identify related pathways with the assistance of the Kyoto Encyclopedia of Genes and Genomes (KEGG) database. The KEGG database facilitated the elucidation of the level functions for the MDM as derived from the proteomic datasets. Statistical significance was determined using a *p*-value < 0.05. Proteins in red and blue, display up- and down- regulation, respectively. Proteins in green belong to the phagosome network and not deregulated by ATV treatment.

A. nativeATV

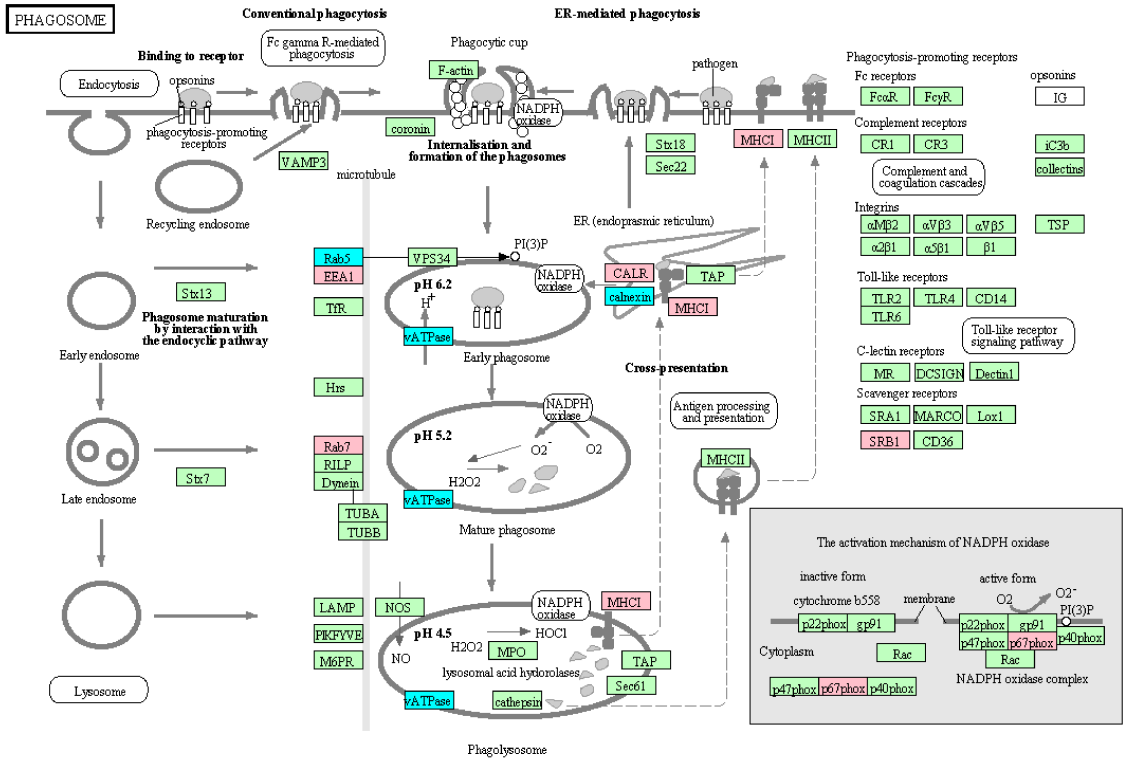

B. nanoATV

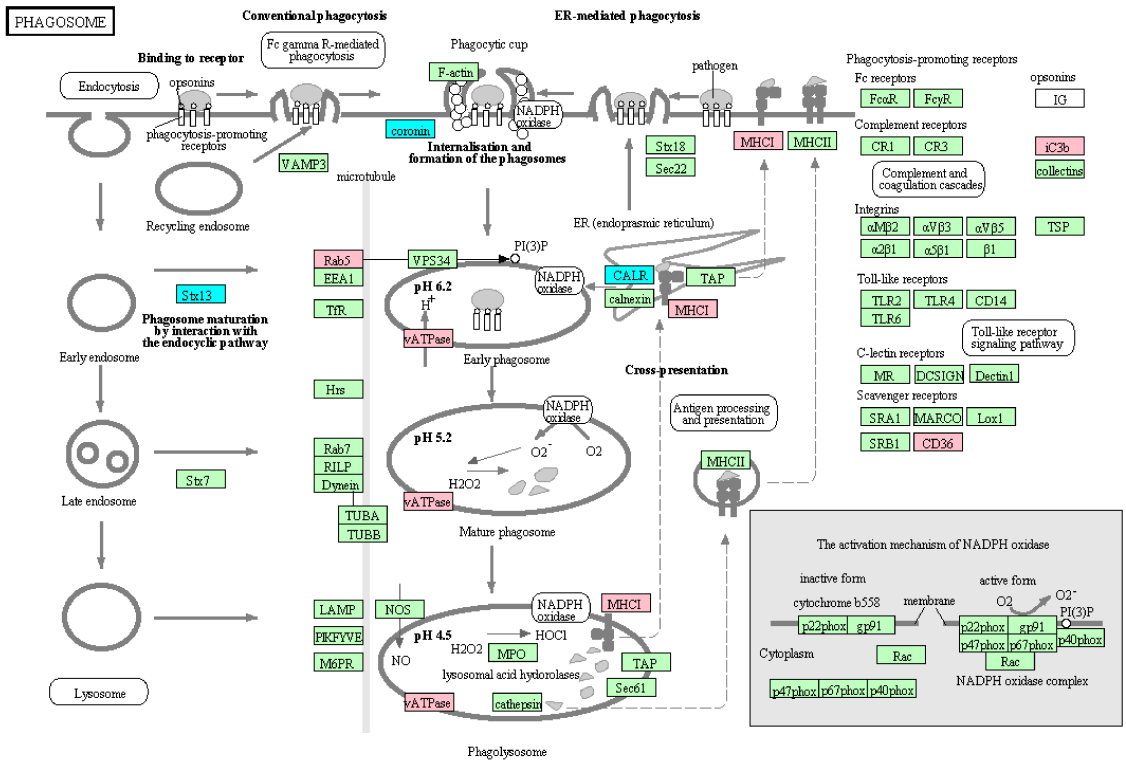

Figure 4.4. Changes in MDM phagosome network for uninfected cells treated treated with nanoATV (A) or native ATV (B).

Proteins were compared to uninfected and untreated MDM controls ($p<0.05$) then bioinformatics analysis performed following parallel procedures described in Figure 4.1. Proteins in red and blue, display up- and down- regulation, respectively. Proteins in green belong to the phagosome network but were not significantly altered by viral infection or treatment.

A. Protein interaction in HIV-1-infected MDM

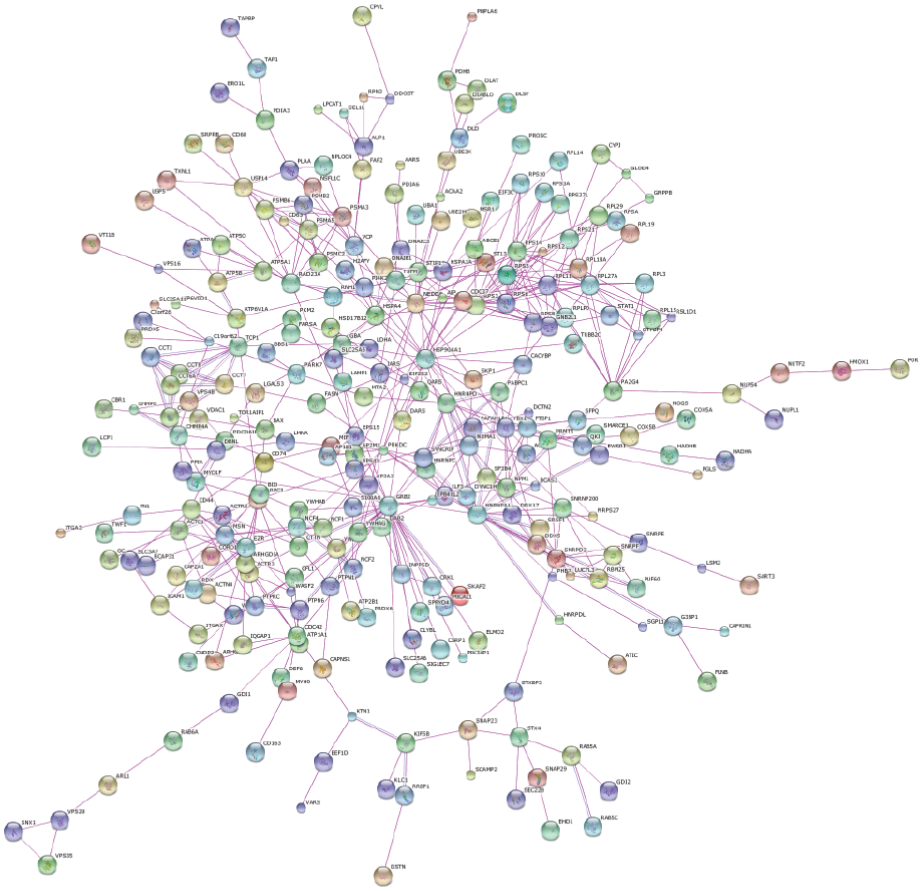

B. Protein interaction in nanoATV treated HIV-1-infected MDM

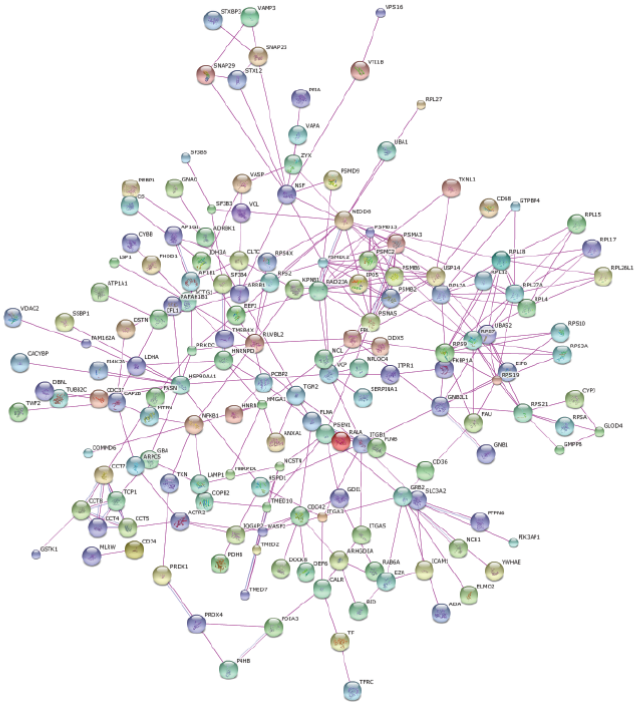

Figure 4.5. Protein interaction in HIV-1-infected MDM or nanoATV treated HIV-1-infected MDM.

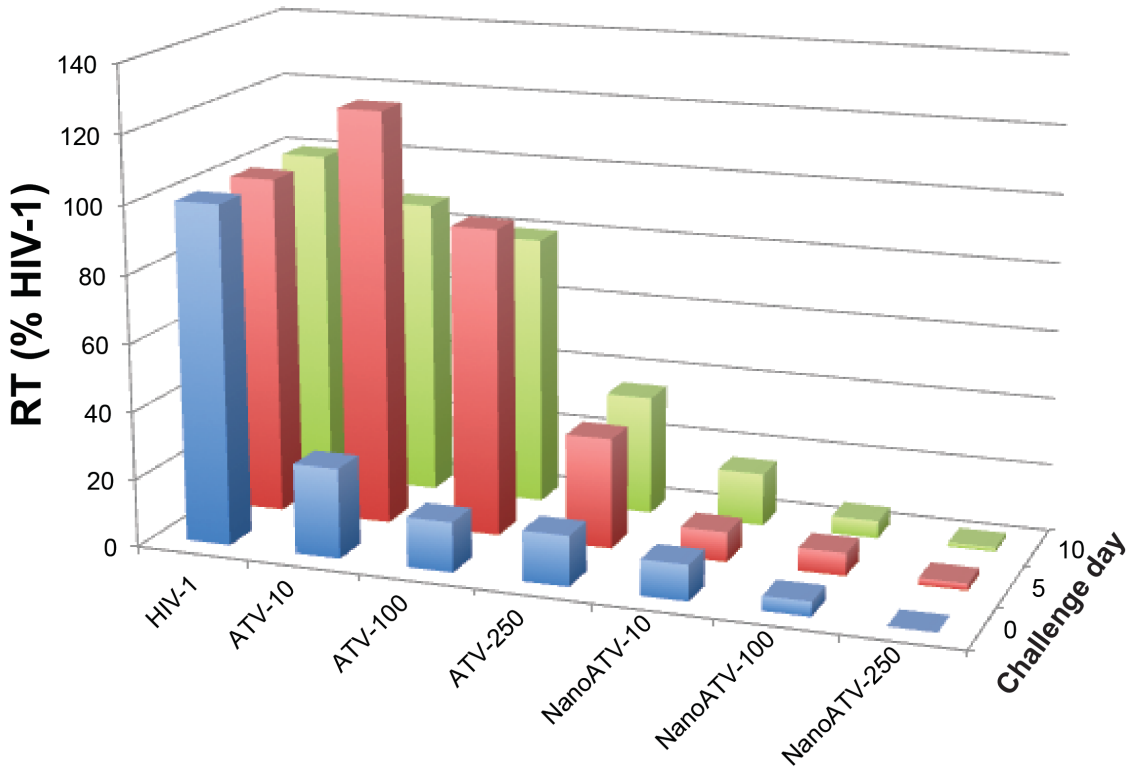

Figure 4.6. NanoATV treatment effects HIV-1 reverse transcriptase (RT) activity. HIV-1 RT activity was determined in treated (native ATV or nanoATV) MDM followed by HIV-1 infection at days 0, 5 or 10. HIV-1 infected cells, without any treatment, served as a positive control for RT activity. All samples were collected after 7 days of viral infection. Results shown are the mean of 5 replicates.

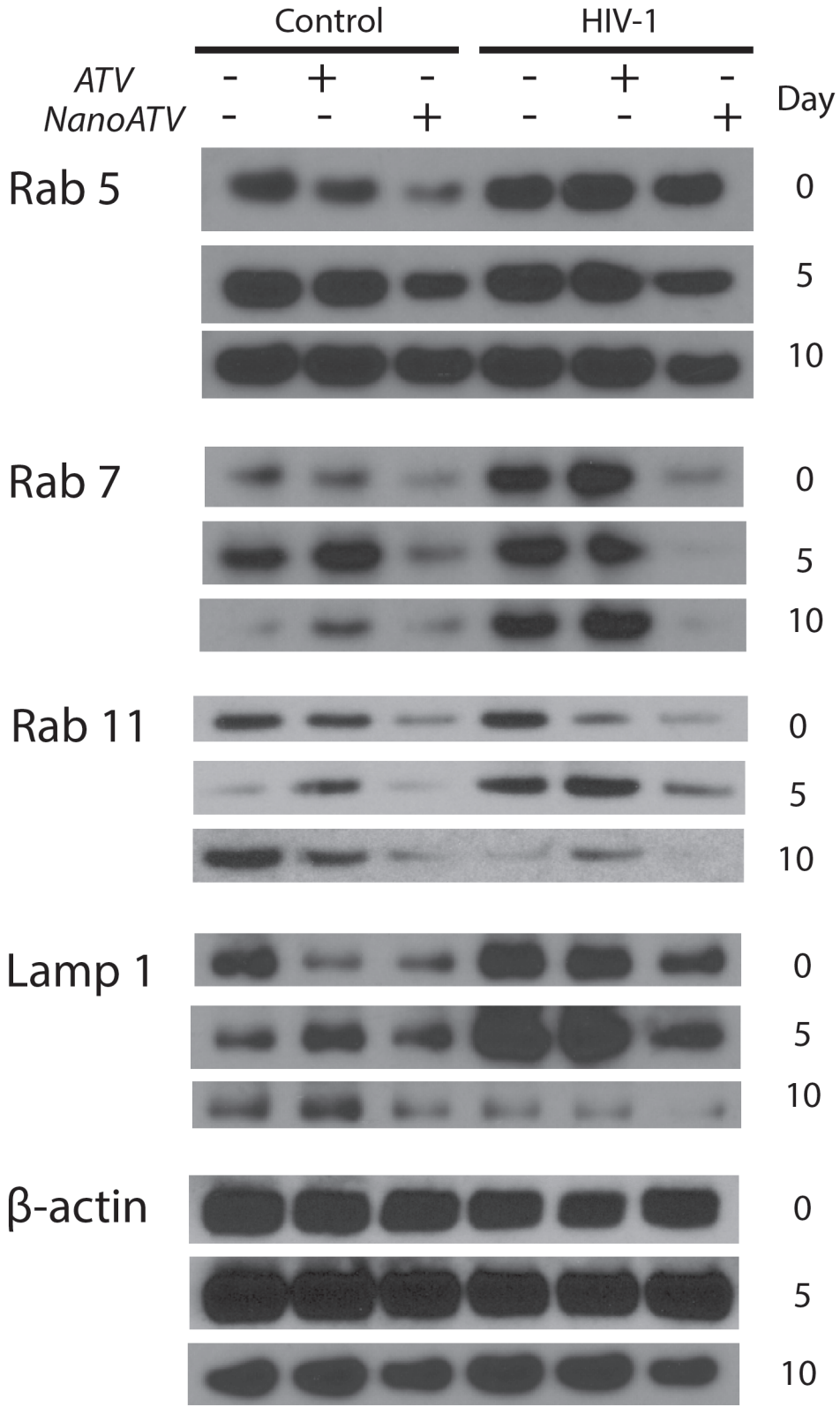
Control
HIV-1
ATV
NanoATV
- + - - + -
- - + - - +
Day
Rab 5
0
5
10
Rab 7
0
5
10
Rab 11
0
5
10
Lamp 1
0
5
10
β-actin
0
5
10

Figure 4.7. NanoATV and HIV-1 endosomal protein regulation.

Western blot of Rab5, -7, -11, LAMP1 and β-actin was performed in cell lysates from MDM treated with native ATV or nanoATV and infected with HIV-1 at day 0, 5 or 10 post-drug treatment then incubated for 7 days. Uninfected cells and infected cells without drug treatment served as negative and positive controls for differential expression of cellular proteins during HIV-1 infection. Blots shown are from one donor and experiment, and equivalent to two independent experiments performed.

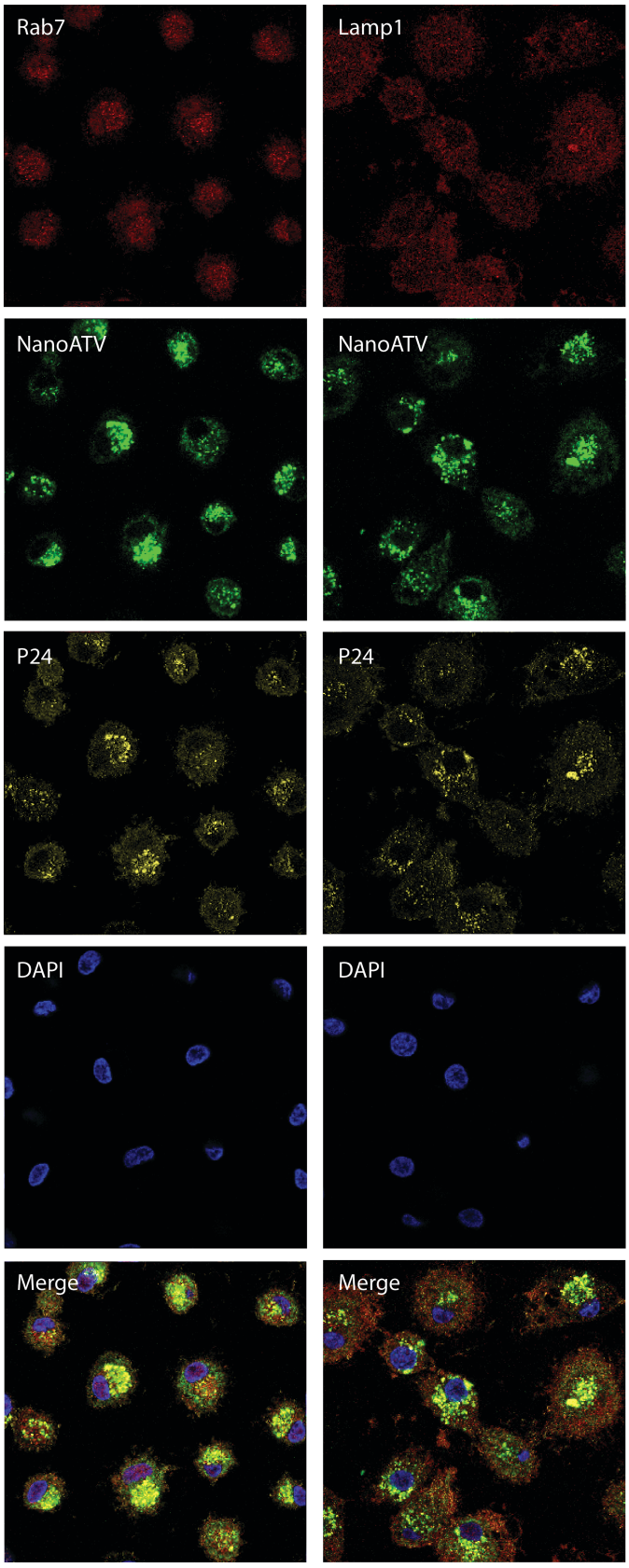
Rab7
Lamp1
NanoATV
NanoATV
P24
P24
DAPI
DAPI
Merge
Merge

Figure 4.8. Subcellular localization of nanoATV, HIV-1 and endolysosomal proteins. Cellular localization of Rab7 or LAMP1 endosomal compartments [51], HIV-1p24 (yellow) and nanoATV [174] are shown by confocal microscopy. Cell nuclei were stained with DAPI (blue). Merged images showed the co-localization of all proteins. Fluorescence images were acquired with a LSM 510 confocal microscopy, 400x magnification.

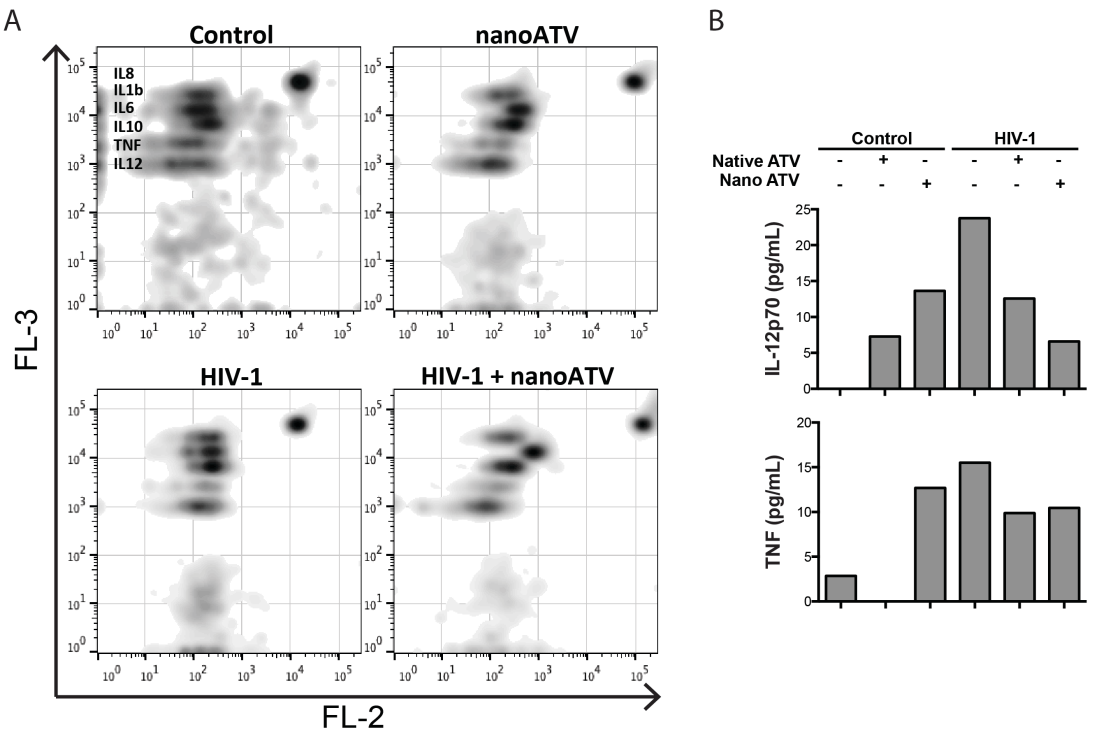

Figure 4.9. NanoATV regulation of cytokine profiles in HIV-1 infected MDM.

MDM were treated with 100 μM native ATV or nanoATV and infected with HIV-1 at day 0, 5 or 10 post-drug treatment. Untreated, uninfected cells were used as controls. After 24 hours of viral infection, cell culture media were collected and analyzed using a cytokine bead array. (A) Density plots show expression of IL-12, TNF, IL-10, IL-6, IL-1b and IL-8 for control, treated, HIV-1 infected and treated infected MDM. Cytokine levels were detected by FACSArray cytometer and data was plotted using FlowJo (version 10.7) software. (B) Levels of IL-12 and TNF after treatment and infection are shown. Data are analyzed using FCAP software and values of cytokine expression were expressed as pg/mL.

Table 4.1. Endolysosomal proteins in HIV-1, HIV+nanoATV, nanoATV and native ATV treated MDM.

Deregulated (up- and down- regulated) proteins from the endolysomal (or phagosome) pathway were grouped into early or late endosomes or lysosomes signalling. Z test values were obtained after proteomics analyses. Up-, down- regulation or unchanged protein expression are represented by red, blue and green arrow, respectively.

		HIV		*HIV+nanoATV*		*nativeATV*		*nanoATV*	
	Protein	Ztest	Regulation	Ztest	Regulation	Z test	Regulation	Z test	Regulation
Early endosomes	Rab5	4.09	↑	-2.57	↓	-2.35	↓	2.87	↑
	TAP	3.38	↑	--	↔	--	↔	--	↔
	TfR	2.62	↑	-3.02	↓	--	↔	--	↔
	vATPase	3.70	↑	2.32	↑	-5.21	↓	-2.02	↓
	Stx13	--	↔	3.47	↑	--	↔	-2.43	↓
	EEA1	--	↔	--	↔	2.62	↑	--	↔
	VPS34	--	↔	--	↔	--	↔	--	↔
	CALR	--	↔	2.03	↑	2.29	↑	-3.73	↓
	Calnexin	--	↔	--	↔	-3.40	↔	--	↔
Late endosomes	Rab7	2.71	↑	-2.62	↓	3.87	↑	--	↔
	vATPase	3.70	↑	2.30	↑	-5.20	↓	-2.02	↓
	Dynein	-2.01	↓	--	↔	--	↔	--	↔
	TUBB	-2.90	↓	2.81	↑	--	↔	--	↔
	TUBA	--	↔	--	↔	--	↔	--	↔
	RILP	--	↔	--	↔	--	↔	--	↔
	Stx7	--	↔	--	↔	--	↔	--	↔
Lysosomes	LAMP	2.88	↑	-2.23	↓	--	↔	--	↔
	vATPase	3.70	↑	2.30	↑	-5.20	↓	-2.02	↓
	TAP	3.40	↑	--	↔	--	↔	--	↔
	M6PR	--	↔	--	↔	--	↔	--	↔
	Cathepsin	--	↔	--	↔	--	↔	--	↔

↓ *Downregulated* ↔ *unchanged* ↑ *Upregulated*

Chapter V.

Small magnetite antiretroviral therapeutic nanoparticle probes

5.1. Abstract

Drug toxicities, patient compliance and limited penetrance into viral reservoirs have diminished the efficacy of long-term antiretroviral therapy (ART) for treatment of human immunodeficiency viral (HIV) infection. In response, cell targeted nanoformulated ART (nanoART) was developed to facilitate drug adherence and improve disease outcomes. However, rapid noninvasive determination of drug biodistribution in virus-target tissues and reservoirs for nanoART have remained unrealized. To this end, small magnetite ART (SMART) particles were made providing, for the first time, noninvasive assessments of antiretroviral drug tissue distribution through magnetic resonance imaging (MRI) techniques. Here, poly(lactic-co-glycolic acid), 1,2-distearoyl-*sn*-glycero-3-phosphocholine and 1,2-distearoyl-*sn*-glycero-3-phosphoethanolamine-N-[methoxy (polyethylene glycol)-2000] encased particles were synthesized that contained atazanavir (ATV) and ultra small paramagnetic iron oxide (referred to as magnetite). Cellular uptake and retention of magnetite and ATV were first performed in human monocyte-derived macrophages (MDM). Here tandem mass spectrometry showed that SMART particles were efficiently taken up and retained in MDM. In mice, magnetite and drug biodistribution paralleled one another, as readily seen after parenteral injections. Three to one ratio of ATV to magnetite allowed drug assessments, for proof of concept experiments, continuously up to 4 and again at 24 hours after particle injection. T_2 maps and 3D spoiled gradient recalled echo image sets confirmed rapid drug tissue distribution in the reticuloendothelial system including spleen, liver, kidney and lung. At four hours, T_2 mapping showed predominant vascular particle distribution. However, by 24 hours signal intensity was seen in liver and spleen with little to no magnetite in kidneys. Significantly, ATV tissue levels correlated with changes in tissue relaxivity

($DR_2=1/T_{2postinjection}-1/T_{2preinjection}$). We conclude that SMART can facilitate the evaluation of drug tissue concentrations in viral reservoirs and provide rapid assessments for the next generation cell and tissue ligand decorated particles.

5.2. Introduction

Eradication of the human immunodeficiency virus type one (HIV-1) in its infected human host will necessitate antiretroviral drug delivery to viral sanctuaries with the secondary elimination of latent or restricted infections [75]. The former could be facilitated through targeted nanoparticle drug delivery but, to achieve its potential, would require improved virus-target tissue drug bioavailability. One major hurdle towards achieving this goal is the dearth of any means to measure antiretroviral therapy (ART) distribution outside of plasma drug levels [76]. We theorized that one way to achieve this is by combinations of small magnetite particles and ART in a single nanoparticle. If realized, such small magnetite ART (SMART) could permit rapid pharmacokinetic and pharmacodynamics evaluations of ART in virus-target tissues, such as the lymph nodes and brain. Drug biodistribution would readily be quantitated by a conventional magnetic resonance imaging (MRI) scan. Such an approach would also provide the potential of delivering packaged medicines to sites of limited viral growth and serve, in part, to eliminate the viral reservoir. The approach was previously used for magnetically targeted cancer drug delivery utilizing T_2- or T_2^*-quantification by MRI [175-178].

To perform proof of concept studies on this theranostic approach we placed magnetite, also referred to as superparamagnetic iron oxide particles, into lipid-coated polylactic-co-glycolic acid (PLGA) nanoparticles with a commonly used antiretroviral protease inhibitor, atazanavir (ATV). By combining PLGA and magnetite, organic/inorganic hybrid composite biomaterials allowed combined diagnostics, or drug distribution assessments,

with therapeutic ART delivery through a single MRI scan [80]. The SMART nanoparticle testing was sped through the availability of *in vitro* cultivated monocyte-derived macrophages (MDM) that determined optimal particle cell uptake and retention. This facilitated studies of the dynamics of *in vivo* drug tissue distribution. All together, the works provide the groundwork for the implementation of SMART systems for noninvasive drug pharmacokinetics for the inevitable goal of viral eradication.

5.3. Materials and methods

5.3.1. Material preparation and characterization

PLGA, 1,2-distearoyl-*sn*-glycero-3-phospho-choline (DSPC) and 1,2-distearoyl-*sn*-glycero-3-phosphoethanolamine-N-[methoxy-(polyethylene glycol)-2000] (DSPE-PEG_{2000}) encased the SMART particle containing ATV and magnetite. The magnetite particles were synthesized as follows: 6 mmol tris(acetylacetonato) iron(III) was mixed with 30 mmol 1,2-hexadecanediol, 18 mmol oleic acid, 18 mmol olylamine and 60 mL benzyl ether in a three-neck round-bottomed flask equipped with condenser, magnetic stirrer, thermograph and heating mantle and stirred under nitrogen. The mixture was slowly heated to 110^{o}C and kept at that temperature for 1 hour, then slowly heated to 200^{o}C. Reflux was kept after it reached 200^{o}C for 2 hours, then slowly heated to 298^{o}C and kept at reflux for another 1.5 hours. After cooling to room temperature, a dark homogeneous colloidal suspension was obtained. The suspension was precipitated in ethanol with a magnetic field. The black precipitate was dissolved in hexane with the presence of oleic acid and oleylamine and the solution was centrifuged at 3,800 x g for 10 min to remove any undispersed residue. The black solution was re-precipitated in ethanol and centrifuged at 10,000 x g for 30 min. Solid products were obtained by drying the precipitate under vacuum, generating the final dry particles.

5.3.2. SMART composition and characterization

Preparation of the drug loaded DSPC/mPEG-DSPE shell and PLGA core particle was as follows. *First*, a weighed amount of PLGA, ATV and magnetite were dissolved in chloroform (oil phase) with a weight ratio of magnetite to ATV of 1:3. *Second*, the aqueous phase was prepared by hydration of DSPC and mPEG-DSPE films. The oil phase was added to the DSPC and mPEG-DSPE aqueous solution drop-by-drop with constant stirring then sonicated for 60 seconds followed by a 20 second break under an ice bath. This procedure was repeated for three cycles. Chloroform was then removed by stirring overnight. *Third*, the particle suspension was centrifuged at 500 x g for 5 min. The supernatant fluids were collected to remove the aggregated nanoparticles. A high speed 50,000 x g centrifugation for 20 min was used to collect the nanoparticles. After washing twice with phosphate-buffered saline (PBS), the nanoparticles were resuspended. SMART size and size distribution were measured by dynamic light scattering (DLS, 90Plus, Brookhaven Instruments Co. USA) then diluted in ultrapure water related to mass concentrations and dispersions. *Fourth*, the surface charge of the SMART particles was determined by ZetaPlus, a zeta-potential analyzer (Brookhaven Instruments Co. USA). The pH value and concentration of the particles dispersion were fixed before measurements of zeta potentials. *Fifth*, the shape and surface morphology of the SMART particles were investigated by transmission electron microscopy performed as previously described [63]. Samples were prepared from dilutions in distilled water of particle suspensions and dropped onto stubs. After air drying the particles were coated with a thin layer of gold then examined by transmission electron microscopy. The magnetic properties were determined by a Physical Property Measurement System [179].

5.3.3. SMART particle stability and release of drug in isotonic solution

SMART particles were dispersed in PBS and placed into a 10 k dialysis tube in 2 L PBS under stirring at 37^{o}C. At 30 min and 1, 2, 3, 4, 6, 8 and 10 days, 100 ml of the suspension was collected. The supernatant was dissolved in 100 µl tetrahydrofuran/methanol (volume ratio 1:10) mixture. The amount of ATV and magnetite was measured by high performance liquid chromatography (HPLC) and inductively coupled plasma mass spectrometry (ICP-MS), respectively [63, 180].

5.3.4. SMART uptake and retention by MDM

Human monocytes were obtained by leukapheresis, from HIV-1 and hepatitis B seronegative donors, then purified by counter-current centrifugal elutriation [106]. Monocytes were cultured in 6-well plates at a density of 1 x 10^6 cells/ml in DMEM containing 10% heat-inactivated pooled human serum, 1% glutamine, 50 mg/ml gentamicin, 10 mg/ml ciprofloxacin and 1,000 U/ml recombinant human macrophage-colony stimulating factor [57]. After 7 days of differentiation, MDM were treated with 100 mM SMART particles, (based upon ATV content). Uptake of SMART particles was assessed without medium change for 8 hours. Adherent MDM were collected by scraping into PBS, at 1, 2, 4 and 8 hours after treatment. Cells were pelleted by centrifugation at 1000 x g for 8 min at 4^{o}C. Cell pellets were briefly sonicated in 200 ml of methanol/acetonitrile (1:1) and centrifuged at 20,000 x g for 10 min at 4^{o}C. To determine cell retention of SMART particles, MDM were exposed to 100 mM SMART particles for 8 hours, washed 3x with PBS, and fresh media without particles was added. MDM were cultured for an additional 15 days with half medium exchanges every other day. On days 1, 5, 10 and 15 after SMART treatment, MDM were collected as described for cell uptake. Cell extracts were stored at -80^{o}C until HPLC analysis [63].

5.3.5. Prussian blue staining of MDM retained SMART particles

MDM were treated with 100 mM SMART particles for 24 hours. Adherent MDM were washed 3x with PBS. Cells were fixed with 2% formalin/2.5% glutaraldehyde in PBS for 10 min then washed 2x with PBS. Fixed macrophages were treated with 5% potassium ferrocyanide/5% hydrochloric acid (1:1) for 10 min at room temperature. Following solution aspiration the cells were washed 2x with PBS. Stained cells were examined by light microscopy.

5.3.6. MRI phantoms and relaxivity measures

MDM were seeded onto 12-well plates at 1 x 10^6 cells/ml. After the cells reached 80% confluence, the medium was changed to medium containing 100 mM SMART particles (based on ATV content). Twenty-four hours later the treatment medium was removed and the cells were washed 3x with 1 ml PBS. Cells were collected and suspended at different cell concentrations (0-5 x 10^6 cells/ml) in 1% agar gel. T_2-relaxtivity was measured by MRI. Magnetite content in the cells was quantitated by ICP-MS.

5.3.7. SMART biodistribution

Biodistribution of SMART particles was determined in male Balb/cJ mice (Jackson Labs, Bar Harbor, ME). SMART particles (30 mg/kg ATV) were injected via a jugular vein cannula in a total volume of 100 ml for each mouse. The mice were scanned by MRI two hours before injection then continuously at 0.25, 1, 2 and 4 hours or at 24 hours after SMART administration. Tissues were collected following the final MRI scan. Tissue drug levels were quantitated by ultra performance liquid chromatography tandem mass spectrometry (UPLC-MS/MS) [181] and magnetite levels were determined by ICP-MS as previously described [180].

5.3.8. MRI acquisition

MRI was acquired using a 7T/16cm Bruker (Ettlingen, Germany) Pharmascan MRI/MRS scanner and a commercial mouse body resonator. SMART detection by MRI was done using T_2 mapping for quantitation and T_2^* weighted high resolution imaging for detection of biodistribution throughout the body. The sequence used for T_2 mapping was a CPMG phase cycled multislice multiecho sequence. Forty-one 0.5 mm thick contiguous interleaved coronal images were acquired with an acquisition matrix of 256 x 192, 40 mm field of view, 12 echoes at 10 ms first echo time and 10 ms echo spacing, repetition time of 4680 ms, three averages, for a total acquisition time of 30 min. T_2^* weighted MRI was acquired using a 3D spoiled gradient recalled echo sequence with echo time = 3 ms, repetition time = 10 ms, 15 degree pulse angle, 50 x 40 x 30 mm FOV, 256 x 196 x 128 acquisition matrix, six averages, for a total scan time of 25min.

5.3.9. MRI analyses

T_2 maps were reconstructed using custom programs written in Interactive Data Language (IDL; Exelis Visual Information Solutions, McLean, VA). Preinjection and 24 hour postinjection maps were constructed using the even-echo images from the CPMG phase cycled imaging data set. Mean tissue T_2 was determined using region of interest [164] analyses before and after SMART injection for the 24 hour results. Magnetite concentration was then determined from the change in relaxivity ($DR_2 = 1/T_{2preinjection} - 1/T_{2postinjection}$) and the per milligram magnetite of SMART particle relaxivity (r_2) determined as the slope of magnetite concentration versus R_2 in phantom studies.

Acute (0-4 hour) data were acquired with in-magnet jugular vein injection, allowing sequential T_2 mapping to be acquired with a T_2^* weighted FLASH image acquired at the end of a four-hour period. The natural coregistration of these data allowed development of magnetite concentration maps based on relaxivity changes using custom programs

written in IDL for the acute scanning session. The ROI analyses were performed using ImageJ (http://imagej.nih.gov/lj) software. For analysis of the acute study, the windows synchronize option was used to simultaneously draw ROIs at same locations on all concentration maps at different time points.

5.3.10. Immunohistochemical identification of cell-SMART uptake

To determine cell localization of SMART spleen and liver were collected after the final MRI scan and fixed in 10% neutral buffered formalin. Tissues were paraffin embedded and sectioned at 5 μm. To identify macrophages, sections were incubated with antibody to ionized calcium binding adaptor molecule 1 (Iba1, Wako Chemicals USA, Inc., Richmond, VA). The polymer-based HRP-conjugated anti-mouse and anti-rabbit Dako EnVision were used as secondary detection reagents and color developed with 3,3'-diaminobenzidine (DAB). All paraffin-embedded sections were stained with Prussian blue to identify magnetite content. Slides were imaged using a Nuance light microscopy system for brightfield imaging.

5.4. Results and discussion

5.4.1. SMART development and in vitro evaluation

The schematic structure of SMART is represented in Figure. 5.1A. This is composed of a hydrophobic PLGA/ATV/magnetite core and an amphiphilic DSPC and DSPE-PEG2k lipid shell. DSPC and DSPE-PEG2k increased SMART stability and facilitated increased systemic formulation circulation times. Both ATV and magnetite are distributed homogeneously within the core of the particle. SMART was made using a single oil-in-water emulsion with lipid surfactants. After sonication amphiphilic lipids self-assembled to the monolayer surrounding PLGA/ATV/magnetite containing oil droplets, achieved

through hydrophobic interactions. Evaporation of chloroform under continuous magnetic stirring allowed for the formation of lipid-coated solid PLGA/ATV/magnetite core. SMART was then purified by ultracentrifugation before further characterization. Our DLS results showed that the average size of the particles is 268 nm with a polydispersity of 0.2. The narrow size distribution is linked to the DSPC, which serves to stabilize the polymeric SMART in the aqueous phase. The zeta potential of the particles is -45.2 mV, which provides its stability when suspended in aqueous media. Although DSPC is neutral when it is used as a particle coat it exhibits non-zero mobilities in an external electric field. This may result in a higher negative charge since some anions bind to the neutral lipids making the surface more negatively charged. Transmission electron microscopy (TEM) was employed to obtain the image that best reflects SMART particle morphology (Figure. 5.1B, right panel). This illustrated that the particles were spherical in shape with narrow size distributions. A representative particle is shown by TEM, showing the ultra small iron oxide contained within the particle's core.

Our preliminary in vitro results showed that SMART is very stable and ATV can slowly release from SMART up to 10 days. After SMART particle characterizations were completed, the *in vitro* kinetics of MDM uptake and retention were determined. Our previous studies of nanoART uptake in MDM showed that > 95% of total uptake occurs by 8 hours for ATV nanoART [62, 63, 82, 182]. Up to 2 mg of ATV/ 10^6 cells was recorded in MDM at 8 hours with magnetite uptake reflective of particle composition (Figure. 5.1C). The majority of the cells took up the magnetite as observed through Prussian blue staining (Figure. 5.1D). Indeed, such staining demonstrated that magnetite-containing particles were readily incorporated in macrophages by 8 hours. The controlled and sustained release profile or ATV facilitates the application of the SMART particles for the delivery of antiretroviral drugs.

5.4.2. Measures of SMART particle relaxivity (r_2)

Concentration dependent relaxivity [r_2 (s^{-1} ml mg^{-1})] causing increased relaxivity (R_2 (s^{-1})) in tissue as a function of concentration (expressed as mg/ml magnetite) of SMART particles were determined using phantoms consisting of both free SMART particles (Figure. 5.2A) and SMART particles taken up by MDM (Figure. 5.2B). The magnetite concentrations in mg/ml contained by SMART in 1% agar gels were plotted against R_2 as measured by MRI. The relationship between R_2 and magnetite concentration of SMART in phantoms was linear within the range of the measured magnetite concentrations. The concentration dependent relaxivity of SMART was found to be r_2 = 6200.2 (s^{-1} ml mg^{-1}) in MDM and r_2 = 7052.1 (s^{-1} ml mg^{-1}) in PBS. The r_2 of SMART in MDM was used for noninvasive in vivo quantitation of magnetite concentration due to SMART influx using MRI.

5.4.3. Real time SMART biodistribution and pharmacokinetics

Magnetite labeling allows MRI to be used to quantify the distribution of SMART particles over time in live animals. This can be seen in Figure. 5.3. Figure. 5.3A shows examples of magnetite concentration (from magnetite in SMART) constructed from MRI T_2 maps measured before and continuously every 30 minutes for four hours after SMART injection. ROI analyses of these data from six animals are shown in Figure. 5.3B. It can be appreciated from the images that a significant amount of the SMART is still within the vasculature, largely leading to the intensity in the kidney, as kidney shows very little uptake by 24 hours. This reflects the measured concentration in kidney reducing over the first four hours while in liver and spleen, organs where SMART accumulates, the mean signal is relatively constant or increases as the particles redistribute from the blood to the tissue. Significant accumulation of SMART was found in liver and spleen at 4 hours as can be appreciated in Figure. 5.4. Figure. 5.4 displays two of the 0.128 mm

thick T_2^* weighted high resolution 3D FLASH images of the same mouse before and 4 hours after injection of SMART. Presence of magnetite in tissue causes a reduction of T2* to the point of complete signal loss at TE = 3 ms in the liver, spleen, and some abdominal regions. This method is not quantitative, however it does allow ready identification of the presence of magnetite throughout the body which can be used to guide quantitative ROI analyses using T_2 maps.

5.4.4. Correlation between magnetite and drug tissue content

Figure. 5.5 shows the relationship between magnetite concentration and ATV concentration of liver, spleen and kidney in four animals 24 hours after injection. It can be appreciated that there is a significant positive correlation (Pearson Correlation, r=0.786, p=0.0008). These results demonstrate the capability of MRI to be used for monitoring nanoART distribution.

5.4.5. Identification of magnetite-ART relationships in systemic tissues

We reasoned that cellular biodistribution of SMART was concordant with our prior results with nanoART [183]. To prove this theory we next studied the relationships between SMART particle biodistribution and macrophages in mice following parenteral SMART injections. Animals were sacrificed 4 hours after injection and tissues collected. Dual Iba-1 (for macrophages) and Prussian blue staining (for magnetite) were performed and evaluated by brightfield microscopic imaging. Prussian blue staining was nearly exclusively in tissue cells identified as macrophages. As shown in Figure. 5.6, Iba-1^+ macrophages were readily seen in both liver and spleen in parallel to distribution of Prussian blue. The dual staining pictures showed that the SMART particles were retained in tissue macrophages. Erythrocyte hemoglobin and its breakdown products are a substantive source of iron. These are degraded after the lifespan of the erythrocyte

[38]. This occurs predominantly in the spleen with iron transferred back into the blood. The highly vascularized spleen contains easily seen red blood cell breakdown products including iron that are phagocytized by macrophages [34]. Thus, the total iron content in the spleen is readily visualized by Prussian blue staining but substantively increased after SMART treatments (Figure. 5.6G and H). The iron content in spleen also changed from 228 μg/g before treatment to 356 μg/g after treatment, measured by ICP-MS. This also explains why background MRI scans are darkened in the spleen but increased after injection of SMART particles.

5.5. Discussion

Our laboratories are responsible for the development of cell-based carriage and delivery of antiretroviral drugs to sites of active HIV-1 replication [63, 82, 95, 106, 182, 184, 185]. This so-called “Trojan Horse” macrophage drug delivery scheme takes full advantage of the cells’ substantive endosomal storage capacity, its phagocytic and secretory functions, and its high degree of mobility to facilitate drug delivery [81]. As the macrophage is a principal cell target for viral growth, the added benefit rests in the abilities to bring ART to subcellular sites of viral assembly [186]. Such a system when used as a weekly or monthly parenteral injection has previously been shown to hold significant gains over conventional native oral drug therapeutic regimens [184, 185].

The principal goal in developing this polymer system rests in the ability to utilize MRI scans to rapidly assess cell and tissue drug biodistribution. The idea is that the polymer-encased dual magnetite and drug particle would permit a clear determination of drug levels in virus-target tissues in a very short time interval (hours). As plasma drug levels remain the gold standard for pharmacokinetic testing this technology clearly opens new opportunities to develop platforms that would accelerate elimination, or some day cure,

of viral infections. Notably, there is a considerable focus amongst HIV/AIDS researchers towards the development of any or all reliable methods to bring drugs to reservoir sites with the explicit goal of eliminating virus. Targeted drug as well as gene delivery when combined with suitable imaging techniques could facilitate this goal by providing a "go/no go" for treatment success [63]. Although this is the first time such "theranostics" has been applied for HIV diagnosis and therapies, similar systems have been developed in recent years for cancer treatments [187]. Here, the application is for early diagnostics. The unique payloads of nanomaterials include fluorescent semiconductor nanocrystals (quantum dots) as well as magnetic nanoparticles as developed in this report. All provide properties that can facilitate in vivo imaging with the help of MRI tests as well as fluorescence based approaches [188]. In all, interest in this idea will likely continue to grow through the development of carrier nanoparticles designed to target specific tissue and effect local chemo-, radio- and gene- directed antiretroviral or immune modulatory therapies [189].

Liposomes and polymer nanoparticles are the two major types of nanoparticles that have been developed and evaluated for diagnostic and therapeutic purposes. Liposomes composed of natural lipids are attractive DDS because of their high biocompatibility, low immunogenicity, long systemic circulation and favorable pharmacokinetic profile. Specific targeted delivery can easily be achieved by conjugating a targeting ligand to the lipid molecule [190-192]. Several liposomal drug formulations have been approved by FDA for clinical application, such as Doxil and DaunoXome [190, 192, 193]. However, the possible intrinsic low drug loading capacity, fast release profiles of hydrophobic drugs and physical instability of liposomes limit their clinical applications of different drugs [194]. Polymeric nanoparticles composed of synthetic PLGA are another widely developed/studied drug delivery platform because of their high stability, relatively high drug loading capacity of all kinds of drugs, biodegradability, low toxicity, and

controlled/sustained drug release profiles. Depending on particle composition, the drug release profiles of PLGA nanoparticles can be modulated to be within days, weeks or even months [195-197]. However, the biocompatibility/immunogenicity of nanoparticles composed of synthetic polymers including PLGA is not as high as liposomes. Without further chemical modification, PLGA nanoparticles are rapidly removed from circulation by the mononuclear phagocyte system (MPS), resulting in short systemic circulation [194]. In summary, both liposomes and PLGA nanoparticles are not independently structurally robust platforms. Thus, lipid-coated polymer nanoparticles, formed by combining synthetic polymers and natural lipids, have been developed as robust drug delivery platform to combine the advantages and avoid the disadvantages of liposomes and polymer nanoparticles [198, 199].

The visualization of cellular function in living organisms is not a new modality [106, 200, 201]. Optical, X-ray, nuclear, MRI and ultrasound allows three-dimensional whole-body scans at high spatial resolution and are adept at morphological and functional evaluations. The data obtained can be enhanced by magnetite and improved image resolution. By immobilizing a specific target molecule on the surface of a magnetic particle, the molecule inherits its magnetic property. Magnetic tissue targeting using multifunctional carrier particles can also facilitate effective treatments by enabling site-directed therapeutic outcomes. To this end, we selected DSPC and DSPE-PEG2k as the shell and PLGA as the core of SMART system. DSPC is used to increase the biocompatibility of SMART, and DSPE-PEG2k is used to build a sterically repulsive shield around SMART that reduces opsonization, prevents interactions with the MPS, escape renal exclusion, and increases systemic circulation. To the best of our knowledge, this is the first attempt to develop lipid-coated PLGA nanoparticles for HIV therapeutics. Our current work sought to use lipid coated PLGA SMART to encase magnetite and antiretroviral therapy to facilitate MDM uptake of drug and its subsequent

slow release. The long-term goals are straightforward. One is to use the synthesized SMART to facilitate drug screening for specific targeting ligands or sugars. The second is to determine the distribution of nanoART in viral reservoirs for the ultimate eradication of HIV. Our in vivo MRI results clearly demonstrated that SMART could facilitate the noninvasive evaluation of drug pharmacokinetics and biodistribution in different tissues, and provide rapid assessments for the next generation cell and tissue ligand decorated particles. This initial study lays the groundwork for what will quickly follow and ultimately, we believe, lead to an effective means to combat and potentially eliminate HIV disease.

5.6. Conclusions

We posit that SMART particles can be developed for noninvasive evaluation of drug distribution and pharmacokinetics. These particles show clear potential in allowing a rapid evaluation of ART content in viral reservoirs that include the brain and lymphoid tissues. Improve in particle delivery have been seen in cell and tissue targeted particles with coated ligands and sugars for future viral elimination studies.

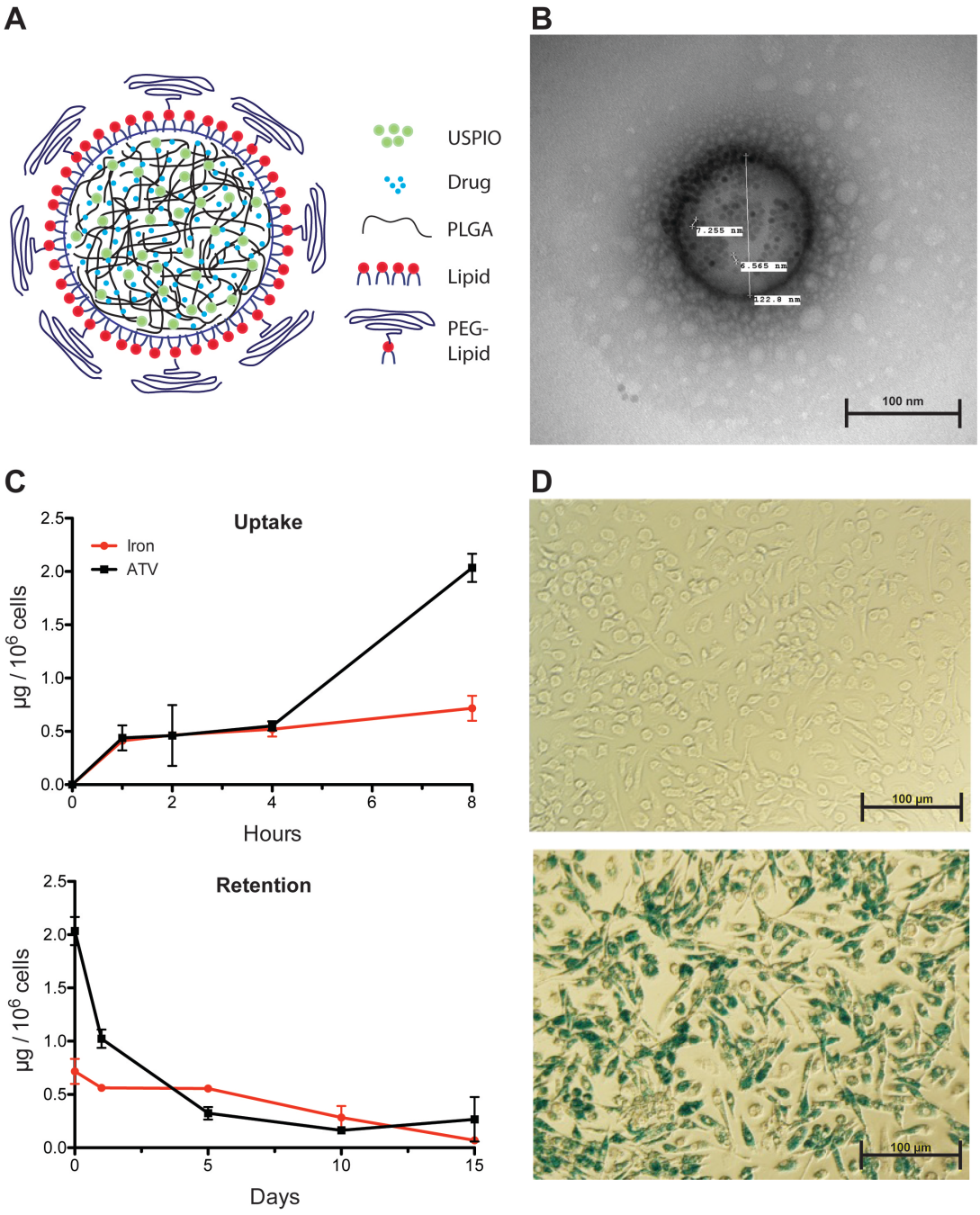

Figure 5.1. Development of SMART nanoparticles.

(A) The schematic structure of lipid-coated PLGA SMART. ATV and SPIO are well distributed within the PLGA matrix to form the core of SMART. The PLGA core is coated with lipid monolayer to form the shell of SMART. (B) Representative transmission electron micrograph (TEM) of a single SMART particle. (C) Timecourse of uptake (upper

panel) and retention (lower panel) of SMART in MDM., MDM were treated with 100 mM SMART (based on ATV content) for 1, 2, 4 and 8 hour uptake studies. For cell retention MDM were treated with 100 mM SMART for 8 hours, cell culture media was changed and cells were cultured for an additional 15 days. The cell lysates at indicated times were analyzed by HPLC and ICP-MS for ATV and magnetite quantification, respectively. Data represent the mean ± SEM, n = 3, for each time point. (D) Prussian blue staining of MDM. MDM were treated with PBS (negative control, upper panel) or 100 mM SMART (lower panel) for 24hours, and then fixed with 2% formalin/2.5% glutaraldehyde and stained with 5% potassium ferrocyanide/5% hydrochloric acid (1:1).

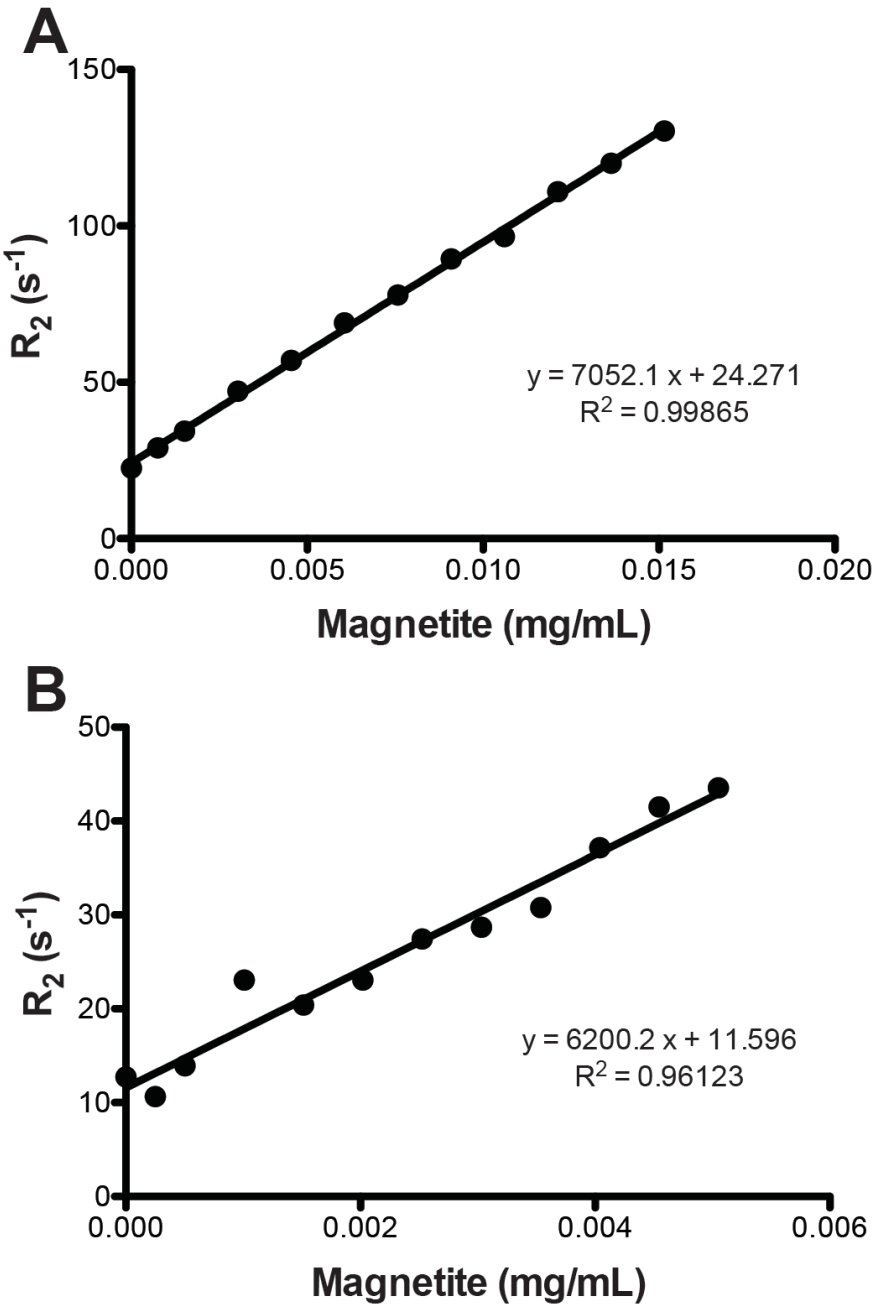

Figure 5.2. Concentration dependence of relaxivity (r_2) of SMART in (A) PBS and (B) MDM.

MDM were incubated with 100 μM SMART (based on ATV content) for 24 hours. Collected MDM and SMART were suspended in 1% agar gel. T_2 was measured by MRI and magnetite content by inductively coupled mass spectrometry (ICP-MS).

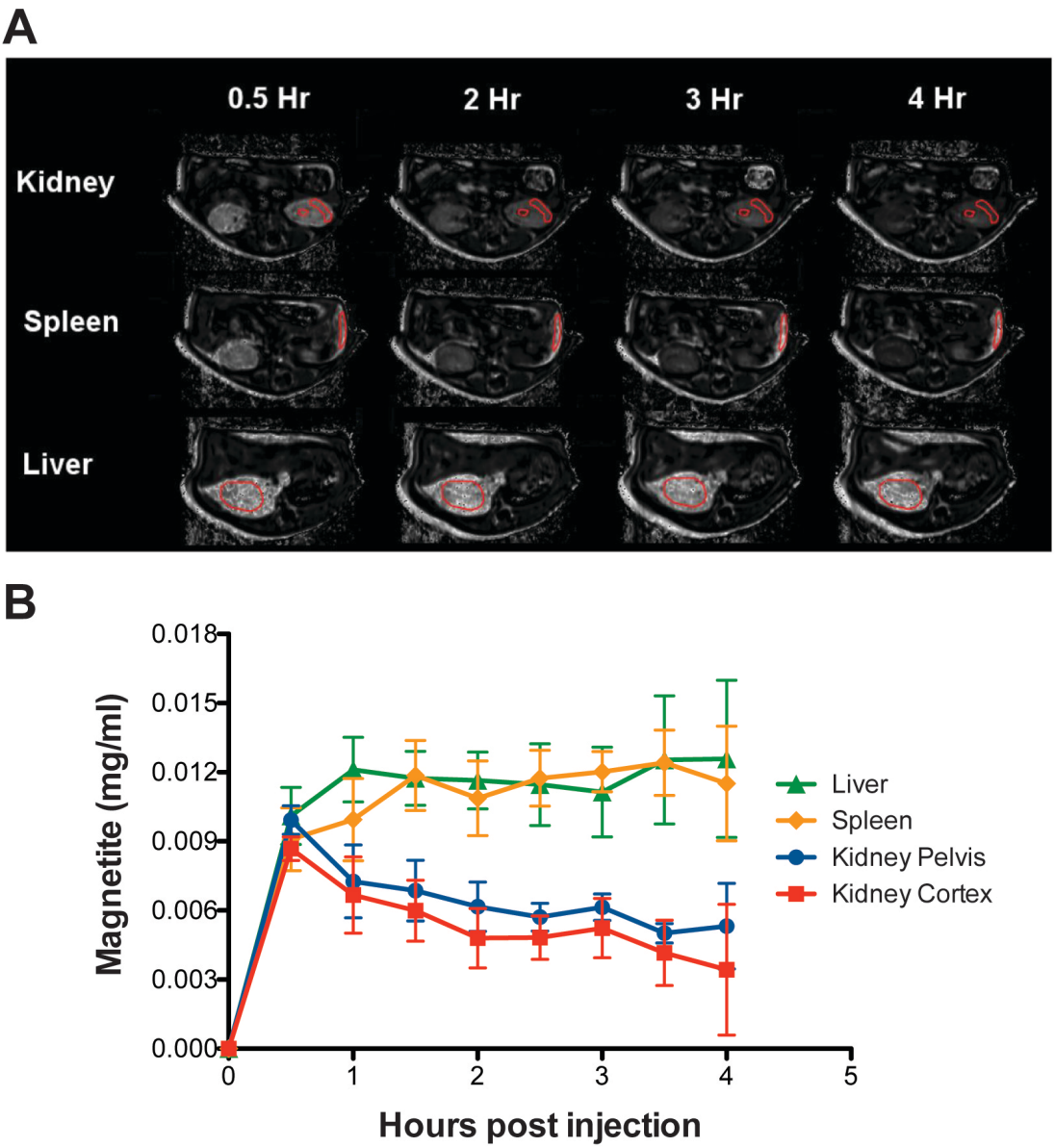

Figure 5.3. MRI assessments of the tissue drug biodistribution and pharmocokinetics by SMART particles.

After pre-MRI scan, mice were injected with SMART through a jugular vein cannula, and then scanned by MRI at continuously at 30 minute intervals up to 4 hours after SMART administration. Mean tissue SMART content was determined as detailed in Materials and Methods. Immediately after the final scan, mice were euthanized and tissues were

collected for ATV quantification by UPLC-MS/MS. (A) MRI based images of magnetite concentration in kidney, spleen and liver from 0.5 h to 4 h following SMART administration. (B) Mean ± SEM (n=6) of magnetite levels in kidney, spleen and liver over 4h following SMART administration.

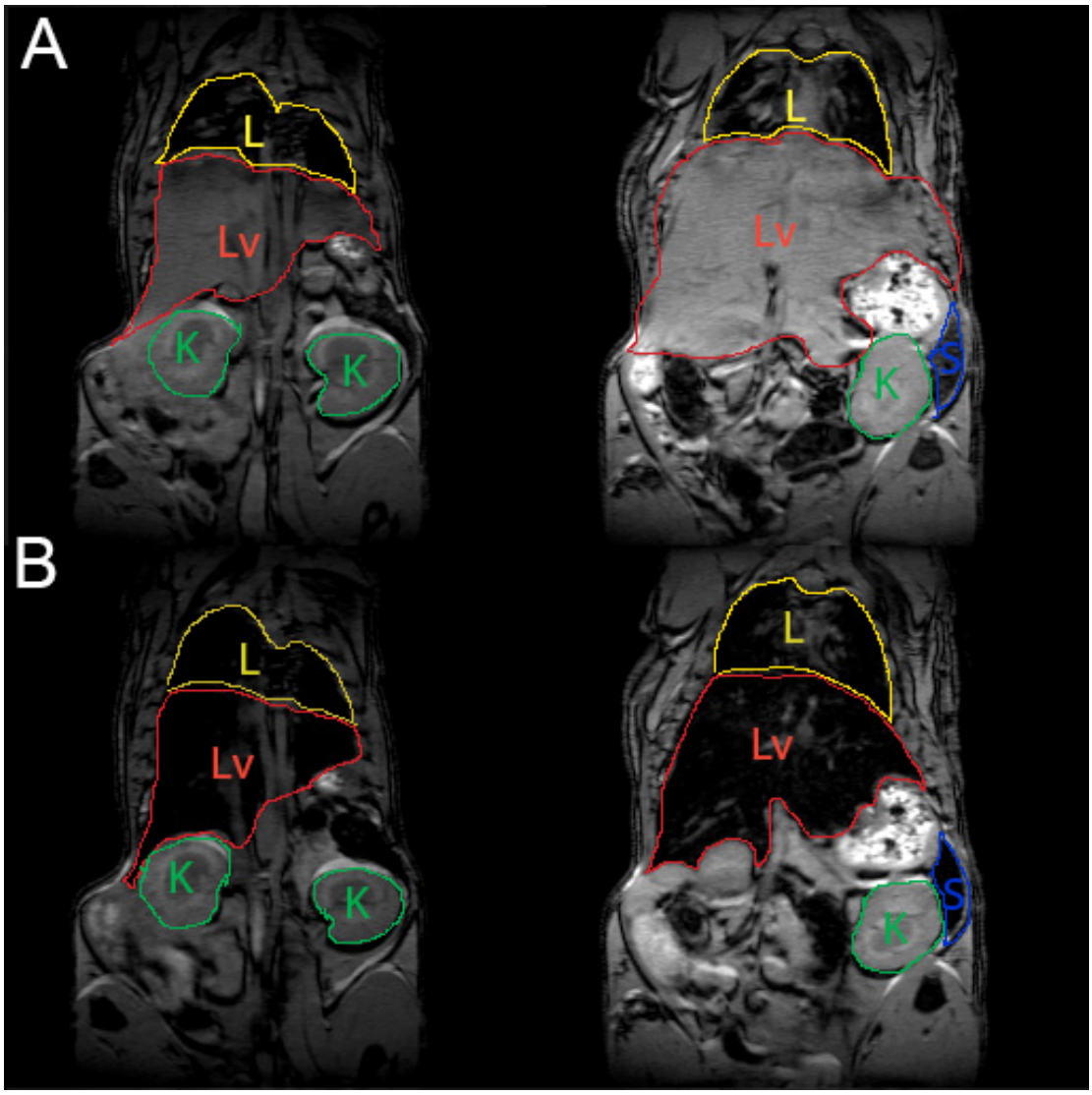

Figure 5.4. 3D gradient recalled echo images of the same mouse before (A) and 4 hours after (B) injection of SMART.

It can be appreciated that the signal from the liver is completely eliminated due to the accumulation of magnetite loaded SMART (L=lung, Lv=liver, K=kidney and S=spleen).

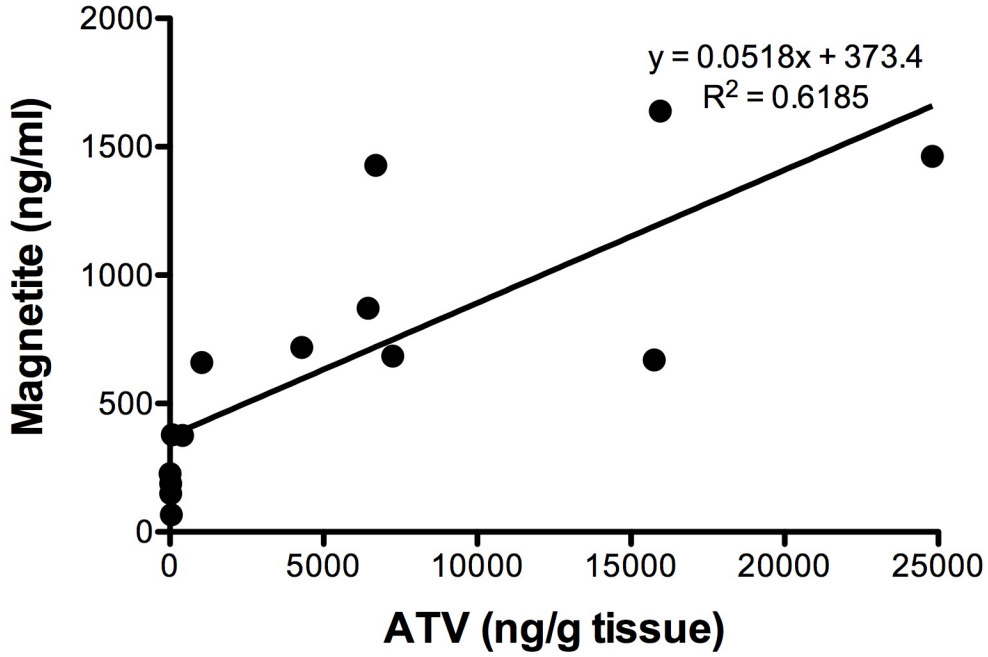

Figure 5.5. Correlation of SMART-associated magnetite and ATV in tissues 24 hours after administration.

The magnetite concentration was quantified from the change in T_2 weighted relaxivity ($DR_2 = 1/T_{2preinjection} - 1/T_{2postinjection}$) and the per milligram magnetite relaxivity (r_2) determined as the slope of magnetite concentration versus R_2 in SMART phantom studies. ATV concentrations were quantified by UPLC-MS/MS following the final 24 hour MRI scan.

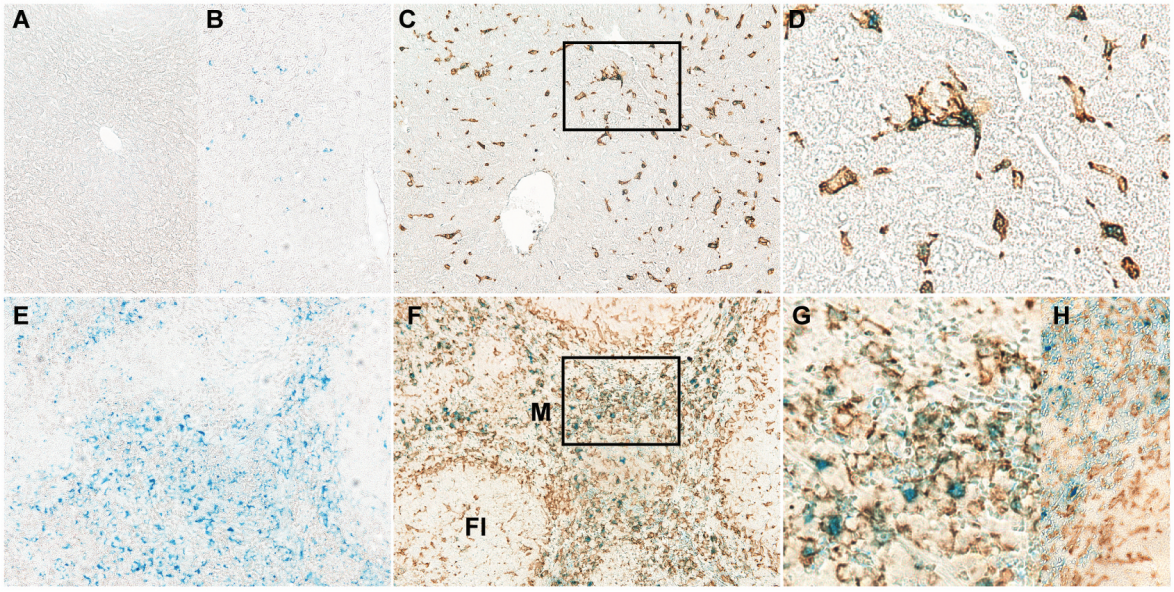

Figure 5.6. Immunohistology of Iba-1 staining and Prussian blue staining.

(A) Liver from control mice with Prussian blue (200×). (B) Liver from SMART treated mice with Prussian blue (200×). (C) Liver from SMART treated mice with Prussian blue and Iba-1 (200×). (D) Enlargement from indicated section in C. (E) Spleen from SMART treated mice with Prussian blue (200×). (F) Spleen from SMART treated mice with Prussian blue and Iba-1 (200×). (G) Enlargement from indicated section in F. (H) Spleen from control mice with Prussian blue and Iba-1 (400×). Livers and spleens were fixed with 10% formalin, paraffin embedded and sectioned for immunohistological analysis after the final MRI scan. Macrophages were identified by Iba1 stains (brown) and magnetite identified by Prussian blue. Fl=lymphoid follicle, M=marginal zone.

Chapter VI.

Conclusions and Future Directions

Our laboratory has developed nanoART for improved formulation stability and bioavailability, higher intracellular drug concentrations, and sustained *in vivo* drug release. It has realized long-acting antiretroviral therapy for types of hydrophobic antiretroviral drugs. In this study, we focused on hydrophilic nucleoside reverse transcriptase inhibitor—lamivudine. A hydrophobic 3TC prodrug was successfully synthesized through myristoylation and incorporated into targeted and non-targeted nanocrystalline formulations to improve drug half-life and reduce cytotoxicity. NMTC exhibited enhanced macrophage uptake and sustained antiretroviral efficacy. FA-NMTC exhibited improved pharmacokinetics and this novel drug delivery system has shown great potential for clinical application. In our subcellular trafficking study, we found macrophages could act as carriers of nanoART to improve drug bioavailability. Late and recycling endosomes are depots for both drug particle and HIV, and nanoATV and HIV-1 utilize similar subcellular pathways. SWATH-MS profiling broad the understanding of complex nanoART-HIV interactions. HIV-1 and nanoART deregulate cellular proteins in opposing manners and specific organelles are action sites for both. Rab5, 7, 11 and LAMP1 serve to coordinate molecular and biological functions of HIV-1 and drug particles. Besides, we developed SMART particles for noninvasive evaluation of drug distribution and pharmacokinetics. These studies unveil a broader understanding of nanomedicine for antiretroviral therapy and exhibit great potential in its future clinical applications.

Overall, this project has exhibited the great potential of our nanoformulated antiretroviral drug delivery system in the clinical applications. In the future, all types of antiretroviral drugs can take advantage of this system for improved antiretroviral efficacy and pharmacokinetics. Besides folic acid, different targeting ligands will be developed and utilized for nanoformulation development, which will uncover new mechanisms for long-acting antiretroviral therapy.

References

[1] HIV epidemic -- a global update. Excerpts from the UN World AIDS Day report. Health for the millions. 1998;24:3-5.

[2] Faria NR, Rambaut A, Suchard MA, Baele G, Bedford T, Ward MJ, et al. HIV epidemiology. The early spread and epidemic ignition of HIV-1 in human populations. Science. 2014;346:56-61.

[3] Berger EA, Doms RW, Fenyo EM, Korber BT, Littman DR, Moore JP, et al. A new classification for HIV-1. Nature. 1998;391:240.

[4] Cohen J. The many states of HIV in America. Science. 2012;337:168-71.

[5] Karlsson Hedestam GB, Fouchier RA, Phogat S, Burton DR, Sodroski J, Wyatt RT. The challenges of eliciting neutralizing antibodies to HIV-1 and to influenza virus. Nature reviews Microbiology. 2008;6:143-55.

[6] Stevenson M, Gendelman HE. Cellular and viral determinants that regulate HIV-1 infection in macrophages. Journal of leukocyte biology. 1994;56:278-88.

[7] Gendelman HE, Orenstein JM, Baca LM, Weiser B, Burger H, Kalter DC, et al. The macrophage in the persistence and pathogenesis of HIV infection. AIDS. 1989;3:475-95.

[8] Gendelman HE, Narayan O, Kennedy-Stoskopf S, Kennedy PG, Ghotbi Z, Clements JE, et al. Tropism of sheep lentiviruses for monocytes: susceptibility to infection and virus gene expression increase during maturation of monocytes to macrophages. Journal of virology. 1986;58:67-74.

[9] Finzi D, Hermankova M, Pierson T, Carruth LM, Buck C, Chaisson RE, et al. Identification of a reservoir for HIV-1 in patients on highly active antiretroviral therapy. Science. 1997;278:1295-300.

[10] Chun TW, Fauci AS. HIV reservoirs: pathogenesis and obstacles to viral eradication and cure. AIDS. 2012;26:1261-8.

[11] Coleman CM, Wu L. HIV interactions with monocytes and dendritic cells: viral latency and reservoirs. Retrovirology. 2009;6:51.

[12] Kurapati KR, Atluri VS, Samikkannu T, Garcia G, Nair MP. Natural Products as Anti-HIV Agents and Role in HIV-Associated Neurocognitive Disorders (HAND): A Brief Overview. Frontiers in microbiology. 2015;6:1444.

[13] Matthews T, Salgo M, Greenberg M, Chung J, DeMasi R, Bolognesi D. Enfuvirtide: the first therapy to inhibit the entry of HIV-1 into host CD4 lymphocytes. Nat Rev Drug Discov. 2004;3:215-25.

[14] MacArthur RD, Novak RM. Reviews of anti-infective agents: maraviroc: the first of a new class of antiretroviral agents. Clinical infectious diseases : an official publication of the Infectious Diseases Society of America. 2008;47:236-41.

[15] Diamond TL, Roshal M, Jamburuthugoda VK, Reynolds HM, Merriam AR, Lee KY, et al. Macrophage tropism of HIV-1 depends on efficient cellular dNTP utilization by reverse transcriptase. The Journal of biological chemistry. 2004;279:51545-53.

[16] Schinazi RF, Hernandez-Santiago BI, Hurwitz SJ. Pharmacology of current and promising nucleosides for the treatment of human immunodeficiency viruses. Antiviral research. 2006;71:322-34.

[17] Souza TM, Cirne-Santos CC, Rodrigues DQ, Abreu CM, Tanuri A, Ferreira VF, et al. The compound 6-chloro-1,4-dihydro-4-oxo-1-(beta-D-ribofuranosyl) quinoline-3-carboxylic acid inhibits HIV-1 replication by targeting the enzyme reverse transcriptase. Current HIV research. 2008;6:209-17.

[18] Patick AK, Potts KE. Protease inhibitors as antiviral agents. Clinical microbiology reviews. 1998;11:614-27.

[19] Anker M, Corales RB. Raltegravir (MK-0518): a novel integrase inhibitor for the treatment of HIV infection. Expert opinion on investigational drugs. 2008;17:97-103.

[20] Imamichi T. Action of anti-HIV drugs and resistance: reverse transcriptase inhibitors and protease inhibitors. Current pharmaceutical design. 2004;10:4039-53.

[21] Chugh P, Bradel-Tretheway B, Monteiro-Filho CM, Planelles V, Maggirwar SB, Dewhurst S, et al. Akt inhibitors as an HIV-1 infected macrophage-specific anti-viral therapy. Retrovirology. 2008;5:11.

[22] Bawarski WE, Chidlowsky E, Bharali DJ, Mousa SA. Emerging nanopharmaceuticals. Nanomedicine. 2008;4:273-82.

[23] Biddlestone-Thorpe L, Marchi N, Guo K, Ghosh C, Janigro D, Valerie K, et al. Nanomaterial-mediated CNS delivery of diagnostic and therapeutic agents. Advanced drug delivery reviews. 2012;64:605-13.

[24] Trivedi R, Kompella UB. Nanomicellar formulations for sustained drug delivery: strategies and underlying principles. Nanomedicine. 2010;5:485-505.

[25] Batrakova EV, Li S, Miller DW, Kabanov AV. Pluronic P85 increases permeability of a broad spectrum of drugs in polarized BBMEC and Caco-2 cell monolayers. Pharmaceutical research. 1999;16:1366-72.

[26] Spitzenberger TJ, Heilman D, Diekmann C, Batrakova EV, Kabanov AV, Gendelman HE, et al. Novel delivery system enhances efficacy of antiretroviral therapy in animal model for HIV-1 encephalitis. Journal of cerebral blood flow and metabolism : official journal of the International Society of Cerebral Blood Flow and Metabolism. 2007;27:1033-42.

[27] Kaur CD, Nahar M, Jain NK. Lymphatic targeting of zidovudine using surface-engineered liposomes. Journal of drug targeting. 2008;16:798-805.

[28] Dou H, Destache CJ, Morehead JR, Mosley RL, Boska MD, Kingsley J, et al. Development of a macrophage-based nanoparticle platform for antiretroviral drug delivery. Blood. 2006;108:2827-35.

[29] Puligujja P, Arainga M, Dash P, Palandri D, Mosley RL, Gorantla S, et al. Pharmacodynamics of folic acid receptor targeted antiretroviral nanotherapy in HIV-1-infected humanized mice. Antiviral research. 2015;120:85-8.

[30] Kuo YC, Su FL. Transport of stavudine, delavirdine, and saquinavir across the blood-brain barrier by polybutylcyanoacrylate, methylmethacrylate-sulfopropylmethacrylate, and solid lipid nanoparticles. International journal of pharmaceutics. 2007;340:143-52.

[31] Nanjwade BK, Bechra HM, Derkar GK, Manvi FV, Nanjwade VK. Dendrimers: emerging polymers for drug-delivery systems. European journal of pharmaceutical

sciences : official journal of the European Federation for Pharmaceutical Sciences. 2009;38:185-96.

[32] Balkundi S, Nowacek AS, Roy U, Martinez-Skinner A, McMillan J, Gendelman HE. Methods development for blood borne macrophage carriage of nanoformulated antiretroviral drugs. J Vis Exp. 2010.

[33] Nair M, Jayant RD, Kaushik A, Sagar V. Getting into the brain: Potential of nanotechnology in the management of NeuroAIDS. Advanced drug delivery reviews. 2016.

[34] Edagwa BJ, Zhou T, McMillan JM, Liu XM, Gendelman HE. Development of HIV reservoir targeted long acting nanoformulated antiretroviral therapies. Current medicinal chemistry. 2014;21:4186-98.

[35] Gendelman HE, Gelbard HA. Adjunctive and long-acting nanoformulated antiretroviral therapies for HIV-associated neurocognitive disorders. Current opinion in HIV and AIDS. 2014;9:585-90.

[36] Lenjisa JL, Woldu MA, Satessa GD. New hope for eradication of HIV from the body: the role of polymeric nanomedicines in HIV/AIDS pharmacotherapy. Journal of nanobiotechnology. 2014;12:9.

[37] Date AA, Destache CJ. A review of nanotechnological approaches for the prophylaxis of HIV/AIDS. Biomaterials. 2013;34:6202-28.

[38] Russo G, Paganotti GM, Soeria-Atmadja S, Haverkamp M, Ramogola-Masire D, Vullo V, et al. Pharmacogenetics of non-nucleoside reverse transcriptase inhibitors (NNRTIs) in resource-limited settings: Influence on antiretroviral therapy response and concomitant anti-tubercular, antimalarial and contraceptive treatments.

Infection, genetics and evolution : journal of molecular epidemiology and evolutionary genetics in infectious diseases. 2016;37:192-207.

[39] Clark DN, Hu J. Hepatitis B virus reverse transcriptase - Target of current antiviral therapy and future drug development. Antiviral research. 2015;123:132-7.

[40] Famiglini V, Silvestri R. Focus on Chirality of HIV-1 Non-Nucleoside Reverse Transcriptase Inhibitors. Molecules. 2016;21.

[41] Lytvyak E, Montano-Loza AJ, Mason AL. Combination antiretroviral studies for patients with primary biliary cirrhosis. World journal of gastroenterology. 2016;22:349-60.

[42] Li X, Jie Y, You X, Shi H, Zhang M, Wu Y, et al. Optimized combination therapies with adefovir dipivoxil (ADV) and lamivudine, telbivudine, or entecavir may be effective for chronic hepatitis B patients with a suboptimal response to ADV monotherapy. International journal of clinical and experimental medicine. 2015;8:21062-70.

[43] Palacios R, Perez-Hernandez IA, Martinez MA, Mayorga ML, Gonzalez-Domenech CM, Omar M, et al. Efficacy and safety of switching to abacavir/lamivudine (ABC/3TC) plus rilpivirine (RPV) in virologically suppressed HIV-infected patients on HAART. European journal of clinical microbiology & infectious diseases : official publication of the European Society of Clinical Microbiology. 2016.

[44] Greig SL, Deeks ED. Abacavir/dolutegravir/lamivudine single-tablet regimen: a review of its use in HIV-1 infection. Drugs. 2015;75:503-14.

[45] Agarwal HK, Chhikara BS, Hanley MJ, Ye G, Doncel GF, Parang K. Synthesis and biological evaluation of fatty acyl ester derivatives of (-)-2',3'-dideoxy-3'-thiacytidine. Journal of medicinal chemistry. 2012;55:4861-71.

[46] Farazi TA, Waksman G, Gordon JI. The biology and enzymology of protein N-myristoylation. The Journal of biological chemistry. 2001;276:39501-4.

[47] Wu Z, Alexandratos J, Ericksen B, Lubkowski J, Gallo RC, Lu W. Total chemical synthesis of N-myristoylated HIV-1 matrix protein p17: structural and mechanistic implications of p17 myristoylation. Proceedings of the National Academy of Sciences of the United States of America. 2004;101:11587-92.

[48] Langner CA, Lodge JK, Travis SJ, Caldwell JE, Lu T, Li Q, et al. 4-oxatetradecanoic acid is fungicidal for Cryptococcus neoformans and inhibits replication of human immunodeficiency virus I. The Journal of biological chemistry. 1992;267:17159-69.

[49] Takamune N, Hamada H, Misumi S, Shoji S. Novel strategy for anti-HIV-1 action: selective cytotoxic effect of N-myristoyltransferase inhibitor on HIV-1-infected cells. FEBS letters. 2002;527:138-42.

[50] Ohta H, Takamune N, Kishimoto N, Shoji S, Misumi S. N-Myristoyltransferase 1 enhances human immunodeficiency virus replication through regulation of viral RNA expression level. Biochemical and biophysical research communications. 2015;463:988-93.

[51] Bahrami B, Mohammadnia-Afrouzi M, Bakhshaei P, Yazdani Y, Ghalamfarsa G, Yousefi M, et al. Folate-conjugated nanoparticles as a potent therapeutic approach in targeted cancer therapy. Tumour biology : the journal of the International Society for Oncodevelopmental Biology and Medicine. 2015;36:5727-42.

[52] Chaudhury A, Das S. Folate receptor targeted liposomes encapsulating anti-cancer drugs. Current pharmaceutical biotechnology. 2015;16:333-43.

[53] Puligujja P, McMillan J, Kendrick L, Li T, Balkundi S, Smith N, et al. Macrophage folate receptor-targeted antiretroviral therapy facilitates drug entry, retention, antiretroviral activities and biodistribution for reduction of human immunodeficiency virus infections. Nanomedicine : nanotechnology, biology, and medicine. 2013;9:1263-73.

[54] Clark SC. Interleukin-6. Multiple activities in regulation of the hematopoietic and immune systems. Annals of the New York Academy of Sciences. 1989;557:438-43.

[55] Guo D, Zhang G, Wysocki TA, Wysocki BJ, Gelbard HA, Liu XM, et al. Endosomal trafficking of nanoformulated antiretroviral therapy facilitates drug particle carriage and HIV clearance. Journal of virology. 2014;88:9504-13.

[56] Arainga M, Guo D, Wiederin J, Ciborowski P, McMillan J, Gendelman HE. Opposing regulation of endolysosomal pathways by long-acting nanoformulated antiretroviral therapy and HIV-1 in human macrophages. Retrovirology. 2015;12:5.

[57] Gendelman HE, Orenstein JM, Martin MA, Ferrua C, Mitra R, Phipps T, et al. Efficient isolation and propagation of human immunodeficiency virus on recombinant colony-stimulating factor 1-treated monocytes. J Exp Med. 1988;167:1428-41.

[58] Guo D, Li T, McMillan J, Sajja BR, Puligujja P, Boska MD, et al. Small magnetite antiretroviral therapeutic nanoparticle probes for MRI of drug biodistribution. Nanomedicine. 2014;9:1341-52.

[59] Bareford LM, Swaan PW. Endocytic mechanisms for targeted drug delivery. Advanced drug delivery reviews. 2007;59:748-58.

[60] Notari S, Sergi M, Montesano C, Ivanovic J, Narciso P, Pucillo LP, et al. Simultaneous determination of lamivudine, lopinavir, ritonavir, and zidovudine concentration in plasma of HIV-infected patients by HPLC-MS/MS. IUBMB life. 2012;64:443-9.

[61] Gray LR, Tachedjian G, Ellett AM, Roche MJ, Cheng WJ, Guillemin GJ, et al. The NRTIs lamivudine, stavudine and zidovudine have reduced HIV-1 inhibitory activity in astrocytes. PloS one. 2013;8:e62196.

[62] Nowacek AS, McMillan J, Miller R, Anderson A, Rabinow B, Gendelman HE. Nanoformulated antiretroviral drug combinations extend drug release and antiretroviral responses in HIV-1-infected macrophages: implications for neuroAIDS therapeutics. J Neuroimmune Pharmacol. 2010;5:592-601.

[63] Nowacek AS, Balkundi S, McMillan J, Roy U, Martinez-Skinner A, Mosley RL, et al. Analyses of nanoformulated antiretroviral drug charge, size, shape and content for uptake, drug release and antiviral activities in human monocyte-derived macrophages. Journal of controlled release : official journal of the Controlled Release Society. 2011;150:204-11.

[64] Zhang G, Guo D, Dash PK, Arainga M, Wiederin JL, Haverland NA, et al. The mixed lineage kinase-3 inhibitor URMC-099 improves therapeutic outcomes for long-acting antiretroviral therapy. Nanomedicine. 2016;12:109-22.

[65] Rampoldi F, Bonrouhi M, Boehm ME, Lehmann WD, Popovic ZV, Kaden S, et al. Immunosuppression and Aberrant T Cell Development in the Absence of N-Myristoylation. Journal of immunology. 2015;195:4228-43.

[66] Perinpanayagam MA, Beauchamp E, Martin DD, Sim JY, Yap MC, Berthiaume LG. Regulation of co- and post-translational myristoylation of proteins during apoptosis: interplay of N-myristoyltransferases and caspases. FASEB journal : official publication of the Federation of American Societies for Experimental Biology. 2013;27:811-21.

[67] Morgan CR, Miglionico BV, Engen JR. Effects of HIV-1 Nef on human N-myristoyltransferase 1. Biochemistry. 2011;50:3394-403.

[68] Shityakov S, Sohajda T, Puskas I, Roewer N, Forster C, Broscheit JA. Ionization states, cellular toxicity and molecular modeling studies of midazolam complexed with trimethyl-beta-cyclodextrin. Molecules. 2014;19:16861-76.

[69] Kumar L, Verma S, Prasad DN, Bhardwaj A, Vaidya B, Jain AK. Nanotechnology: a magic bullet for HIV AIDS treatment. Artificial cells, nanomedicine, and biotechnology. 2015;43:71-86.

[70] Zaki NM, Tirelli N. Gateways for the intracellular access of nanocarriers: a review of receptor-mediated endocytosis mechanisms and of strategies in receptor targeting. Expert opinion on drug delivery. 2010;7:895-913.

[71] Hattori Y, Sakaguchi M, Maitani Y. Folate-linked lipid-based nanoparticles deliver a NFkappaB decoy into activated murine macrophage-like RAW264.7 cells. Biological & pharmaceutical bulletin. 2006;29:1516-20.

[72] Kularatne SA, Low PS. Targeting of nanoparticles: folate receptor. Methods in molecular biology. 2010;624:249-65.

[73] Sahay G, Alakhova DY, Kabanov AV. Endocytosis of nanomedicines. J Control Release. 2010;145:182-95.

[74] Rijnboutt S, Jansen G, Posthuma G, Hynes JB, Schornagel JH, Strous GJ. Endocytosis of GPI-linked membrane folate receptor-alpha. The Journal of cell biology. 1996;132:35-47.

[75] Wainberg MA. AIDS: Drugs that prevent HIV infection. Nature. 2011;469:306-7.

[76] Pretorius E, Klinker H, Rosenkranz B. The role of therapeutic drug monitoring in the management of patients with human immunodeficiency virus infection. Ther Drug Monit. 2011;33:265-74.

[77] Beyrer C, Malinowska-Sempruch K, Kamarulzaman A, Kazatchkine M, Sidibe M, Strathdee SA. Time to act: a call for comprehensive responses to HIV in people who use drugs. Lancet. 2010;376:551-63.

[78] Chulamokha L, DeSimone JA, Pomerantz RJ. Antiretroviral therapy in the developing world. J Neurovirol. 2005;11 Suppl 1:76-80.

[79] Wang X, Li J, Wang Y, Cho KJ, Kim G, Gjyrezi A, et al. HFT-T, a targeting nanoparticle, enhances specific delivery of paclitaxel to folate receptor-positive tumors. Acs Nano. 2009;3:3165-74.

[80] Kabanov AV, Gendelman HE. Nanomedicine in the diagnosis and therapy of neurodegenerative disorders. Prog Polym Sci. 2007;32:1054-82.

[81] Kadiu I, Nowacek A, McMillan J, Gendelman HE. Macrophage endocytic trafficking of antiretroviral nanoparticles. Nanomedicine (Lond). 2011;6:975-94.

[82] Nowacek AS, Miller RL, McMillan J, Kanmogne G, Kanmogne M, Mosley RL, et al. NanoART synthesis, characterization, uptake, release and toxicology for human monocyte-macrophage drug delivery. Nanomedicine (Lond). 2009;4:903-17.

[83] Kingsley JD, Dou H, Morehead J, Rabinow B, Gendelman HE, Destache CJ. Nanotechnology: a focus on nanoparticles as a drug delivery system. J Neuroimmune Pharmacol. 2006;1:340-50.

[84] Wood R. Atazanavir: its role in HIV treatment. Expert Rev Anti Infect Ther. 2008;6:785-96.

[85] Schwarcz SK, Hsu LC, Vittinghoff E, Katz MH. Impact of protease inhibitors and other antiretroviral treatments on acquired immunodeficiency syndrome survival in San Francisco, California, 1987-1996. Am J Epidemiol. 2000;152:178-85.

[86] Arribas JR, Eron J. Advances in antiretroviral therapy. Current opinion in HIV and AIDS. 2013;8:341-9.

[87] Rowell JF, Stanhope PE, Siliciano RF. Endocytosis of endogenously synthesized HIV-1 envelope protein. Mechanism and role in processing for association with class II MHC. Journal of immunology. 1995;155:473-88.

[88] Raposo G, Moore M, Innes D, Leijendekker R, Leigh-Brown A, Benaroch P, et al. Human macrophages accumulate HIV-1 particles in MHC II compartments. Traffic. 2002;3:718-29.

[89] Pelchen-Matthews A, Kramer B, Marsh M. Infectious HIV-1 assembles in late endosomes in primary macrophages. The Journal of cell biology. 2003;162:443-55.

[90] Goncalves E, Bucher J, Ryll A, Niklas J, Mauch K, Klamt S, et al. Bridging the layers: towards integration of signal transduction, regulation and metabolism into mathematical models. Mol Biosyst. 2013;9:1576-83.

[91] Karr JR, Sanghvi JC, Macklin DN, Gutschow MV, Jacobs JM, Bolival B, Jr., et al. A whole-cell computational model predicts phenotype from genotype. Cell. 2012;150:389-401.

[92] Liszewski MK, Yu JJ, O'Doherty U. Detecting HIV-1 integration by repetitive-sampling Alu-gag PCR. Methods. 2009;47:254-60.

[93] Kumar R, Vandegraaff N, Mundy L, Burrell CJ, Li P. Evaluation of PCR-based methods for the quantitation of integrated HIV-1 DNA. J Virol Methods. 2002;105:233-46.

[94] Kalter DC, Nakamura M, Turpin JA, Baca LM, Hoover DL, Dieffenbach C, et al. Enhanced HIV replication in macrophage colony-stimulating factor-treated monocytes. Journal of immunology. 1991;146:298-306.

[95] Dou H, Grotepas CB, McMillan JM, Destache CJ, Chaubal M, Werling J, et al. Macrophage delivery of nanoformulated antiretroviral drug to the brain in a murine model of neuroAIDS. Journal of immunology. 2009;183:661-9.

[96] Hutagalung AH, Novick PJ. Role of Rab GTPases in membrane traffic and cell physiology. Physiol Rev. 2011;91:119-49.

[97] Martin TM, Wysocki BJ, Beyersdorf JP, Wysocki TA, Pannier AK. Integrating mitosis, toxicity, and transgene expression in a telecommunications packet-switched network model of lipoplex-mediated gene delivery. Biotechnology and Bioengineering. 2014:n/a-n/a.

[98] Junghanns JU, Muller RH. Nanocrystal technology, drug delivery and clinical applications. International journal of nanomedicine. 2008;3:295-309.

[99] Kumar L, Verma S, Prasad DN, Bhardwaj A, Vaidya B, Jain AK. Nanotechnology: A magic bullet for HIV AIDS treatment. Artificial cells, nanomedicine, and biotechnology. 2014.

[100] Ramana LN, Sharma S, Sethuraman S, Ranga U, Krishnan UM. Evaluation of chitosan nanoformulations as potent anti-HIV therapeutic systems. Biochim Biophys Acta. 2014;1840:476-84.

[101] Rabinow BE. Nanosuspensions in drug delivery. Nat Rev Drug Discov. 2004;3:785-96.

[102] Gollapudi K, Galet C, Grogan T, Zhang H, Said JW, Huang J, et al. Association between tumor-associated macrophage infiltration, high grade prostate cancer, and biochemical recurrence after radical prostatectomy. Am J Cancer Res. 2013;3:523-9.

[103] Schulz R, Moll UM. Targeting the heat shock protein 90: a rational way to inhibit macrophage migration inhibitory factor function in cancer. Curr Opin Oncol. 2014;26:108-13.

[104] Goshima F, Esaki S, Luo C, Kamakura M, Kimura H, Nishiyama Y. Oncolytic viral therapy with a combination of HF10, a herpes simplex virus type 1 variant and granulocyte-macrophage colony-stimulating factor for murine ovarian cancer. Int J Cancer. 2013.

[105] Gautam N, Roy U, Balkundi S, Puligujja P, Guo D, Smith N, et al. Preclinical pharmacokinetics and tissue distribution of long-acting nanoformulated antiretroviral therapy. Antimicrobial agents and chemotherapy. 2013;57:3110-20.

[106] Beduneau A, Ma Z, Grotepas CB, Kabanov A, Rabinow BE, Gong N, et al. Facilitated monocyte-macrophage uptake and tissue distribution of superparmagnetic iron-oxide nanoparticles. PloS one. 2009;4:e4343.

[107] Meltzer MS, Gendelman HE. Mononuclear phagocytes as targets, tissue reservoirs, and immunoregulatory cells in human immunodeficiency virus disease. Curr Top Microbiol Immunol. 1992;181:239-63.

[108] Meltzer MS, Nakamura M, Hansen BD, Turpin JA, Kalter DC, Gendelman HE. Macrophages as susceptible targets for HIV infection, persistent viral reservoirs in tissue, and key immunoregulatory cells that control levels of virus replication and extent of disease. AIDS Res Hum Retroviruses. 1990;6:967-71.

[109] Feng Y, Press B, Wandinger-Ness A. Rab 7: an important regulator of late endocytic membrane traffic. The Journal of cell biology. 1995;131:1435-52.

[110] Meng B, Lever AM. Wrapping up the bad news: HIV assembly and release. Retrovirology. 2013;10:5.

[111] Bell NM, Lever AM. HIV Gag polyprotein: processing and early viral particle assembly. Trends in microbiology. 2013;21:136-44.

[112] Bell NM, L'Hernault A, Murat P, Richards JE, Lever AM, Balasubramanian S. Targeting RNA-protein interactions within the human immunodeficiency virus type 1 lifecycle. Biochemistry. 2013;52:9269-74.

[113] Benaroch P, Billard E, Gaudin R, Schindler M, Jouve M. HIV-1 assembly in macrophages. Retrovirology. 2010;7:29.

[114] Varthakavi V, Smith RM, Martin KL, Derdowski A, Lapierre LA, Goldenring JR, et al. The pericentriolar recycling endosome plays a key role in Vpu-mediated enhancement of HIV-1 particle release. Traffic. 2006;7:298-307.

[115] Kumari S, Mg S, Mayor S. Endocytosis unplugged: multiple ways to enter the cell. Cell Res. 2010;20:256-75.

[116] McMahon HT, Boucrot E. Molecular mechanism and physiological functions of clathrin-mediated endocytosis. Nat Rev Mol Cell Biol. 2011;12:517-33.

[117] Jordens I, Marsman M, Kuijl C, Neefjes J. Rab proteins, connecting transport and vesicle fusion. Traffic. 2005;6:1070-7.

[118] Sonnichsen B, De Renzis S, Nielsen E, Rietdorf J, Zerial M. Distinct membrane domains on endosomes in the recycling pathway visualized by multicolor imaging of Rab4, Rab5, and Rab11. The Journal of cell biology. 2000;149:901-14.

[119] Schonteich E, Wilson GM, Burden J, Hopkins CR, Anderson K, Goldenring JR, et al. The Rip11/Rab11-FIP5 and kinesin II complex regulates endocytic protein recycling. Journal of cell science. 2008;121:3824-33.

[120] Parent A, Hamelin E, Germain P, Parent JL. Rab11 regulates the recycling of the beta2-adrenergic receptor through a direct interaction. Biochem J. 2009;418:163-72.

[121] Yamamoto H, Koga H, Katoh Y, Takahashi S, Nakayama K, Shin HW. Functional cross-talk between Rab14 and Rab4 through a dual effector, RUFY1/Rabip4. Mol Biol Cell. 2010;21:2746-55.

[122] Zerial M, McBride H. Rab proteins as membrane organizers. Nat Rev Mol Cell Biol. 2001;2:107-17.

[123] Boffito M, Jackson A, Owen A, Becker S. New approaches to antiretroviral drug delivery: challenges and opportunities associated with the use of long-acting injectable agents. Drugs. 2014;74:7-13.

[124] Puligujja P, Balkundi SS, Kendrick LM, Baldridge HM, Hilaire JR, Bade AN, et al. Pharmacodynamics of long-acting folic acid-receptor targeted ritonavir-boosted atazanavir nanoformulations. Biomaterials. 2015;41C:141-50.

[125] Rajoli RK, Back DJ, Rannard S, Freel Meyers CL, Flexner C, Owen A, et al. Physiologically Based Pharmacokinetic Modelling to Inform Development of Intramuscular Long-Acting Nanoformulations for HIV. Clinical pharmacokinetics. 2014.

[126] Spreen WR, Margolis DA, Pottage JC, Jr. Long-acting injectable antiretrovirals for HIV treatment and prevention. Current opinion in HIV and AIDS. 2013;8:565-71.

[127] Gautam N, Puligujja P, Balkundi S, Thakare R, Liu XM, Fox HS, et al. Pharmacokinetics, biodistribution, and toxicity of folic Acid-coated antiretroviral nanoformulations. Antimicrobial agents and chemotherapy. 2014;58:7510-9.

[128] Roy U, McMillan J, Alnouti Y, Gautum N, Smith N, Balkundi S, et al. Pharmacodynamic and antiretroviral activities of combination nanoformulated antiretrovirals in HIV-1-infected human peripheral blood lymphocyte-reconstituted mice. The Journal of infectious diseases. 2012;206:1577-88.

[129] Haverland NA, Fox HS, Ciborowski P. Quantitative proteomics by SWATH-MS reveals altered expression of nucleic acid binding and regulatory proteins in HIV-1-infected macrophages. Journal of proteome research. 2014;13:2109-19.

[130] Kudoh A, Takahama S, Sawasaki T, Ode H, Yokoyama M, Okayama A, et al. The phosphorylation of HIV-1 Gag by atypical protein kinase C facilitates viral infectivity by promoting Vpr incorporation into virions. Retrovirology. 2014;11:9.

[131] Levine AJ, Panos SE, Horvath S. Genetic, transcriptomic, and epigenetic studies of HIV-associated neurocognitive disorder. Journal of acquired immune deficiency syndromes. 2014;65:481-503.

[132] Linde ME, Colquhoun DR, Ubaida Mohien C, Kole T, Aquino V, Cotter R, et al. The conserved set of host proteins incorporated into HIV-1 virions suggests a common egress pathway in multiple cell types. Journal of proteome research. 2013;12:2045-54.

[133] Schweitzer CJ, Jagadish T, Haverland N, Ciborowski P, Belshan M. Proteomic analysis of early HIV-1 nucleoprotein complexes. Journal of proteome research. 2013;12:559-72.

[134] Wisniewski JR, Rakus D. Multi-enzyme digestion FASP and the 'Total Protein Approach'-based absolute quantification of the Escherichia coli proteome. Journal of proteomics. 2014;109C:322-31.

[135] Drabik A, Bodzon-Kulakowska A, Suder P, Ciborowski P, Silberring J. iTRAQ analysis with Paul ion trap-obstacle solved. Journal of proteome research. 2013;12:4607-11.

[136] Peng H, Wu Y, Duan Z, Ciborowski P, Zheng JC. Proteolytic processing of SDF-1alpha by matrix metalloproteinase-2 impairs CXCR4 signaling and reduces neural progenitor cell migration. Protein & cell. 2012;3:875-82.

[137] Huang da W, Sherman BT, Lempicki RA. Systematic and integrative analysis of large gene lists using DAVID bioinformatics resources. Nature protocols. 2009;4:44-57.

[138] Raska M, Czernekova L, Moldoveanu Z, Zachova K, Elliott MC, Novak Z, et al. Differential glycosylation of envelope gp120 is associated with differential recognition of HIV-1 by virus-specific antibodies and cell infection. AIDS research and therapy. 2014;11:23.

[139] Edagwa BJ, Guo D, Puligujja P, Chen H, McMillan J, Liu X, et al. Long-acting antituberculous therapeutic nanoparticles target macrophage endosomes. FASEB journal : official publication of the Federation of American Societies for Experimental Biology. 2014.

[140] Cook EB, Stahl JL, Lowe L, Chen R, Morgan E, Wilson J, et al. Simultaneous measurement of six cytokines in a single sample of human tears using microparticle-based flow cytometry: allergics vs. non-allergics. Journal of immunological methods. 2001;254:109-18.

[141] Murray JL, Mavrakis M, McDonald NJ, Yilla M, Sheng J, Bellini WJ, et al. Rab9 GTPase is required for replication of human immunodeficiency virus type 1, filoviruses, and measles virus. Journal of virology. 2005;79:11742-51.

[142] Li M, Ablan SD, Miao C, Zheng YM, Fuller MS, Rennert PD, et al. TIM-family proteins inhibit HIV-1 release. Proceedings of the National Academy of Sciences of the United States of America. 2014;111:E3699-707.

[143] Chen AK, Sengupta P, Waki K, Van Engelenburg SB, Ochiya T, Ablan SD, et al. MicroRNA binding to the HIV-1 Gag protein inhibits Gag assembly and virus

production. Proceedings of the National Academy of Sciences of the United States of America. 2014;111:E2676-83.

[144] Liu C, Zhang X, Huang F, Yang B, Li J, Liu B, et al. APOBEC3G inhibits microRNA-mediated repression of translation by interfering with the interaction between Argonaute-2 and MOV10. The Journal of biological chemistry. 2012;287:29373-83.

[145] Welsch S, Groot F, Krausslich HG, Keppler OT, Sattentau QJ. Architecture and regulation of the HIV-1 assembly and holding compartment in macrophages. Journal of virology. 2011;85:7922-7.

[146] Tan J, Sattentau QJ. The HIV-1-containing macrophage compartment: a perfect cellular niche? Trends in microbiology. 2013;21:405-12.

[147] Mlcochova P, Pelchen-Matthews A, Marsh M. Organization and regulation of intracellular plasma membrane-connected HIV-1 assembly compartments in macrophages. BMC biology. 2013;11:89.

[148] Jouve M, Sol-Foulon N, Watson S, Schwartz O, Benaroch P. HIV-1 buds and accumulates in "nonacidic" endosomes of macrophages. Cell host & microbe. 2007;2:85-95.

[149] Ono A. Subcellular locations at which HIV-1 assembles. Uirusu. 2007;57:9-18.

[150] Deneka M, Pelchen-Matthews A, Byland R, Ruiz-Mateos E, Marsh M. In macrophages, HIV-1 assembles into an intracellular plasma membrane domain containing the tetraspanins CD81, CD9, and CD53. The Journal of cell biology. 2007;177:329-41.

[151] Chang Y, Finnemann SC. Tetraspanin CD81 is required for the alpha v beta5-integrin-dependent particle-binding step of RPE phagocytosis. Journal of cell science. 2007;120:3053-63.

[152] Dijkstra S, Geisert EE, Jr., Dijkstra CD, Bar PR, Joosten EA. CD81 and microglial activation in vitro: proliferation, phagocytosis and nitric oxide production. Journal of neuroimmunology. 2001;114:151-9.

[153] Takeda Y, Tachibana I, Miyado K, Kobayashi M, Miyazaki T, Funakoshi T, et al. Tetraspanins CD9 and CD81 function to prevent the fusion of mononuclear phagocytes. The Journal of cell biology. 2003;161:945-56.

[154] Stein MP, Muller MP, Wandinger-Ness A. Bacterial pathogens commandeer Rab GTPases to establish intracellular niches. Traffic. 2012;13:1565-88.

[155] Tippett E, Cameron PU, Marsh M, Crowe SM. Characterization of tetraspanins CD9, CD53, CD63, and CD81 in monocytes and macrophages in HIV-1 infection. Journal of leukocyte biology. 2013;93:913-20.

[156] Poteryaev D, Datta S, Ackema K, Zerial M, Spang A. Identification of the switch in early-to-late endosome transition. Cell. 2010;141:497-508.

[157] Collier ME, Mah PM, Xiao Y, Maraveyas A, Ettelaie C. Microparticle-associated tissue factor is recycled by endothelial cells resulting in enhanced surface tissue factor activity. Thrombosis and haemostasis. 2013;110:966-76.

[158] Bastin G, Heximer SP. Rab family proteins regulate the endosomal trafficking and function of RGS4. The Journal of biological chemistry. 2013;288:21836-49.

[159] Gulappa T, Clouser CL, Menon KM. The role of Rab5a GTPase in endocytosis and post-endocytic trafficking of the hCG-human luteinizing hormone receptor complex. Cellular and molecular life sciences : CMLS. 2011;68:2785-95.

[160] Mendoza P, Ortiz R, Diaz J, Quest AF, Leyton L, Stupack D, et al. Rab5 activation promotes focal adhesion disassembly, migration and invasiveness in tumor cells. Journal of cell science. 2013;126:3835-47.

[161] Liu SS, Chen XM, Zheng HX, Shi SL, Li Y. Knockdown of Rab5a expression decreases cancer cell motility and invasion through integrin-mediated signaling pathway. Journal of biomedical science. 2011;18:58.

[162] Macovei A, Petrareanu C, Lazar C, Florian P, Branza-Nichita N. Regulation of hepatitis B virus infection by Rab5, Rab7, and the endolysosomal compartment. Journal of virology. 2013;87:6415-27.

[163] Vitelli R, Santillo M, Lattero D, Chiariello M, Bifulco M, Bruni CB, et al. Role of the small GTPase Rab7 in the late endocytic pathway. The Journal of biological chemistry. 1997;272:4391-7.

[164] Caillet M, Janvier K, Pelchen-Matthews A, Delcroix-Genete D, Camus G, Marsh M, et al. Rab7A is required for efficient production of infectious HIV-1. PLoS pathogens. 2011;7:e1002347.

[165] Amet T, Nonaka M, Dewan MZ, Saitoh Y, Qi X, Ichinose S, et al. Statin-induced inhibition of HIV-1 release from latently infected U1 cells reveals a critical role for protein prenylation in HIV-1 replication. Microbes and infection / Institut Pasteur. 2008;10:471-80.

[166] Ullrich O, Reinsch S, Urbe S, Zerial M, Parton RG. Rab11 regulates recycling through the pericentriolar recycling endosome. The Journal of cell biology. 1996;135:913-24.

[167] Milev MP, Brown CM, Mouland AJ. Live cell visualization of the interactions between HIV-1 Gag and the cellular RNA-binding protein Staufen1. Retrovirology. 2010;7:41.

[168] Sandgren KJ, Smed-Sorensen A, Forsell MN, Soldemo M, Adams WC, Liang F, et al. Human plasmacytoid dendritic cells efficiently capture HIV-1 envelope glycoproteins via CD4 for antigen presentation. Journal of immunology. 2013;191:60-9.

[169] Fanales-Belasio E, Moretti S, Fiorelli V, Tripiciano A, Pavone Cossut MR, Scoglio A, et al. HIV-1 Tat addresses dendritic cells to induce a predominant Th1-type adaptive immune response that appears prevalent in the asymptomatic stage of infection. Journal of immunology. 2009;182:2888-97.

[170] Fanales-Belasio E, Moretti S, Nappi F, Barillari G, Micheletti F, Cafaro A, et al. Native HIV-1 Tat protein targets monocyte-derived dendritic cells and enhances their maturation, function, and antigen-specific T cell responses. Journal of immunology. 2002;168:197-206.

[171] Micaroni M, Stanley AC, Khromykh T, Venturato J, Wong CX, Lim JP, et al. Rab6a/a' are important Golgi regulators of pro-inflammatory TNF secretion in macrophages. PloS one. 2013;8:e57034.

[172] Mori R, Ikematsu K, Kitaguchi T, Kim SE, Okamoto M, Chiba T, et al. Release of TNF-alpha from macrophages is mediated by small GTPase Rab37. European journal of immunology. 2011;41:3230-9.

[173] Bhattacharya M, Ojha N, Solanki S, Mukhopadhyay CK, Madan R, Patel N, et al. IL-6 and IL-12 specifically regulate the expression of Rab5 and Rab7 via distinct signaling pathways. The EMBO journal. 2006;25:2878-88.

[174] Green DA, Masliah E, Vinters HV, Beizai P, Moore DJ, Achim CL. Brain deposition of beta-amyloid is a common pathologic feature in HIV positive patients. Aids. 2005;19:407-11.

[175] Guthi JS, Yang SG, Huang G, Li S, Khemtong C, Kessinger CW, et al. MRI-visible micellar nanomedicine for targeted drug delivery to lung cancer cells. Molecular pharmaceutics. 2010;7:32-40.

[176] Lebel RM, Menon RS, Bowen CV. Relaxometry model of strong dipolar perturbers for balanced-SSFP: application to quantification of SPIO loaded cells. Magnetic resonance in medicine : official journal of the Society of Magnetic Resonance in Medicine / Society of Magnetic Resonance in Medicine. 2006;55:583-91.

[177] Liu W, Dahnke H, Rahmer J, Jordan EK, Frank JA. Ultrashort T2* relaxometry for quantitation of highly concentrated superparamagnetic iron oxide (SPIO) nanoparticle labeled cells. Magnetic resonance in medicine : official journal of the Society of Magnetic Resonance in Medicine / Society of Magnetic Resonance in Medicine. 2009;61:761-6.

[178] Girard OM, Ramirez R, McCarty S, Mattrey RF. Toward absolute quantification of iron oxide nanoparticles as well as cell internalized fraction using multiparametric MRI. Contrast media & molecular imaging. 2012;7:411-7.

[179] Boska M, Liu Y, Uberti M, Sajja BR, Balkundi S, McMillan J, et al. Registered bioimaging of nanomaterials for diagnostic and therapeutic monitoring. J Vis Exp. 2010.

[180] Mascheri N, Dharmakumar R, Zhang Z, Paunesku T, Woloschak G, Li D. Fast low-angle positive contrast steady-state free precession imaging of USPIO-labeled macrophages: theory and in vitro experiment. Magnetic resonance imaging. 2009;27:961-9.

[181] Huang J, Gautam N, Bathena SP, Roy U, McMillan J, Gendelman HE, et al. UPLC-MS/MS quantification of nanoformulated ritonavir, indinavir, atazanavir, and efavirenz in mouse serum and tissues. Journal of chromatography B, Analytical technologies in the biomedical and life sciences. 2011;879:2332-8.

[182] Balkundi S, Nowacek AS, Veerubhotla RS, Chen H, Martinez-Skinner A, Roy U, et al. Comparative manufacture and cell-based delivery of antiretroviral nanoformulations. International journal of nanomedicine. 2011;6:3393-404.

[183] Roy U, McMillan J, Alnouti Y, Gautum N, Smith N, Balkundi S, et al. Pharmacodynamic and antiretroviral activities of combination nanoformulated antiretrovirals in HIV-1-infected human peripheral blood lymphocyte-reconstituted mice. The Journal of infectious diseases. 2012;206:1577-88.

[184] Dash PK, Gendelman HE, Roy U, Balkundi S, Alnouti Y, Mosley RL, et al. Long-acting nanoART elicits potent antiretroviral and neuroprotective responses in HIV-1-infected humanized mice. AIDS. 2012;26:2135-44.

[185] Roy U, McMillan J, Alnouti Y, Gautum N, Smith N, Balkundi S, et al. Pharmacodynamic and antiretroviral activities of combination nanoformulated antiretrovirals in HIV-1-infected human peripheral blood lymphocyte-reconstituted mice. The Journal of infectious diseases. 2012;206:1577-88.

[186] Gendelman HE, Gelbard, H. and Swindells S. The neurological manifestations of HIV-1 infection. Philadelphia: Lippincott-Raven Publishers; 2003.

[187] Choi KY, Liu G, Lee S, Chen X. Theranostic nanoplatforms for simultaneous cancer imaging and therapy: current approaches and future perspectives. Nanoscale. 2012;4:330-42.

[188] Boska M, Dou D., Liu, Y., Destache, C., Bartoletti, T.M., Uberti, M., Rabinow, B.E., and Gendelman, H.E. Magnetic resonance imaging and histological co-registration for blood-borne macrophage nanoformulated drug delivery in HIV-1 encephalitis Glia. 2007;submitted.

[189] Kibuule D, Dou H, Uberti M, Nelson J, Mellon M, Bradley J, et al. Magnetic labeled macrophages migrate across the blood brain barrier in mice with HIV-1 encephalitis. The 12th Annual Meeting of the Society on NeuroImmune Pharmacology, La Fonda on the Plaza, Santa Fe, New Mexico, abstract (TP-17). 2006.

[190] Torchilin VP. Recent advances with liposomes as pharmaceutical carriers. Nature reviews Drug discovery. 2005;4:145-60.

[191] Lasic DD. Doxorubicin in sterically stabilized liposomes. Nature. 1996;380:561-2.

[192] Barenholz Y. Doxil(R)--the first FDA-approved nano-drug: lessons learned. Journal of controlled release : official journal of the Controlled Release Society. 2012;160:117-34.

[193] Petre CE, Dittmer DP. Liposomal daunorubicin as treatment for Kaposi's sarcoma. International journal of nanomedicine. 2007;2:277-88.

[194] Liu Y, Pan J, Feng SS. Nanoparticles of lipid monolayer shell and biodegradable polymer core for controlled release of paclitaxel: effects of surfactants on particles size, characteristics and in vitro performance. International journal of pharmaceutics. 2010;395:243-50.

[195] Avgoustakis K. Pegylated poly(lactide) and poly(lactide-co-glycolide) nanoparticles: preparation, properties and possible applications in drug delivery. Current drug delivery. 2004;1:321-33.

[196] Panyam J, Labhasetwar V. Biodegradable nanoparticles for drug and gene delivery to cells and tissue. Advanced drug delivery reviews. 2003;55:329-47.

[197] Cho K, Wang X, Nie S, Chen ZG, Shin DM. Therapeutic nanoparticles for drug delivery in cancer. Clinical cancer research : an official journal of the American Association for Cancer Research. 2008;14:1310-6.

[198] Chan JM, Zhang L, Yuet KP, Liao G, Rhee JW, Langer R, et al. PLGA-lecithin-PEG core-shell nanoparticles for controlled drug delivery. Biomaterials. 2009;30:1627-34.

[199] Li B, Xu H, Li Z, Yao M, Xie M, Shen H, et al. Bypassing multidrug resistance in human breast cancer cells with lipid/polymer particle assemblies. International journal of nanomedicine. 2012;7:187-97.

[200] Wessels E, Simpson JC. Impact of live cell imaging on coated vesicle research. Seminars in cell & developmental biology. 2007;18:412-23.

[201] Kingsley J, Dou H, Morehead J, Rabinow B, Gendelman H, Destache C. Nanotechnology: a focus on Nanoparticles as a Drug delivery System J neuroimmune Pharmacol. 2006; 1:340-50.